Institutional Repository - Research Portal
Dépôt Institutionnel - Portail de la Recherche
researchportal.unamur.be
University of Namur

THESIS / THÈSE

DOCTOR OF SCIENCES

Design of novel imidazolium based nanostructures for sastainable catalytic applications

Calabrese, Carla

Award date:
2019

Awarding institution:
University of Namur

Link to publication

General rights
Copyright and moral rights for the publications made accessible in the public portal are retained by the authors and/or other copyright owners and it is a condition of accessing publications that users recognise and abide by the legal requirements associated with these rights.

- Users may download and print one copy of any publication from the public portal for the purpose of private study or research.
- You may not further distribute the material or use it for any profit-making activity or commercial gain
- You may freely distribute the URL identifying the publication in the public portal ?

Take down policy
If you believe that this document breaches copyright please contact us providing details, and we will remove access to the work immediately and investigate your claim.

Download date: 17. Apr. 2024

Università degli Studi di Palermo
Dottorato di Ricerca in
Scienze Molecolari e Biomolecolari
Dipartimento STEBICEF
S. S. D. – CHIM/06

Université de Namur
Doctorat en Sciences
Faculté de Sciences
Département de Chimie

DESIGN OF NOVEL IMIDAZOLIUM BASED NANOSTRUCTURES FOR SUSTAINABLE CATALYTIC APPLICATIONS

PhD STUDENT
CARLA CALABRESE

COORDINATOR
PROF. PATRIZIA DIANA

TUTOR
PROF. MICHELANGELO GRUTTADAURIA

TUTOR
PROF. CARMELA APRILE

CICLO XXXI
2019

Table of contents

Preface *iv*

Acknowledgements *vi*

CHAPTER I 1
General Introduction

1.1 Catalysis and Sustainable Development 2

1.2 Supported Organic Salts: Imidazolium Based Hybrid materials 4

1.3 Catalytic Supports for Imidazolium-Based Organic Salts 6

1.4 Carbon Nanoforms 7

1.4.1 Carbon Nanotubes 7

1.4.2 Carbon Nanohorns 9

1.5 Amorphous Silica 10

1.6 Ordered Mesoporous Silica 13

1.7 Polyhedral Oligomeric Silsesquioxanes 15

1.8 References 19

CHAPTER II 24
Carbon Dioxide Conversion into Cyclic Carbonates: An Introduction to Chapters III, IV, V

2.1 Carbon Dioxide: from a waste to a feedstock 25

2.2 Carbon Dioxide Conversion into Cyclic Carbonates 27

2.3 Catalytic Systems for the Synthesis of Cyclic Carbonates 29

2.4 References 32

CHAPTER III 34
Imidazolium Functionalized Carbon Nanohorns for the Conversion of Carbon Dioxide. Unprecedented Increase of Catalytic Activity after Recycling

3.1 Abstract 35

3.2 Results and Discussion 36
3.3 Conclusions 49
3.4 Experimental Section 50
3.5 References 52

CHAPTER IV 53
Supported Imidazolium Modified POSS Hybrids for the Conversion of Carbon Dioxide into Cyclic Carbonates
4.1 Introduction 54
4.2 Results and Discussion 55
4.3 Conclusions 67
4.4 Experimental Section 68
4.5 References 71

CHAPTER V 73
Imidazolium Based Cross-Linked Nanostructures from POSS Molecular Bricks for the Efficient Conversion of Carbon Dioxide
5.1 Abstract 74
5.2 Results and Discussion 75
5.3 Conclusions 84
5.4 Experimental Section 85
5.5 References 88

CHAPTER VI 89
Carbon–Carbon Cross Coupling Reactions Catalyzed by Supported Palladium Species: An Introduction to Chapters VI, VII
6.1 Palladium Catalyzed C–C Couplings 90
6.2 Imidazolium Salts as Palladium Support 91
6.3 References 94

CHAPTER VII 96
Imidazolium Functionalized Carbon Nanohorns and Carbon Nanotubes as Pd Nanoparticles Support for C–C Cross Couplings
7.1 Abstract 97
7.2 Results and Discussion 98

7.3 Conclusions 111

7.4 Experimental Section 113

7.5 References 118

CHAPTER VIII 119

Supported Imidazolium Modified POSS Hybrids as Palladium Platform for C–C Cross Couplings

8.1 Abstract 120

8.2 Results and Discussion 121

8.3 Conclusions 133

8.4 Experimental Section 134

8.5 References 138

CHAPTER IX 139

General Conclusions

List of abbreviations 143

Curriculum vitae 145

Preface

In a growing quest for greener processes able to reduce chemical wastes, the design of recoverable and recyclable catalysts represents a topic of paramount importance for the industry, the environment preservation, and the societal progress. The possibility of recovering and reusing a selected catalytic system for consecutive runs is the main pillar of the heterogeneous catalysis.

In this scenario, finding an ideal balance between homogeneous and heterogeneous catalysis is not an easy task. Herein, the PhD project has been focused on the development of highly performing heterogeneous catalysts for sustainable applications, namely the conversion of carbon dioxide into cyclic carbonates and the formation of C–C bond.

The mitigation of CO_2 emission is a contemporary challenge to be tackled from both environmental and economic perspectives. The conversion of carbon dioxide into cyclic carbonates *via* reaction with epoxides is one of the most attractive strategies to switch from a waste to a feedstock for the synthesis of value added products endowed with 100% of atom economy. On the other hand, the importance of palladium catalyzed C–C bond formation is well known in organic chemistry as key steps for the production of pharmaceuticals, agrochemicals, natural products, and conjugated polymers. In this project, imidazolium salts have been selected, from one hand, as active sites for CO_2 fixation, from the other hand, as stabilizing support for palladium species. The design of the catalytic materials was carried out by the covalent immobilization of imidazolium based organic salts onto novel nanostructures: carbon nanohorns, multi-walled carbon nanotubes, and polyhedral oligomeric silsesquioxanes.

The first chapter of the dissertation introduce the reader into the field of heterogeneous catalysis based on imidazolium salts with a focus on the nanostructured supports herein employed. After this introductory chapter, the dissertation is split into two main parties dealing with the specific catalytic

application of the proposed materials. The first part (*Chapters II-IV*) presents the catalytic systems for the conversion of carbon dioxide into cyclic carbonates, whereas the second one (*Chapters V-VIII*) is concerned with palladium supported hybrids for Suzuki-Miyaura and Mizoroki-Heck C–C cross couplings.

Acknowledgements

This research was supported by a co-funded PhD fellowship between the University of Palermo (Italy) and the University of Namur (Belgium).

Firstly, I would like to express my sincere gratitude to my advisors *Prof. Michelangelo Gruttadauria* and *Prof. Carmela Aprile* for their precious scientific and human support during my PhD experience. They gave me the opportunity to explore the world of scientific research with enthusiasm and criticism. It was a pleasure being part of their research groups and working in the field of heterogeneous catalysis.

A special thank goes to *Prof. Francesco Giacalone* for his encouragement, scientific support, and mentoring since I started my bachelor thesis under the wise supervision of *Prof. Gruttadauria*.

I would like to thank *Dr. Leonarda Francesca Liotta* for providing a significant scientific support and for kindly discussing together my results.

I'm grateful to *Prof. Steve Lanners* and *Dr. Luca Fusaro*, my *comité d'accompagnement*, for the help and the advices they offered to me.

I want to thank *Dr. Esther Carbonell* and *Dr. Vincenzo Campisciano* who have been involved in my research activity.

Many thanks to my labmates, colleagues, and friends of the University of Palermo and the University of Namur.

Finally, I wish to thank my family for its support, encouragement, and unconditional love.

CHAPTER I

General Introduction

CHAPTER I

General Introduction

1.1 Catalysis and Sustainable Development

Nowadays, the sustainable development of new technologies and processes is one of the main goals from both academic and industrial parties. In 1987 Brundtland described the sustainable development as "*meeting the needs of the present generation without compromising the ability of future generations to meet their own needs*".[1] In this context, the design of novel processes with a low environmental impact is closely associated to the Twelve Principles of Green Chemistry proposed by Anastas and Warner in 1998.[2] It is widely recognized that Green Chemistry is a field of great interest for the environment and the economic progress. Green Chemistry is notably defined as "*the design and application of chemical products and processes to reduce or to eliminate the use and generation of hazardous substances*".[2] The eco-friendly design criteria of new materials, products and processes include the key concepts of waste prevention, atom economy, use of renewable feedstocks with regard to human health and environmental viability.[3]

According to Green Chemistry Principles, catalytic processes are one of the most important pillars for the sustainable development.[4] It is well known that the traditional use of stoichiometric amounts of reagents leads to a remarkable production of waste. Catalysis, therefore, plays a pivotal role in the improvement of the efficiency of chemical reactions leading to lower energy, feedstock, and waste consumption. The advantages of using catalytic processes result from the intrinsic features of the catalyst defined as sub-stoichiometric substance able to properly decrease the activation energy of a selected reaction.

The design of an efficient catalytic system should be planned with the aim to achieve appealing performances in terms of chemical stability, selectivity toward the desired product, and high turnover number values. Catalysts can be classified,

on the basis of their physical state, into homogeneous and heterogeneous. In the first case, the catalyst is molecularly dispersed in the same phase as the reactants whereas, in heterogeneous catalysis, the catalyst and the reactants are in different phases. These two branches of catalysis display different strengths and weaknesses.[5] Homogeneous catalysts lead to the synthesis of the target product in high yield and selectivity. However, the tedious separation of homogeneous catalysts from the reaction medium limits their industrial applications. On the other hand, heterogeneous catalysts usually display lower activity compared to the analogous homogeneous, but they can be easily recovered from the reaction mixture, recycled for consecutive runs and also used in large-scale applications such as in fixed-bed technology. Furthermore, the use of solid catalysts in liquid or gas phase is quite common and involves mass transfer and diffusion processes among the reactants, products and the catalyst itself.

From the above, it is evident that finding an ideal balance between homogeneous and heterogeneous catalysis is a challenging objective. In this respect, different strategies have been developed for the design of heterogeneous catalyst *via* immobilization of molecular catalysts onto a plethora of solid supports.[6] On the basis of the covalent or non-covalent interaction between the catalyst and the support, it is possible to distinguish two general synthetic approaches. Moreover, the covalent immobilization of the catalyst onto the support, in turns, includes post-synthetic or co-synthetic strategies. In the co-synthetic strategy, the heterogeneous catalyst is prepared by using a one-pot procedure in which both the catalyst and the molecular precursors of the support are reacted together. On the other hand, the post-synthetic approach, showed in Scheme 1, involves the grafting of the catalytic moieties onto a pre-formed solid support. Furthermore, the solid support can be used as pristine or previously modified with a proper linker bearing a double functionality able to react from one end with the solid, and from the other with the selected catalyst.

Scheme 1. Post-synthetic covalent immobilization of catalytic moieties.

In this PhD dissertation, the post-synthetic approach has been adopted for the synthesis of imidazolium-based hybrid materials as heterogeneous catalysts for the conversion of carbon dioxide into cyclic carbonates (Chapters II, III, IV, V).

Finally, the non-covalent immobilization pathway for the synthesis of heterogeneous catalysts, can be performed by using electrostatic interaction, inclusion, or adsorption procedures. Herein, imidazolium-based nanostructures have been employed as catalytic support able to provide electrostatic and steric stabilization of palladium species for C−C cross coupling reactions (Chapters VI, VII, VIII).

1.2 Supported Organic Salts: Imidazolium Based Hybrid Materials

Organic salts (OSs) are a class of ionic compounds made up of at least an organic cation or anion. On the lines of the common inorganic salts, the primary interactions between cation and anion of an organic salt are merely coulombic. Moreover, the specific ions structure of the OSs can involve strong secondary interactions, such as hydrogen bonds, π–π or cation-π interactions. The properties of OSs can be finely modulated by changing either the nature of the cation, the anion, or by tuning their structure with selected functionalities. Owing to their wide range of applications, a growing interest of the scientific research is focused on the design of novel technologies based on both mono- and poly-cationic OSs. In particular, mono-cationic OSs are mainly included in the broad family of ionic liquids (ILs), commonly defined as salts with melting point below 100 °C. Typically, such systems are characterized by low vapor pressure, low flammability, wide liquid range, high ionic conductivity and excellent thermal and chemical stability. All these features make ILs good candidates in numerous fields of research. Moreover, ILs can be modulated for specific tasks by tuning the structure as well as their physicochemical properties including melting point, viscosity, density, solubility, and hydrophobicity. In this context, the introduction of specific functional groups into ILs structures gives rise to the so-called "*Task Specific Ionic Liquids*" (TSILs). In particular, Davis described the design of TSILs as "*the covalent tethering of a*

functional group to one or both of the ions of an otherwise ordinary ionic liquid can imbue the resulting salt with a capacity to interact with dissolved substrates in specific ways".[7] The cationic structures forming ILs are based on aromatic or aliphatic moieties. Some of the most common cations are imidazolium, thiazolium, pyridinium, ammonium, and phosphonium. They can be easily prepared by quaternization of the heterocycle, amine or phosphate core. Among the most used anions in ionic liquids, it is possible to find chloride, bromide, iodide, tetrafluoroborate, and hexafluorophosphate. The tuning of the anionic species can be carried out by anionic metathesis procedures. The above-mentioned components of ionic liquids are summarized in Figure 1.

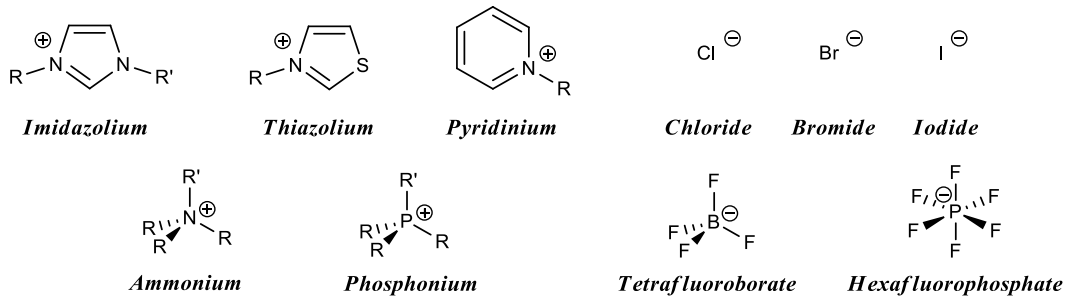

Figure 1. Some commonly used cations and anions in ionic liquids.

Thanks to their huge spectrum of properties, ILs find applications in organic synthesis, as alternative reaction media to conventional organic solvents, in catalysis,[8] biotechnology,[9] separation techniques,[10] energy storage,[11] electrochemistry[12].

In the field of catalysis, supported ionic liquids (SILs) emerged as a promising class of functional materials.[13] A wide range of reported SILs catalytic systems is based on imidazolium salts covalently grafted onto many types of solid supports such as amorphous or mesostructured silica, zeolites, polymers, magnetic nanoparticles, carbon nanostructures, and others.[14] Imidazolium based SILs materials have been employed as support for organocatalysts, as catalysts themselves, and as stabilizing support for metal-based catalysts.

The covalent immobilization of ILs frameworks onto a suitable support is a synthetic strategy that offers attractive advantages compared to the unsupported analogous. The resulting hybrids imply: *i)* a much lower use of ILs; *ii)* easy

separation of the catalyst from the reaction media; *iii)* transfer of the physicochemical properties of ILs to the final material.

It is worth to mention that the choice of the support is of paramount importance for the implementation of the catalytic performance of the obtained material.

Herein, the dissertation will be focused on the design of imidazolium-based hybrids as heterogeneous catalysts for *i)* carbon dioxide conversion into cyclic carbonates and, *ii)* palladium catalyzed C–C cross-coupling reactions. For this purpose, several solid supports have been considered such as carbon nanohorns (CNHs), multiwalled carbon nanotubes (MWCNTs), amorphous silica (SiO_2), mesostructured SBA-15, and polyhedral oligomeric silsesquioxanes (POSS).

1.3 Catalytic Supports for Imidazolium-Based Organic Salts

In the area of heterogeneous catalysis, the preparation of hybrid solids by post-synthetic strategies requires special attention to the choice of the support. In general, the main features of the final material are: *i)* grain and pore size; *ii)* surface area; *iii)* location of the active phase; *iv)* interaction of the active phase with the support; *v)* particle size; *vi)* mechanical properties, and *vii)* thermal stability. Therefore, considering the key role of the support in the catalytic performance, a good solid support should display high chemical, thermal and mechanical stability, large surface area, good amount of functionalization sites, and fast mass transport of reactants and products to and from the active sites. Among the most used solids, alumina, silica and carbons deserve to be mentioned. Based on the structural properties, solid supports can be classified as *i)* structured porous materials, *ii)* layered materials, and *iii)* unstructured materials. Herein, a broad series of heterogeneous catalysts bearing imidazolium salts as active sites will be presented. The idea was to propose imidazolium-based nanostructures able to bridge the gap between the homogeneous and heterogeneous catalysts: highly dispersible, easily recoverable and reusable. In the next sections, the selected solid supports will be briefly presented.

1.4 Carbon Nanostructures

Nanocarbon based hybrid materials have drawn the interest of the scientific community thanks to their potential applications in a plethora of research fields. Structured carbon nanoforms (CNFs) are a class of materials at the forefront of new nanotechnologies.[15] The wide family of carbon nanostructures includes graphenes, fullerenes, single- and multi-walled nanotubes, nanodiamonds, nano-onions, and nanohorns.[16] The unique properties of both nanocarbons and imidazolium-based OSs led to the development of a growing family of hybrid materials for heterogeneous catalysis.[17]

1.4.1 Carbon Nanohorns

Among CNFs, in the last few years, carbon nanohorns (CNHs) have emerged because of their particular morphology and their high degree of purity linked to the absence of metal nanoparticles. CNHs are conical carbon nanostructures made up of single rolled graphene sheets.[18] Individual CNHs have a diameter of approximately 2–5 nm and a length of 40–50 nm. Moreover, they have a conical front tip section followed by a short cylindrical nanotube section. CNHs can be produced *via* arc-discharge, laser ablation, and Joule heating. During the synthesis, CNHs cluster together into spherical aggregates that look like dahlia flowers. The average diameter of such aggregates is approximately 100 nm.

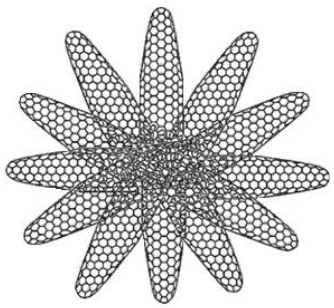

Figure 2. Pristine CNHs.

The synthesis of CNHs does not involve the use of metal catalysts and can be performed in high yield and at a high rate of production. Typically, the synthesis methods consist in a suitable injection of energy able to vaporize and restructure a carbon target, followed by rapid quenching under inert conditions. Pristine CNHs present a good thermal stability, micro- and mesoporosity, internal pore accessibility, and semiconducting properties. All these features pave the way to a wide range of nanotechnological applications for CNH-

based materials such as gas storage, biosensors, drug delivery systems, and catalysis.[19] The chemical functionalization of CNHs sidewalls represents a cornerstone for the design of novel hybrid materials based on this promising carbon nanostructure. The main pathways for the chemical modification of CNHs involve covalent attachment of organic moieties, noncovalent interactions between CNHs and aromatic organic units, and the immobilization of metal nanoparticles.[20] Furthermore, the covalent functionalization of CNHs can be carried out by following two approaches: *i)* oxidation of the conical tips in order to introduce carboxylic moieties able to react for further chemical modifications, and *ii)* direct covalent bond formation onto CNHs sidewalls.

Conversely to the case of others CNFs, the applications of CNHs, were less explored. Excluding the materials presented in this PhD dissertation, there is just one example in literature about imidazolium functionalized CNHs. In particular, Tagmatarchis *et al.*[21] prepared a series of hybrid materials starting from oxidized CNHs. After their activation upon reaction with oxalyl chloride, the obtained CNHs were covalently coupled with (3-aminopropyl)imidazole, while further reaction with n-butyl bromide allowed to the formation of the N-n-butylimidazolium-modified CNHs as a stable dispersion in aqueous media.

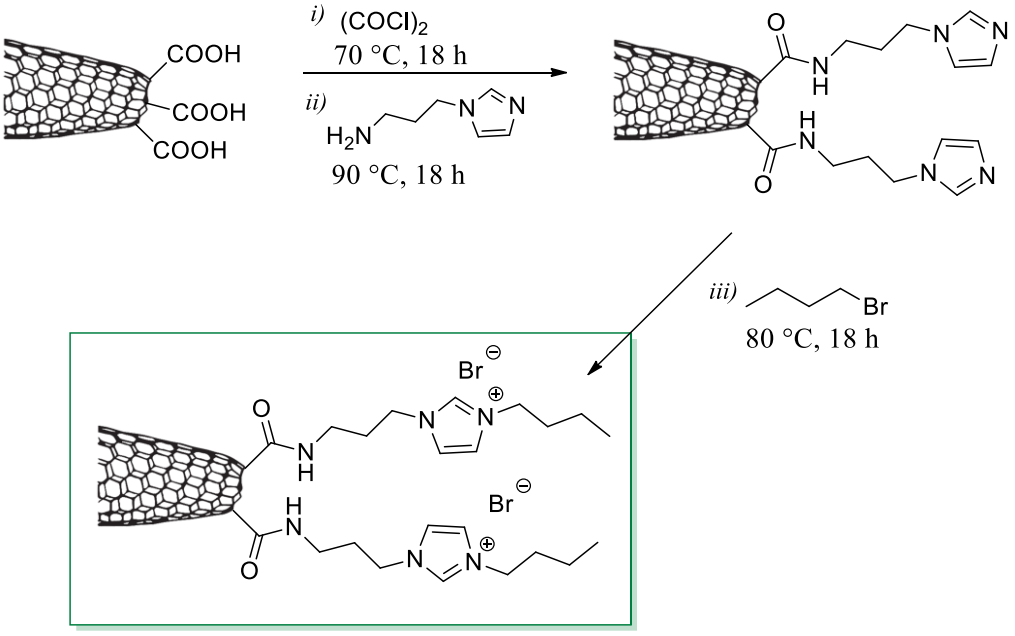

Scheme 2. Synthesis of imidazolium functionalized CNHs hybrid materials.[21]

Moreover, the bromide anion of the material, was exchanged by [PF_6^-], [ClO_4^-] and [BF_4^-] anions with a solubility switch of the hybrid from aqueous to organic solvents. On the other hand, when the [PF_6^-] N-n-butylimidazolium-modified CNHs were treated with Na_2SO_4, $NaNO_3$ or NaCl, the solubility of the as prepared materials was switched to aqueous media again. In addition, these hybrids have been used as stabilizers to grow platinum and palladium nanoparticles.

1.4.2 Carbon Nanotubes

Since their discovery in 1991, carbon nanotubes (CNTs) have attracted increasing attention from the scientific research as promising candidates for a huge spectrum of applications in materials science and nanotechnology.[22] CNTs have a cylindrical nanostructure resulting from graphene layers wrapped into a seamless tube. Based on the number of the walls, it is possible to classify CNTs into: *i)* single-walled carbon nanotubes (SWCNTs), *ii)* double-walled carbon nanotubes (DWCNTs), and *iii)* multi-walled carbon nanotubes (MWCNTs). Nanotube external diameters are in the range between 0.4–4 nm for SWCNTs, and up to 100 nm for MWCNTs. Moreover, the way in which the graphene layer is rolled gives rise to armchair, zigzag, and chiral nanostructures with different electronic properties (Figure 3).

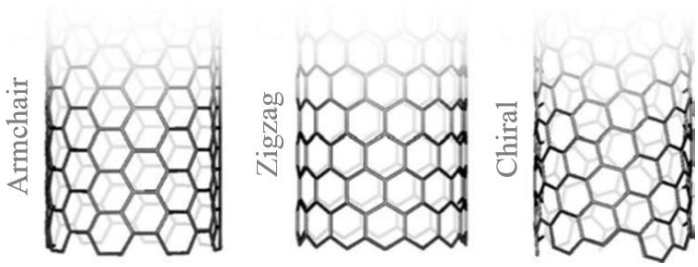

Figure 3. Different chirality of single walled carbon nanotubes.[23]

CNTs properties such as diameter, number of walls, and length are influenced by their specific production method. The synthesis can be carried out by using arc-discharge, laser ablation, and chemical vapor deposition (CVD) techniques in the presence of metal catalysts.

CNTs display high thermal and electrical conductivity, mechanical resistance, low density, and tunable semiconductivity. These features introduce them to numerous industrial applications, such as components in electronics, solar cells, sensors, energy storage devices, and as filler in polymeric composites in mechanical applications. Moreover, the use of CNTs for catalytic applications is an ongoing research study involving CNTs as heterogeneous supports for molecular catalysts, metal nanoparticles, metal oxides, metal-free catalytic systems and hierarchical hybrids. The broad variety of catalytic processes covers standard organic synthesis, electrocatalysis, photocatalysis and many others.[24]

Pristine CNTs are usually packed into bundles owing to van der Waals and π–π stacking interactions between the walls of the tubes. For this reason, their tangled network is not able to form stable and fine dispersions in both aqueous solutions and organic solvents. In order to improve CNTs dispersibility as well as their application fields, a crucial approach is represented by the chemical functionalization of CNTs.[25] Pristine CNTs can be modified by following three main methodologies: *i)* the covalent attachment of chemical moieties onto the π-conjugated nanotube skeleton; *ii)* the non-covalent adsorption or wrapping of the tubular surface by several functional molecules; and *iii)* the endohedral filling of their inner empty cavity.[25b] According to literature, it was found that the functionalization of CNTs with imidazolium based organic salts allowed to obtain a wide variety of hybrid materials and nanocomposites.[17a, 26] Herein, imidazolium modified MWCNTs and CNHs have been used as support for palladium nanoparticles in order to obtain novel hybrid catalytic systems for C–C coupling reactions.

1.5 Amorphous Silica Gel

Synthetic Amorphous Silica (SAS) is highly pure silicon dioxide which may be produced as pyrogenic silica, precipitated silica, and silica gel.[27]

Silica gels can be described as a rigid 3D-network made up of micro-sized random aggregates of polymerized amorphous silicate particles.[28] Typically, their production requires the controlled neutralization of aqueous sodium silicate

solutions by sulfuric acid. Then, the obtained hydrogel is aged, washed, and dried. The textural properties of silica gels, such as pore sizes and high surface area (300–1000 $m^2\ g^{-1}$), can be tuned by changing the reaction parameters (pH, temperature, the type of acid, drying conditions). Based on the adopted drying protocol, it is possible to classify silica gel into: *i)* xerogel, if aqueous phase in the pores is removed by evaporation; *ii)* aerogel, when the solvent is removed by supercritical extraction; *iii)* cryogel (freeze drying). A further method for the preparation of silica gels is represented by the sol-gel polymerization of silicon alkoxides, such as tetraethylorthosilicate ($Si(OC_2H_5)_4$) in the presence of ethanol and water.[29]

Silica gel displays useful features, *e.g.* high surface area, narrow range of pore sizes (microporous to mesoporous), good thermal and mechanical stability, widespread availability, and easy covalent functionalization strategies covering a broad range of organic or organo-metallic moieties. All these features lead to several applications as ultrafilters, adsorbents, chromatography column packing materials, catalytic supports and many others.

The huge variety of chemical modifications onto silica surface is linked to the presence of silanol groups. Moreover, these functional groups play a key role when acting as the centers of molecular adsorption during their specific interaction with adsorbates able to form a hydrogen bond with the –OH groups, or, more generally, undergo donor–acceptor interaction.[30]

As evidenced by Zhuravlev,[30] pure silica shows surface –OH groups which can be distinguished in: *i)* isolated free silanols, *ii)* geminal silanols, and *iii)* vicinal, or bridged, or –OH groups bound through the hydrogen bond (H-bonded single silanols, H-bonded geminals, and their H-bonded combinations). According to the nomenclature commonly used in NMR spectroscopy (Figure 4), silica is composed of Q^n structural units, where *n* indicates the number of bridging bonds (–O–Si) linked to the central silicon atom. From the above, it is possible to find geminal silanols in both Q^1 and Q^2 units, single silanols in Q^3 frameworks, whereas Q^4 corresponds to siloxanes moieties.

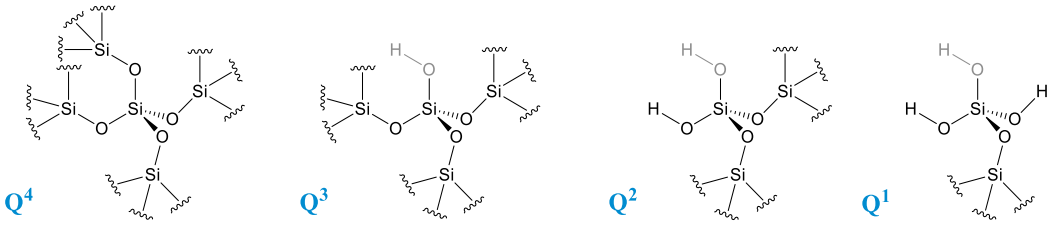

Figure 4. Q^n silicon units nomenclature.

The covalent functionalization of silica surface is usually performed by condensation reactions between the silanol groups and a selected organo-silane. Therefore, silylating coupling agents such as chlorosilanes, alkoxy-silanes and silyl-amines have found widespread application. Their reaction with surface silanol functionalities usually occurs on free and geminal silanol groups, whereas hydrogen bonded silanol moieties are less reactive owing to the local hydrophilic networks. Silica gels have been employed as supports for the covalent grafting of organic salts in order to improve their applicability and reusability in industrially catalytic processes. In particular, several studies report the use of silica gels as inorganic supports for the design of recyclable and efficient catalytic systems based on imidazolium salts. In the field of catalysis, one of the first examples of organic salts covalently grafted onto amorphous silica is given by the immobilization of an acidic chloroaluminate imidazolium ionic liquid. In particular, Valkenberg *et al.*[31] proposed novel hybrids where either anion or cation was covalently bonded to the solid support (Scheme 3).

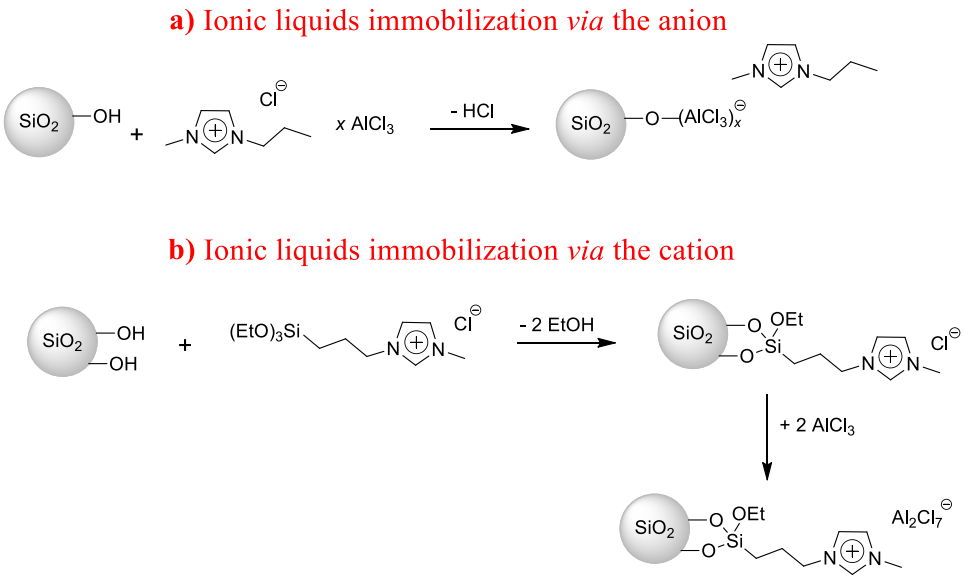

Scheme 3. Covalent grafting of imidazolium salts *via* the anion (a) or the cation (b).[31]

The resulting materials were tested as catalysts in the Friedel–Crafts alkylation of aromatic compounds.

Considering the pivotal catalytic applications of this PhD thesis, herein, it is worth to mention the use of imidazolium supported silica gel for *i)* the conversion of CO_2 into cyclic carbonates,[32] or *ii)* as catalytic and stabilizing platform for palladium nanoparticles.[33]

1.6 Ordered Mesoporous SBA-15

Ordered mesoporous materials, emerged in the early 1990s, represent an interdisciplinary research focus. This class of materials is characterized by high surface areas, a large and uniform pore size (1.5–50 nm), and high regularity of order array of pores. The design of periodically arranged organic-inorganic nanohybrids is one of the main topics of interest which explain the continuous research activity on functional mesostructured materials. In particular, ordered mesoporous silicas have received widespread attention owing to their broad range potential applications as supports for catalysis, selective adsorption, novel functional materials, separation, and use as hosts to confine guest molecules.[28, 34] Such materials display a well-ordered arrangement of building units resulting from self-organization processes around molecular assemblies. Several templating methodologies have been developed for the synthesis of materials with different types of pore arrangement. In this context, MCM-41 and SBA-15 deserve to be mentioned as the two most representative of mesoporous silicas with hexagonal phases.[35] In particular, their ideal structural model corresponds to hexagonally close-packed cylinder-like pore channels, ascribed to *p6mm* space group.

SBA-15 (Santa Barbara Amorphous) mesoporous silica structures were introduced by Zhao *et al.* in the late 1990s.[36] Since then, SBA-15 family has attracted a growing interest in many fields of research such as catalysis, adsorption, chemical sensing, drug delivery systems, and separation science (*e.g.* high-performance liquid chromatography, HPLC). The main attractive features of this class of materials are represented by high surface areas (690–1040 $m^2\ g^{-1}$), well-defined pore structure, high biocompatibility, and high thermal and hydrothermal

stability. Furthermore, SBA-15 mesostructures have pore size in the range 4.6–30 nm and thick pore walls (3.1–6.4 nm). Compared to the above-mentioned MCM-41 family, SBA-15 solids present higher hydrothermal and thermal stabilities because of their thicker pore walls. Owing to the presence of a non-regular microporosity with pore sizes in the range 0.5–2 nm, SBA-15 texture may be considered as a combination of micro- and mesoporosity. The synthesis of SBA-15 is performed under acidic conditions and involves the use of a sacrificial structuring template such as amphiphilic triblock copolymers able to direct the organization of polymerizing silica species. For doing so, poly(alkylene oxide) triblock copolymers are commonly used as organic structure-templating agents. In particular, poly(alkylene oxide) triblock copolymers such as poly(ethylene oxide)-poly(propylene oxide)-poly(ethylene oxide) (PEO–PPO–PEO) emerged as sacrificial surfactants, because of their mesostructural ordering properties, amphiphilic character, low-cost commercial availability, and biodegradability. At the end of the synthetic procedure, the organic-inorganic mesostructures, arising from both polymerization and condensation phenomena between the silica precursors, are calcinated in order to remove the surfactant (Scheme 4).

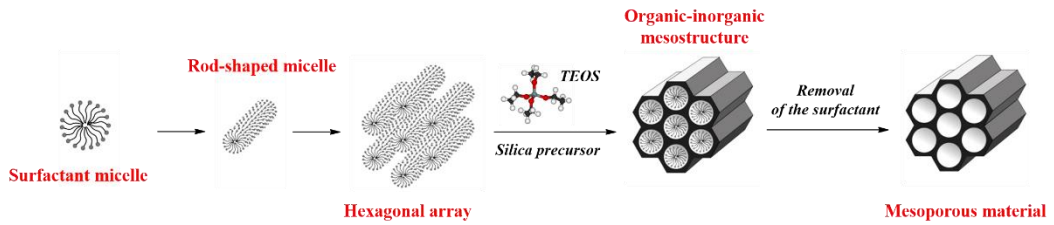

Scheme 4. Synthetic protocol of ordered mesoporous silica.

The large SBA-15 mesopores result interconnected by many irregular tunneling micropores. The presence of such micropores is due to the chains of the polymeric surfactant that, during the synthesis, may be trapped into the silica walls leading to the formation of the micropores after the calcination step. The specific textural properties of the obtained mesoporous material can be finally tuned to get a broad spectrum of morphologies. Based on the selected reaction conditions,[28] it is possible to increase the pore sizes of the material by changing some parameters such as the hydrothermal temperature, or the length of the hydrophobic part of the surfactant. A further approach to modulate the size of the pore is represented by the

use of a nonpolar organic swelling agent such as 1,3,5-trimethylbenzene (TMB). A larger amount of swelling agent usually results in larger pore sizes (up to 30 nm). However, it is worth that too high a concentration of TMB may decrease the regularity of mesopore order. Moving on some literature applications, SBA-15 mesostructures have been employed for the design of novel materials based on imidazolium moieties as SO_2 adsorbents,[37] composite membrane for alkaline fuel cell,[38] catalytic supports for gold[39] or palladium[33a, 40] nanoparticles, or as catalysts themselves for Henry reactions,[41] Knoevenagel–Michael-cyclization processes,[42] and for the conversion of carbon dioxide into cyclic carbonates.[43]

1.7 Polyhedral Oligomeric Silsesquioxanes

The huge demand for novel hybrid materials with specific technological applications encouraged a prosperous research activity focused on the design of modular and efficient synthetic strategies. In the recent years, polyhedral oligomeric silsesquioxanes (POSS) emerged as building blocks for the preparation of multifunctional nanohybrids and nanocomposites with tunable hierarchical structures. Usually considered as the smallest hybrid particles of silica, POSS are a class of organic-inorganic hybrid molecules made up of an inorganic nanocaged silicate core surrounded by organic functional groups dangling in a three dimensional arrangement.[44] The general formula of these hybrid molecules is $(R\text{-}SiO_{1.5})_n$, where *n* is commonly 6, 8, 10 and 12, the ratio O/Si is 1.5, and R is the vertex functional group. Among them, POSS molecules with a T_8 cubic inorganic core composed of silicon−oxygen bonds ($R_8Si_8O_{12}$) represent the most investigated nanostructure.

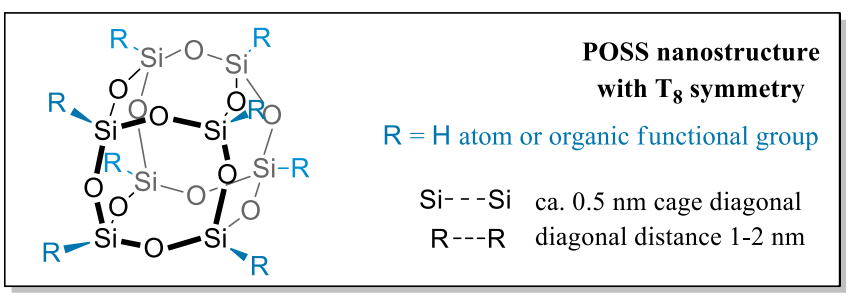

Figure 5. T_8 POSS nanocage.

In this PhD dissertation, the nomenclature of conventional silicon nuclear magnetic resonance (^{29}Si NMR) will be used by considering T^n and Q^n as silicon atoms bonded to three or four oxygen atoms (*n*), respectively (Figure 4 and 6). Typically, based on the nature of the R-group, cubic POSS have a size in the range 1–2 nm, and an inner Si–Si diameter of approximately 0.5 nm. POSS structures display high chemical and thermal stability together with a rigid molecular skeleton that can be functionalized with a plethora of organic side groups. On these grounds, the peculiar POSS molecular structure can be easily tuned to get a broad spectrum of properties. For instance, the presence of the R-groups ensures the solubility POSS in many organic solvents paving the way to several applications.

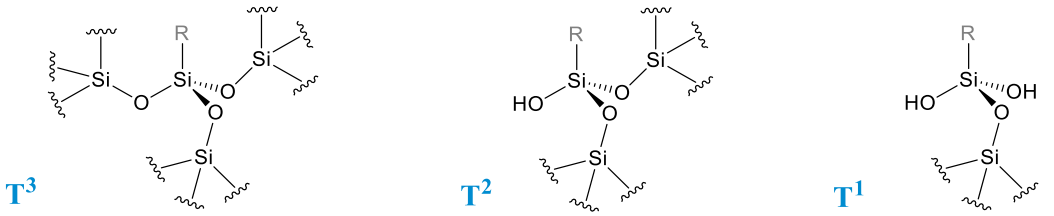

Figure 6. T^n silicon unit nomenclature.

The synthesis of cubic POSS nanocages can be performed by following three main approaches: *i)* the hydrolytic condensation of monosilanes; *ii)* the corner capping of partially condensed silsesquioxanes, $Si_7O_9R_7(OH)_3$; *iii)* the chemical modification of the functional groups of an already existing T_8 core to give a new POSS derivative.[44-45] Among them, the first strategy is the most general and widely used. According to literature, in the proposed mechanism for the synthesis of the completely condensed POSS, firstly, the hydrolysis of the monosilane $RSiX_3$ (where R is an hydrogen atom or an organic group and X = Cl, OMe, OEt, etc.) lead to the corresponding trisilanol, $RSi(OH)_3$. Then, the monomeric trisilanol gives rise to consecutive condensation steps through the formation of the dimer, of the cyclic tetramer, and finally, of the cubic silsesquioxanes (Scheme 5).[46] It is worth to mention that the good outcoming of the synthesis is strongly influenced by many factors such as: *i)* the nature of both R- and X-group; *ii)* the concentration of the monosilane $RSiX_3$; *iii)* the type of solvent; *iv)* the presence of water; *v)* the temperature; *vi)* the pH; *vii)* the reaction time.

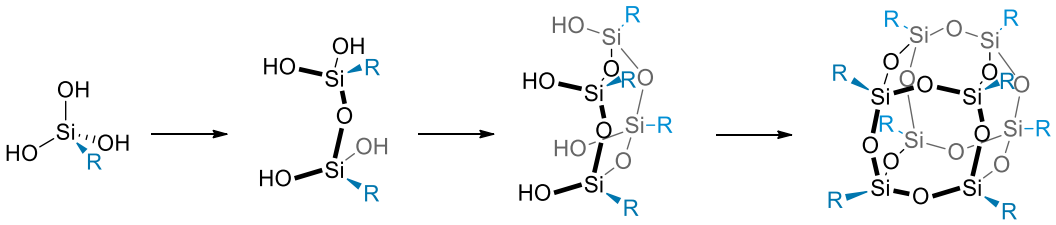

Scheme 5. Proposed mechanism of T_8 POSS formation.

POSS family is attracting the attention of the scientific arena owing to their wide range of applications in materials science ranging from soft electronics to nanomedicine.[47] POSS molecules have been widely employed for the design of hybrid polymer and nanocomposites. As showed in Figure 7, POSS may be integrated into composites through four main strategies: *i)* POSS molecule bearing unreactive groups (*e.g.* -alkyl) as a blender in a polymeric network; *ii)* mono-functional POSS grafted onto a polymer backbone, leading to polymers with pedant POSS units; *iii)* multi-functional POSS as local initiator of the polymerization from the surface of the nanocage, allowing a star-like macromolecule; *iv)* POSS with multi-reactive groups as local initiator to produce a heavily cross-linked polymeric network.[44, 47b, 48] The incorporation of such nanosized building blocks into polymeric matrices gives rise to novel local molecular interactions, giving rise to a nanocomposite with modulated physical properties such as modulus, strength, glass transition temperature, thermal stability, and dimensional stability.

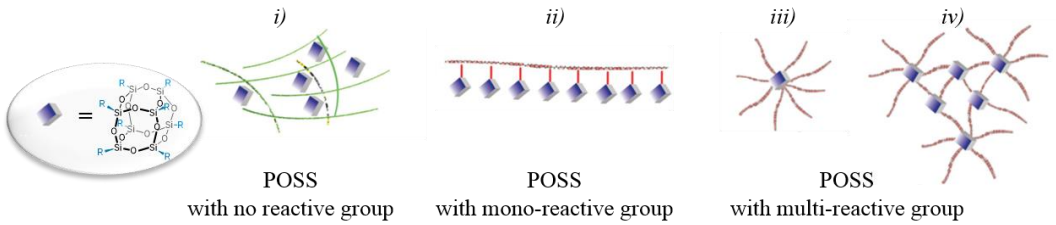

Figure 7. POSS as nano-building blocks for polymeric nanocomposites.[47b]

Chen and co-workers[49] introduced the first family of POSS based porous frameworks with enriched organic salts structures and tunable textural properties. In particular, POSS building blocks bearing eight chloropropyl chains were reacted with several bis-N-heterocyclic linkers allowing to obtain a series of cross-linked ionic materials. The applicability of POSS in imidazolium salts has been upgraded by introducing POSS-based filler materials into ionic liquids. As reported in

literature, sulfonic acid POSS[50] and octa-substituted carboxy-POSS[51] have been used efficient filler able to improve the thermal stability and lower the melting temperature of imidazolium salts for using as ionic liquids. Recently, Shang *et al.*[52] employed a series of novel imidazolium-based POSS nanostructures for the design of new solid polymer electrolytes for lithium ion batteries with high ionic conductivity and wide electrochemical windows. Moreover, imidazolium modified POSS found application as solid-state electrolytes in solid-state dye-sensitized solar cells (ssDSSCs).[53]

Finally, imidazolium decorated POSS nanostructures have been applied in the area of catalysis. In this context, there are only few examples (Figure 8). POSS units have been functionalized with imidazolium peripheries in order to be used as *i)* homogeneous catalyst for the conversion of CO_2 into cyclic carbonates,[54] and *ii)* catalytic platform for palladium species for C−C coupling reactions.[55]

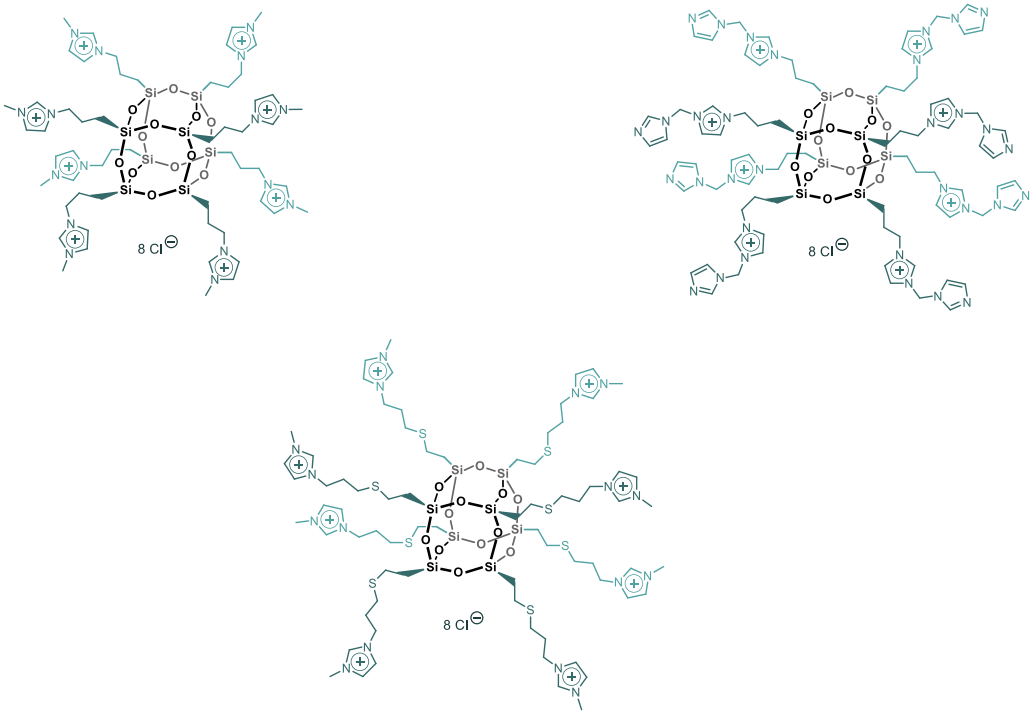

Figure 8. Imidazolium modified POSS nanostructure for catalytic applications.[55]

Herein, based on the promising features of both POSS nanostructures and imidazolium based organic salts, a wide series of novel hybrid materials was designed to be used as heterogeneous catalytic systems for the conversion of carbon dioxide and for Pd catalyzed Suzuki and Heck couplings.

1.8 References

[1] C. G. Brundtland, Oxford University Press, Oxford, **1987**.

[2] P. T. Anastas, J. C. Warner, *Green chemistry : theory and practice*, Oxford University Press, Oxford [England]; New York, **1998**.

[3] a) P. Anastas, N. Eghbali, *Chemical Society Reviews* **2010**, *39*, 301-312; b) R. A. Sheldon, *Chemical Society Reviews* **2012**, *41*, 1437-1451.

[4] a) P. T. Anastas, M. M. Kirchhoff, T. C. Williamson, *Applied Catalysis A: General* **2001**, *221*, 3-13; b) G. Centi, S. Perathoner, *Catalysis Today* **2003**, *77*, 287-297.

[5] S.-E. Park, E.-Y. Jeong, in *Bridging Heterogeneous and Homogeneous Catalysis: Concepts, Strategies, and Applications* (Eds.: L. Can, L. Yan), Wiley-VCH, **2014**, pp. 85-110.

[6] C. Aprile, H. Garcia, P. P. Pescarmona, in *Catalytic Methods in Asymmetric Synthesis* (Eds.: M. Gruttadauria, F. Giacalone), Wiley, **2011**, pp. 177-208.

[7] J. J. H. Davis, *Chemistry Letters* **2004**, *33*, 1072-1077.

[8] a) P. Wasserscheid, W. Keim, *Angewandte Chemie International Edition* **2000**, *39*, 3772-3789; b) R. Sheldon, *Chemical Communications* **2001**, 2399-2407; c) T. Welton, *Coordination Chemistry Reviews* **2004**, *248*, 2459-2477; d) H. Olivier-Bourbigou, L. Magna, D. Morvan, *Applied Catalysis A: General* **2010**, *373*, 1-56; e) J. P. Hallett, T. Welton, *Chemical Reviews* **2011**, *111*, 3508-3576; f) C. Dai, J. Zhang, C. Huang, Z. Lei, *Chemical Reviews* **2017**, *117*, 6929-6983; g) Y. Qiao, W. Ma, N. Theyssen, C. Chen, Z. Hou, *Chemical Reviews* **2017**, *117*, 6881-6928; h) R. L. Vekariya, *Journal of Molecular Liquids* **2017**, *227*, 44-60.

[9] a) S. N. Riduan, Y. Zhang, *Chemical Society Reviews* **2013**, *42*, 9055-9070; b) K. S. Egorova, E. G. Gordeev, V. P. Ananikov, *Chemical Reviews* **2017**, *117*, 7132-7189.

[10] a) V. Pino, A. M. Afonso, *Analytica Chimica Acta* **2012**, *714*, 20-37; b) M. D. Joshi, J. L. Anderson, *RSC Advances* **2012**, *2*, 5470-5484; c) X. Shi, L. Qiao, G. Xu, *Journal of Chromatography A* **2015**, *1420*, 1-15; d) A. Berthod, M. J. Ruiz-Ángel, S. Carda-Broch, *Journal of Chromatography A* **2018**, *1559*, 2-16.

[11] a) G. Gebresilassie Eshetu, M. Armand, B. Scrosati, S. Passerini, *Angewandte Chemie International Edition* **2014**, *53*, 13342-13359; b) D. R. MacFarlane, M. Forsyth, P. C. Howlett, M. Kar, S. Passerini, J. M. Pringle, H. Ohno, M. Watanabe, F. Yan, W. Zheng, S. Zhang, J. Zhang, *Nature Reviews Materials* **2016**, *1*, 15005; c) M. Watanabe, M. L. Thomas, S. Zhang, K. Ueno, T. Yasuda, K. Dokko, *Chemical Reviews* **2017**, *117*, 7190-7239; d) A. Basile, M. Hilder, F. Makhlooghiazad, C. Pozo-Gonzalo, D. R.

MacFarlane, P. C. Howlett, M. Forsyth, *Advanced Energy Materials* **2018**, *8*, 1703491.

[12] a) K. Fujita, K. Murata, M. Masuda, N. Nakamura, H. Ohno, *RSC Advances* **2012**, *2*, 4018-4030; b) A. Vioux, B. Coasne, *Advanced Energy Materials* **2017**, *7*, 1700883.

[13] a) F. Giacalone, M. Gruttadauria, *ChemCatChem* **2016**, *8*, 664-684; b) V. Campisciano, F. Giacalone, M. Gruttadauria, *The Chemical Record* **2017**, *17*, 918-938.

[14] a) T. Selvam, A. Machoke, W. Schwieger, *Applied Catalysis A: General* **2012**, *445-446*, 92-101; b) B. Xin, J. Hao, *Chemical Society Reviews* **2014**, *43*, 7171-7187.

[15] a) T. Akasaka, F. Wudl, S. Nagase, *Chemistry of Nanocarbons*, Wiley, **2010**; b) C. Kumar, *Carbon Nanomaterials, Vol. 9*, Wiley-WCH, **2011**; c) N. Tagmatarchis, *Advances in Carbon Nanomaterials: Science and Applications*, Pan Stanford, **2012**; d) T. Gatti, N. Vicentini, M. Mba, E. Menna, *European Journal of Organic Chemistry* **2016**, *2016*, 1071-1090.

[16] a) J. L. Delgado, M. a. Á. Herranz, N. Martín, *Journal of Materials Chemistry* **2008**, *18*, 1417-1426; b) I. Suarez-Martinez, N. Grobert, C. P. Ewels, *Carbon* **2012**, *50*, 741-747.

[17] a) M. Tunckol, J. Durand, P. Serp, *Carbon* **2012**, *50*, 4303-4334; b) B. Huang, Z. Xie, in *Hybrid Organic-Inorganic Interfaces* (Eds.: M. Delville, A. Taubert), Wiley-WCH, **2017**, pp. 497-533; c) V. Campisciano, M. Gruttadauria, F. Giacalone, *ChemCatChem* **2018**, doi:10.1002/cctc.201801414.

[18] a) G. Pagona, G. Mountrichas, G. Rotas, N. Karousis, S. Pispas, N. Tagmatarchis, *International Journal of Nanotechnology* **2008**, *6*, 176-195; b) N. Karousis, I. Suarez-Martinez, C. P. Ewels, N. Tagmatarchis, *Chemical Reviews* **2016**, *116*, 4850-4883.

[19] S. Zhu, G. Xu, *Nanoscale* **2010**, *2*, 2538-2549.

[20] G. Pagona, N. Tagmatarchis, in *Advances in Carbon Nanomaterials: Science and Applications* (Ed.: N. Tagmatarchis), Pan Stanford, **2012**, pp. 239-268.

[21] N. Karousis, T. Ichihashi, S. Chen, H. Shinohara, M. Yudasaka, S. Iijima, N. Tagmatarchis, *Journal of Materials Chemistry* **2010**, *20*, 2959-2964.

[22] a) M. Ghiazza, G. Vietti, I. Fenoglio, in *Health and Environmental Safety of Nanomaterials* (Eds.: J. Njuguna, K. Pielichowski, H. Zhu), Woodhead Publishing, **2014**, pp. 147-174; b) S. Merum, J. B. Veluru, R. Seeram, *Materials Science and Engineering: B* **2017**, *223*, 43-63; c) X. Jia, F. Wei, *Topics in Current Chemistry* **2017**, *375*, 18.

[23] I. Suarez-Martinez, N. Grobert, C. P. Ewels, in *Advances in Carbon Nanomaterials: Science and Applications* (Ed.: N. Tagmatarchis), **2012**, pp. 1-65.

[24] a) M. Melchionna, S. Marchesan, M. Prato, P. Fornasiero, *Catalysis Science & Technology* **2015**, *5*, 3859-3875; b) Y. Zhai, Z. Zhu, S. Dong, *ChemCatChem* **2015**, *7*, 2806-2815.

[25] a) A. Hirsch, *Angewandte Chemie International Edition* **2002**, *41*, 1853-1859; b) D. Tasis, N. Tagmatarchis, A. Bianco, M. Prato, *Chemical Reviews* **2006**, *106*, 1105-1136.

[26] a) S. Guo, S. Dong, E. Wang, *Advanced Materials* **2010**, *22*, 1269-1272; b) L. Rodríguez-Pérez, C. Pradel, P. Serp, M. Gómez, E. Teuma, *ChemCatChem* **2011**, *3*, 749-754; c) M. Tunckol, S. Fantini, F. Malbosc, J. Durand, P. Serp, *Carbon* **2013**, *57*, 209-216; d) A. R. Hajipour, Z. Khorsandi, H. Karimi, *Applied Organometallic Chemistry* **2015**, *29*, 805-808; e) Y. Ren, Z. Zhou, G. Yin, G.-X. Chen, Q. Li, *Materials Letters* **2016**, *166*, 133-136; f) T. Li, Z. Cui, W. Yuan, C. M. Li, *RSC Advances* **2016**, *6*, 12792-12796; g) M. Buaki-Sogó, A. Vivian, L. A. Bivona, H. García, M. Gruttadauria, C. Aprile, *Catalysis Science & Technology* **2016**, *6*, 8418-8427; h) C. M. Q. Le, X. T. Cao, Y. T. Jeong, K. T. Lim, *Journal of Industrial and Engineering Chemistry* **2018**, *64*, 337-343.

[27] N. Auner, J. Weis, in *Organosilicon Chemistry VI* (Eds.: N. Auner, J. Weis), Wiley-VCH Verlag GmbH & Co, **2008**, pp. 858-1007.

[28] W. Schwieger, T. Selvam, M. Klumpp, M. Hartmann, in *Supported Ionic Liquids* (Eds.: R. Fehrmann, A. Riisager, M. Haumann), Wiley-VCH, **2014**, pp. 37-74.

[29] A. M. Buckley, M. Greenblatt, *Journal of Chemical Education* **1994**, *71*, 599-602.

[30] L. T. Zhuravlev, *Colloids and Surfaces A: Physicochemical and Engineering Aspects* **2000**, *173*, 1-38.

[31] M. H. Valkenberg, C. deCastro, W. F. Hölderich, *Green Chemistry* **2002**, *4*, 88-93.

[32] a) L. Han, S.-W. Park, D.-W. Park, *Energy & Environmental Science* **2009**, *2*, 1286-1292; b) S. Udayakumar, V. Raman, H.-L. Shim, D.-W. Park, *Applied Catalysis A: General* **2009**, *368*, 97-104; c) P. Agrigento, S. M. Al-Amsyar, B. Sorée, M. Taherimehr, M. Gruttadauria, C. Aprile, P. P. Pescarmona, *Catalysis Science & Technology* **2014**, *4*, 1598-1607.

[33] a) M. Gruttadauria, L. F. Liotta, A. M. P. Salvo, F. Giacalone, V. La Parola, C. Aprile, R. Noto, *Advanced Synthesis & Catalysis* **2011**, *353*, 2119-2130; b) C. Pavia, F. Giacalone, L. A. Bivona, A. M. P. Salvo, C. Petrucci, G. Strappaveccia, L. Vaccaro, C. Aprile, M. Gruttadauria, *Journal of Molecular Catalysis A: Chemical* **2014**, *387*, 57-62.

[34] A. Z. Alothman, *Materials* **2012**, *5*, 2874-2902.

[35] D. Zhao, Y. Wan, W. Zhou, in *Ordered Mesoporous Materials* (Eds.: D. Zhao, Y. Wan, W. Zhou), Wiley-VCH, **2013**, pp. 153-217.

[36] a) D. Zhao, J. Feng, Q. Huo, N. Melosh, G. H. Fredrickson, B. F. Chmelka, G. D. Stucky, *Science* **1998**, *279*, 548-552; b) D. Zhao, Q. Huo, J. Feng, B. F. Chmelka, G. D. Stucky, *Journal of the American Chemical Society* **1998**, *120*, 6024-6036.

[37] L. Zhang, L. Xiao, Y. Zhang, L. J. France, Y. Yu, J. Long, D. Guo, X. Li, *Energy & Fuels* **2018**, *32*, 678-687.

[38] V. Elumalai, S. Dharmalingam, *Microporous and Mesoporous Materials* **2016**, *236*, 260-268.

[39] E. N. Kusumawati, D. Nishio-Hamane, T. Sasaki, *Catalysis Today* **2018**, *309*, 109-118.

[40] F. Giacalone, V. Campisciano, C. Calabrese, V. La Parola, L. F. Liotta, C. Aprile, M. Gruttadauria, *Journal of Materials Chemistry A* **2016**, *4*, 17193-17206.

[41] B. Motos-Pérez, J. Roeser, A. Thomas, P. Hesemann, *Applied Organometallic Chemistry* **2013**, *27*, 290-299.

[42] S. Rostamnia, A. Hassankhani, H. G. Hossieni, B. Gholipour, H. Xin, *Journal of Molecular Catalysis A: Chemical* **2014**, *395*, 463-469.

[43] C. Aprile, F. Giacalone, P. Agrigento, L. F. Liotta, J. A. Martens, P. P. Pescarmona, M. Gruttadauria, *ChemSusChem* **2011**, *4*, 1830-1837.

[44] D. B. Cordes, P. D. Lickiss, F. Rataboul, *Chemical Reviews* **2010**, *110*, 2081-2173.

[45] Y. Li, X.-H. Dong, Y. Zou, Z. Wang, K. Yue, M. Huang, H. Liu, X. Feng, Z. Lin, W. Zhang, W.-B. Zhang, S. Z. D. Cheng, *Polymer* **2017**, *125*, 303-329.

[46] P. P. Pescarmona, C. Aprile, S. Swaminathan, in *New and Future Developments in Catalysis* (Ed.: S. L. Suib), Elsevier, Amsterdam, **2013**, pp. 385-422.

[47] a) H. Ghanbari, B. G. Cousins, A. M. Seifalian, *Macromolecular Rapid Communications* **2011**, *32*, 1032-1046; b) H. Zhou, Q. Ye, J. Xu, *Materials Chemistry Frontiers* **2017**, *1*, 212-230; c) Z. Li, J. Kong, F. Wang, C. He, *Journal of Materials Chemistry C* **2017**, *5*, 5283-5298.

[48] E. Carbonell, L. A. Bivona, L. Fusaro, C. Aprile, *Inorganic Chemistry* **2017**, *56*, 6393-6403.

[49] G. Chen, Y. Zhou, X. Wang, J. Li, S. Xue, Y. Liu, Q. Wang, J. Wang, *Scientific Reports* **2015**, *5*, 11236.

[50] J.-H. Jeon, K. Tanaka, Y. Chujo, *RSC Advances* **2013**, *3*, 2422-2427.

[51] J.-H. Jeon, K. Tanaka, Y. Chujo, *Journal of Materials Chemistry A* **2014**, *2*, 624-630.

[52] D. Shang, J. Fu, Q. Lu, L. Chen, J. Yin, X. Dong, Y. Xu, R. Jia, S. Yuan, Y. Chen, W. Deng, *Solid State Ionics* **2018**, *319*, 247-255.

[53] a) W. Zhang, J. Li, S. Jiang, Z.-S. Wang, *Chemical Communications* **2014**, *50*, 1685-1687; b) K. Lv, W. Zhang, L. Zhang, Z.-S. Wang, *ACS Applied Materials & Interfaces* **2016**, *8*, 5343-5350.

[54] L. A. Bivona, O. Fichera, L. Fusaro, F. Giacalone, M. Buaki-Sogo, M. Gruttadauria, C. Aprile, *Catalysis Science & Technology* **2015**, *5*, 5000-5007.

[55] a) L. A. Bivona, F. Giacalone, E. Carbonell, M. Gruttadauria, C. Aprile, *ChemCatChem* **2016**, *8*, 1685-1691; b) V. Somjit, M. Wong Chi Man, A. Ouali, P. Sangtrirutnugul, V. Ervithayasuporn, *ChemistrySelect* **2018**, *3*, 753-759; c) S. Mohapatra, T. Chaiprasert, R. Sodkhomkhum, R. Kunthom, S. Hanprasit, P. Sangtrirutnugul, V. Ervithayasuporn, *ChemistrySelect* **2016**, *1*, 5353-5357.

CHAPTER II

Carbon Dioxide Conversion into Cyclic Carbonates

An Introduction to Chapters III, IV, V

CHAPTER II

Carbon Dioxide Conversion into Cyclic Carbonates An Introduction to Chapters III, IV, V

2.1 Carbon Dioxide: from a waste to a feedstock

The design of new technologies able to mitigate CO_2 environmental impact is an issue of growing interest from both academic and industrial standpoint. CO_2 is a common product of biological processes such as the aerobic respiration or the alcoholic fermentation of sugars. However, carbon dioxide emission is also associated to the combustion of fossil fuels arising from the anthropogenic activities for the production of energy, transportation and industrial processes.

Since the Industrial Revolution, the concentration of carbon dioxide in the atmosphere has steadily increased becoming an environmental issue to be addressed.

In this scenario, carbon dioxide capture, utilization and storage emerged as tangible processes moving toward a sustainable development.[1] Focusing on its utilization, carbon dioxide has found application in separation processes, dry-cleaning, refrigerators, fire extinguishers, in the food or agrochemical industry, or as solvent for several reactions under supercritical conditions.[2]

The conversion of carbon dioxide into valuable chemicals is attracting the attention of the scientific community due to the possibility to valorise an industrial waste into an inexpensive, available, nontoxic, and renewable carbon feedstock.[3] In nature, CO_2 is converted into carbohydrates through a series of cascade reactions promoted by specific metalloenzymes present in photosynthetic organisms. Moreover, carbon dioxide has been tested as one-carbon (C1) building block in organic synthesis for the preparation of several chemicals including methanol, urea,

lactones, various heterocycles, biodegradable polymers, and carboxylated structures among others.[4]

Scheme 1 summarizes some industrial organic synthesis using carbon dioxide as C1 synthon.

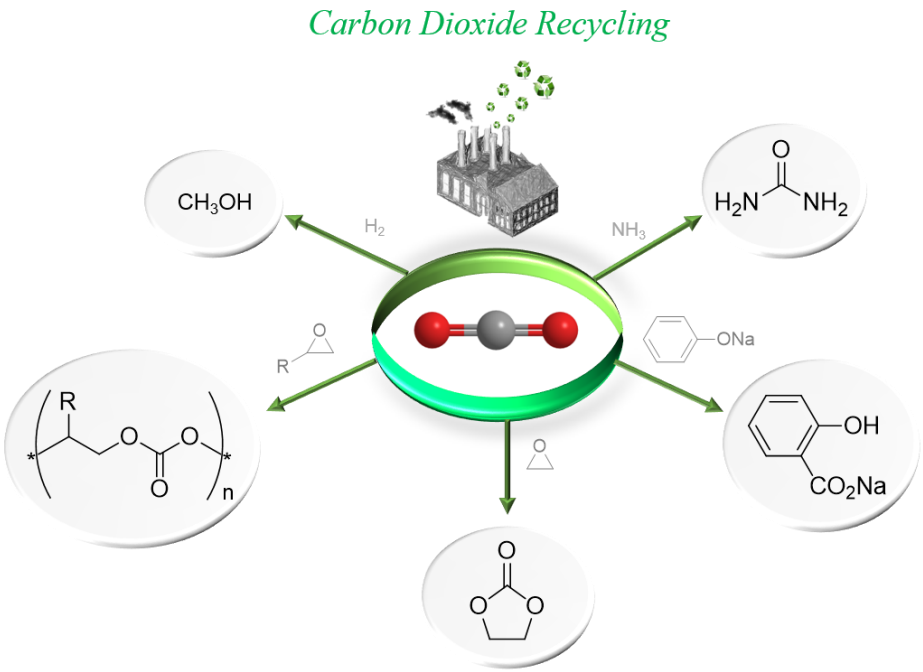

Scheme 1. Industrialized organic synthesis using CO_2 as C1 feedstock.

All these processes make CO_2 a key pillar for the sustainable and resource-efficient production of chemicals.[5]

Independently from the specific application, the drawback of the conversion of carbon dioxide is mainly represented by its elevated thermodynamic stability.

The carbon atom in CO_2 is present in its most oxidized state resulting into a low molecular reactivity. To overcome this problem, highly energetic starting materials such as hydrogen, epoxides, and amine among others are usually employed together with a catalyst able to properly decrease the activation energy of the selected reaction (Figure 1). For doing so, in the last decades several catalytic systems, able to work under both homogeneous and heterogeneous conditions have been developed in the perspective of greener chemical processes.

The activation of carbon dioxide is pivotal for its effective transformation. The basic features of CO_2 reactivity must be considered to reach a good conversion of this molecule into useful chemicals.

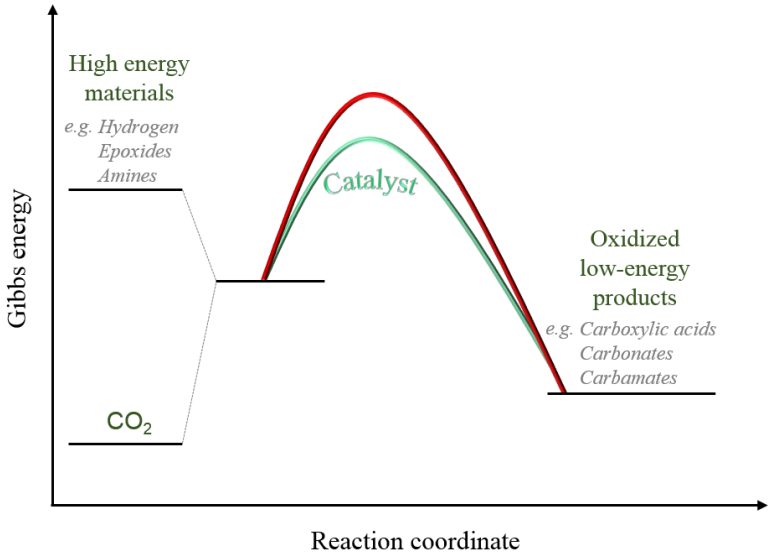

Figure 1. Organic synthesis using CO_2 as building block.

Carbon dioxide is a linear molecule in which the carbon–oxygen bonds are polar with a net partial charge on carbon and oxygen atoms. Therefore, the carbon atom, bearing a partial positive charge, can behave as an electrophile. On the other hand, the oxygen atoms, with a partial negative charge, can act as nucleophiles. Owing to the linear geometry of the molecule, being the two dipole moments opposite each other, the overall molecule is apolar. From the above, the amphoteric CO_2 behaviour lead to two possible activation pathways: the oxygen atoms can exhibit a Lewis base character, while the carbon atom can play the role of a Lewis acid centre. As the electrophilic character of carbon is higher than the nucleophilicity of the oxygen atoms, carbon dioxide is a better acceptor than donor of electron density.

Herein, the conversion of carbon dioxide into cyclic carbonates by reaction with epoxides will be discussed.

2.2 Carbon Dioxide Conversion into Cyclic Carbonates

One of the most interesting pathways to valorise CO_2 is represented by carbon dioxide fixation into epoxides for the production of cyclic carbonates.[6]

Cyclic carbonates are organic compounds with interesting properties such as low vapor pressure, high boiling point, low toxicity, and biodegradability. Based on these features, cyclic carbonates find widespread applications as aprotic high-

boiling polar solvents, electrolytes for batteries, precursors for polymeric materials, fuel additives, plastic materials, and intermediates for the synthesis of fine chemicals such as dialkyl carbonates, glycols, carbamates, pyrimidines among others.[7] These structures can be found in some natural compounds within fungi, bacteria, or plants. In industry, cyclic carbonates are traditionally prepared by synthetic methodologies involving the use of phosgene. However, such procedures allow the production of equimolar amounts of carbonate and chlorinated salts and of large volumes of chlorinated solvents. Moreover, even if phosgene is a versatile building block widely used in the production of plastics and pesticides, it is also a hazardous, toxic, corrosive, and difficult to handle. The exposure to phosgene may cause collateral health effects. Therefore, its application as feedstock in industrial large-scale synthesis should be replaced with sustainable alternative routes having a lower environmental impact. Among them, the synthesis of cyclic carbonates from carbon dioxide and epoxide emerged as a low toxic alternative.

For instance, Scheme 1 shows three possible synthetic routes for the conversion of ethene into the corresponding cyclic carbonate: *i)* hydrochlorination of ethylene, followed by hydrolysis, and conversion with $COCl_2$; *ii)* formation of ethylene oxide, subsequent hydrolysis, and conversion with $COCl_2$; *iii)* formation of ethylene oxide and CO_2 fixation. Life cycle assessment (LCA) methodology has been applied to evaluated the ratio between the amount of CO_2 emitted and ethene carbonate produced.[3a] The obtained results clearly identified the reaction between ethylene oxide and CO_2 as the most sustainable route for the production of ethylene carbonate.

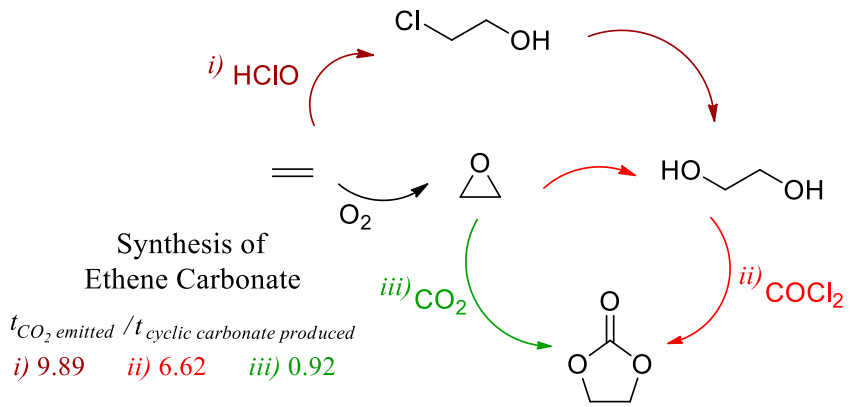

Scheme 2. Synthetic routes for the production of ethene carbonate.[3a]

According to green chemistry principles,[8] carbon dioxide fixation into epoxides for the synthesis of five-membered cyclic carbonates is a productive catalytic process displaying an atom economy of 100%. In order to face the challenging thermodynamic stability of carbon dioxide, epoxides have to be used combined with a catalyst to reduce the activation energy of the process.

2.3 Catalytic Systems for the Synthesis of Cyclic Carbonates

In this context, a growing interest toward the synthesis of cyclic carbonates *via* reaction of CO_2 with epoxides led to the design of catalytic systems bearing Lewis acid sites for the electrophilic activation of epoxide and/or carbon dioxide and Lewis base sites as nucleophilic species. Both sites can be included into two different systems (*e.g.* the metal of a complex as Lewis acid and the anion of a salt as Lewis base) or belong to a sole bifunctional catalyst (*e.g.* a complex with a cationic metal centre and a labile anionic ligand). Several catalysts, working under both homogeneous and heterogeneous conditions, have been developed for the conversion of CO_2 into cyclic carbonates by reaction with epoxides. In particular, metal oxides,[9] metal organic frameworks (MOF),[10] metal salts,[11] metal complexes,[12] Lewis base systems,[13] ionic liquids (ILs),[14] and organic polymers[14c, 15] have been proposed as catalyst for this reaction. Based on the environmental impact and the cost efficiency, the overall sustainability of this process has to be evaluated and improved according to some key criteria such as: *i)* the presence of solvents, *ii)* the use of metal species, *iii)* the achieved yields and selectivity, *iv)* the required reaction conditions (temperature, pressure, reaction time). The choice between metal-based or organo-catalysts for the CO_2 fixation brings strengths and weaknesses. Metal-based systems lead to milder reaction conditions (*e.g.* lower temperature, reduced catalytic loading) owing to their ability to activate and/or stabilize substrates or intermediates *via* coordination interactions. On the other hand, organo-catalysts can be considered as suitable and safer alternative for the design of sustainable processes because of their low cost, non-toxic nature, and good stability and inertness towards moisture and air. To increase the catalyst lifetime several heterogeneous organo-catalysts have been developed

providing simplified work-up procedures combined with the possibility to use them under continuous flow conditions. It is well known that the design of heterogeneous catalysts is particularly envisaged from industrial parties because of their simple recovery from the reaction medium and the possibility of using them in fixed bed reactors. The evident advantages of heterogeneous catalytic systems encouraged the development of supported ionic liquids hybrids for the production of cyclic carbonates. In particular, imidazolium salts have been immobilized on several solid supports such as cross-linked polymers,[16] silicon-based main chain polyimidazolium salts,[17] silica,[18] and carbon nanostructures.[19] In the synthesis of cyclic carbonates, the activity of ionic liquid based catalysts strongly depends on the nucleophilicity of the anionic species towards the attack into the epoxide as well as on its ability as leaving group.[20] Therefore, taking into account previously mentioned catalytic systems, imidazolium counterions play a crucial role in the reaction mechanism by promoting epoxide ring opening followed by the CO_2 insertion (Scheme 3).

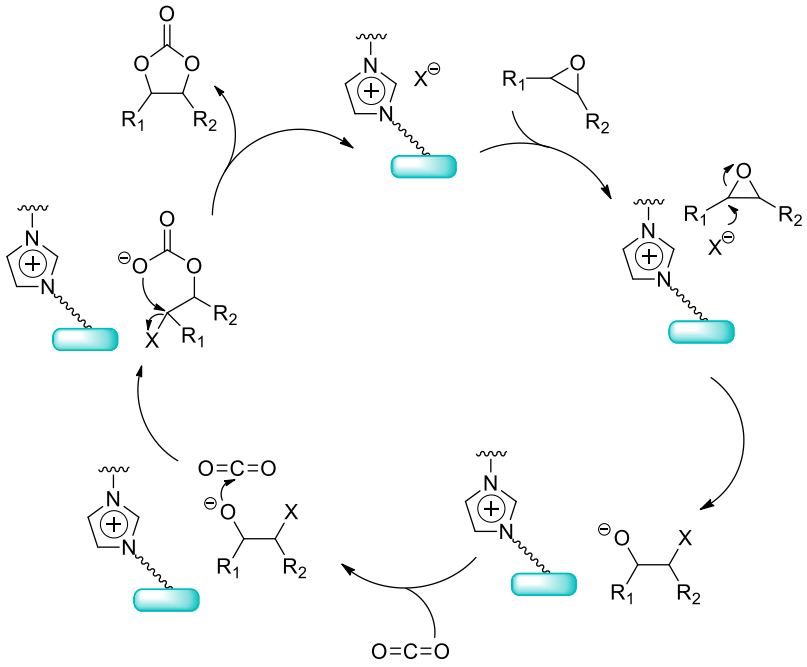

Scheme 3. Reaction mechanism of CO_2 fixation into cyclic carbonates promoted by supported imidazolium salts.

Furthermore, the design of hybrid materials able to combine the high activity and selectivity achieved by homogeneous catalysts and the intrinsic advantages of

heterogeneous ones is still a challenging task. In order to introduce the catalytic materials developed during the PhD project, two literature examples on the production of cyclic carbonates deserve to be mentioned (Figure 2).

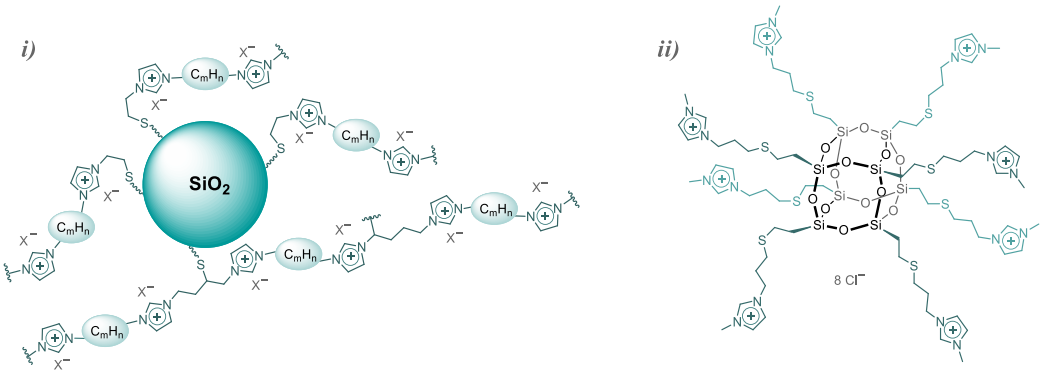

Figure 2. Imidazolium based organo-catalysts for the conversion of CO_2.

Firstly, highly cross-linked imidazolium networks have been immobilized onto silica supports for the design of heterogeneous hybrids bearing bromide and iodide as nucleophilic active species.[18] Such materials were prepared by grafting different bis-vinylimidazolium salts on thiol-functionalized silica. The synthetic protocol allowed to obtain a series of materials showing good thermal stability combined with high catalytic loadings. These features are of paramount importance in terms of both catalyst recyclability and productivity (calculated as the ratio between the amount of cyclic carbonate produced and the amount of catalyst used). Moving onto homogeneous reaction conditions, POSS nanostructures modified with imidazolium chloride moieties showed improved catalytic performances compared to the unsupported 1-butyl-3-methylimidazolium chloride.[21] This behavior was ascribed to a proximity effect due to the higher local concentration of imidazolium active sites surrounding the inorganic silsesquioxane core. However, in this case, the recovery of the catalyst from the reaction mixture was tricky and the material was not recycled. Herein, on the ground of this findings, a wide series of imidazolium-based hybrids have been developed by following three main synthetic methodologies: *i)* grafting of several bis-vinylimidazolium salts onto carbon nanohorns; *ii)* covalent immobilization of imidazolium modified POSS nanocages onto amorphous silica and mesostructured SBA-15; *iii)* direct heterogenization of POSS nanostructures with bis-imidazolium salts.

2.4 References

[1] F. A. Rahman, M. M. A. Aziz, R. Saidur, W. A. W. A. Bakar, M. R. Hainin, R. Putrajaya, N. A. Hassan, *Renewable and Sustainable Energy Reviews* **2017**, *71*, 112-126.

[2] E. Alper, O. Yuksel Orhan, *Petroleum* **2017**, *3*, 109-126.

[3] a) M. Aresta, A. Dibenedetto, A. Angelini, *Chemical Reviews* **2014**, *114*, 1709-1742; b) T. Sakakura, J.-C. Choi, H. Yasuda, *Chemical Reviews* **2007**, *107*, 2365-2387; c) Q.-W. Song, Z.-H. Zhou, L.-N. He, *Green Chemistry* **2017**, *19*, 3707-3728.

[4] a) Q. Liu, L. Wu, R. Jackstell, M. Beller, *Nature Communications* **2015**, *6*, 5933; b) C. Maeda, Y. Miyazaki, T. Ema, *Catalysis Science & Technology* **2014**, *4*, 1482-1497.

[5] E. A. Quadrelli, G. Centi, J.-L. Duplan, S. Perathoner, *ChemSusChem* **2011**, *4*, 1194-1215.

[6] M. North, R. Pasquale, C. Young, *Green Chemistry* **2010**, *12*, 1514-1539.

[7] a) T. Sakakura, K. Kohno, *Chemical Communications* **2009**, 1312-1330; b) W. Clegg, R. W. Harrington, M. North, F. Pizzato, P. Villuendas, *Tetrahedron: Asymmetry* **2010**, *21*, 1262-1271; c) Q. Li, J. Chen, L. Fan, X. Kong, Y. Lu, *Green Energy & Environment* **2016**, *1*, 18-42.

[8] P. Anastas, J. Warner, *Green Chemistry: Theory and Practice*, Oxford University Press, **2000**.

[9] B. M. Bhanage, S.-i. Fujita, Y. Ikushima, M. Arai, *Applied Catalysis A: General* **2001**, *219*, 259-266.

[10] a) P. T. K. Nguyen, H. T. D. Nguyen, H. N. Nguyen, C. A. Trickett, Q. T. Ton, E. Gutiérrez-Puebla, M. A. Monge, K. E. Cordova, F. Gándara, *ACS Applied Materials & Interfaces* **2018**, *10*, 733-744; b) W.-Y. Gao, Y. Chen, Y. Niu, K. Williams, L. Cash, P. J. Perez, L. Wojtas, J. Cai, Y.-S. Chen, S. Ma, *Angewandte Chemie International Edition* **2014**, *53*, 2615-2619.

[11] J. Song, Z. Zhang, B. Han, S. Hu, W. Li, Y. Xie, *Green Chemistry* **2008**, *10*, 1337-1341.

[12] a) H. Vignesh Babu, K. Muralidharan, *Dalton Transactions* **2013**, *42*, 1238-1248; b) D. Tian, B. Liu, Q. Gan, H. Li, D. J. Darensbourg, *ACS Catalysis* **2012**, *2*, 2029-2035; c) J. A. Castro-Osma, K. J. Lamb, M. North, *ACS Catalysis* **2016**, *6*, 5012-5025; d) C. Martín, G. Fiorani, A. W. Kleij, *ACS Catalysis* **2015**, *5*, 1353-1370.

[13] H. Zhou, X. Lu, *Science China Chemistry* **2017**, *60*, 904-911.

[14] a) V. B. Saptal, B. M. Bhanage, *ChemSusChem* **2016**, *10*, 1145-1151; b) V. B. Saptal, B. M. Bhanage, *ChemCatChem* **2015**, *8*, 244-250; c) R. Luo, Y. Chen, Q. He, X. Lin, Q. Xu, X. He, W. Zhang, X. Zhou, H. Ji, *ChemSusChem* **2017**, *10*, 1526-1533; d) S. Yue, X.-J. Hao, P.-P. Wang, J.

Li, *Molecular Catalysis* **2017**, *433*, 420-429; e) F. Jutz, J.-M. Andanson, A. Baiker, *Chemical Reviews* **2011**, *111*, 322-353; f) A.-L. Girard, N. Simon, M. Zanatta, S. Marmitt, P. Gonçalves, J. Dupont, *Green Chemistry* **2014**, *16*, 2815-2825.

[15] a) H. Zhong, Y. Su, X. Chen, X. Li, R. Wang, *ChemSusChem* **2017**, *10*, 4855-4863; b) W. Wang, C. Li, L. Yan, Y. Wang, M. Jiang, Y. Ding, *ACS Catalysis* **2016**, *6*, 6091-6100.

[16] a) T. Wang, W. Wang, Y. Lyu, X. Chen, C. Li, Y. Zhang, X. Song, Y. Ding, *RSC Advances* **2017**, *7*, 2836-2841; b) A. H. Jadhav, G. M. Thorat, K. Lee, A. C. Lim, H. Kang, J. G. Seo, *Catalysis Today* **2016**, *265*, 56-67.

[17] J. Wang, J. Leong, Y. Zhang, *Green Chemistry* **2014**, *16*, 4515-4519.

[18] a) P. Agrigento, S. M. Al-Amsyar, B. Sorée, M. Taherimehr, M. Gruttadauria, C. Aprile, P. P. Pescarmona, *Catalysis Science & Technology* **2014**, *4*, 1598-1607; b) C. Aprile, F. Giacalone, P. Agrigento, L. F. Liotta, J. A. Martens, P. P. Pescarmona, M. Gruttadauria, *ChemSusChem* **2011**, *4*, 1830-1837.

[19] a) L. Han, H. Li, S.-J. Choi, M.-S. Park, S.-M. Lee, Y.-J. Kim, D.-W. Park, *Applied Catalysis A: General* **2012**, *429-430*, 67-72; b) M. Buaki-Sogó, A. Vivian, L. A. Bivona, H. García, M. Gruttadauria, C. Aprile, *Catalysis Science & Technology* **2016**, *6*, 8418-8427; c) C. Calabrese, L. F. Liotta, E. Carbonell, F. Giacalone, M. Gruttadauria, C. Aprile, *ChemSusChem* **2016**, *10*, 1202-1209.

[20] P. P. Pescarmona, M. Taherimehr, *Catalysis Science & Technology* **2012**, *2*, 2169-2187.

[21] L. A. Bivona, O. Fichera, L. Fusaro, F. Giacalone, M. Buaki-Sogo, M. Gruttadauria, C. Aprile, *Catalysis Science & Technology* **2015**, *5*, 5000-5007.

CHAPTER III

Imidazolium-Functionalized Carbon Nanohorns for the Conversion of Carbon Dioxide: Unprecedented Increase of Catalytic Activity after Recycling

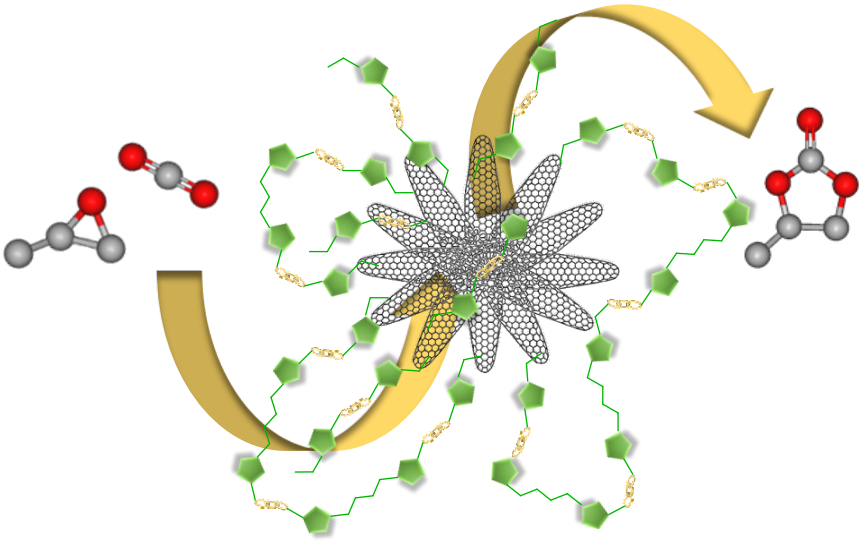

This chapter is based on:

ChemSusChem **2017**, *10*, 1202–1209

CHAPTER III

Imidazolium-Functionalized Carbon Nanohorns for the Conversion of Carbon Dioxide: Unprecedented Increase of Catalytic Activity after Recycling

3.1 Abstract

Six new hybrid materials composed of carbon nanohorns (CNHs) and highly cross-linked imidazolium salts were easily synthesized using a one-step procedure based on the radical polymerization of bis-vinylimidazolium salts (bVImiX) in the presence of pristine CNHs. The hybrid materials were characterized and employed as the sole catalysts for the conversion of carbon dioxide into cyclic carbonate by reaction with epoxides. The solids displayed excellent turnover number and productivity values. Moreover, four catalysts were investigated in recycling experiments. Two catalysts containing an octyl linker between the imidazolium units and a bromide or an iodide anion showed no loss in activity after three cycles. The other two catalysts containing a *p*-xylyl linker and a bromide anion and different CNHs/bVImiX ratios showed an unprecedented increase of activity after recycling.

3.2 Results and Discussion

In the panorama of carbon dioxide conversion into valuable chemicals, the development of highly performing heterogeneous catalysts for the synthesis of cyclic carbonates is one of the main focus of this PhD dissertation. In a quest for improved performance, several cross-linked imidazolium networks have been grafted onto carbon nanohorns as solid support. The choice of CNHs as novel catalytic platform arises from their specific features. Such exotic carbon nanoform appears as an attractive support for the design of heterogeneous catalytic systems due to their chemical stability and mechanical strength. Furthermore, the preparation of CNHs gives rise to a specific conical morphology resulting in spherical dahlia-like clusters without involving the presence of metal catalysts during the synthesis. The local chemical reactivity of their surface is enhanced in regions of higher curvature due to pyramidal distortion of the sp^2 carbon bonding. According to literature, the covalent functionalization of CNHs can be achieved through different approaches.[1] Among them, the double bonds on the walls can react with radical species.[2] Herein, the synthesis of functionalized CNHs (Scheme 1) was performed by *in situ* radical polymerization of different bis-vinylimidazolium salts (**2a-d**).

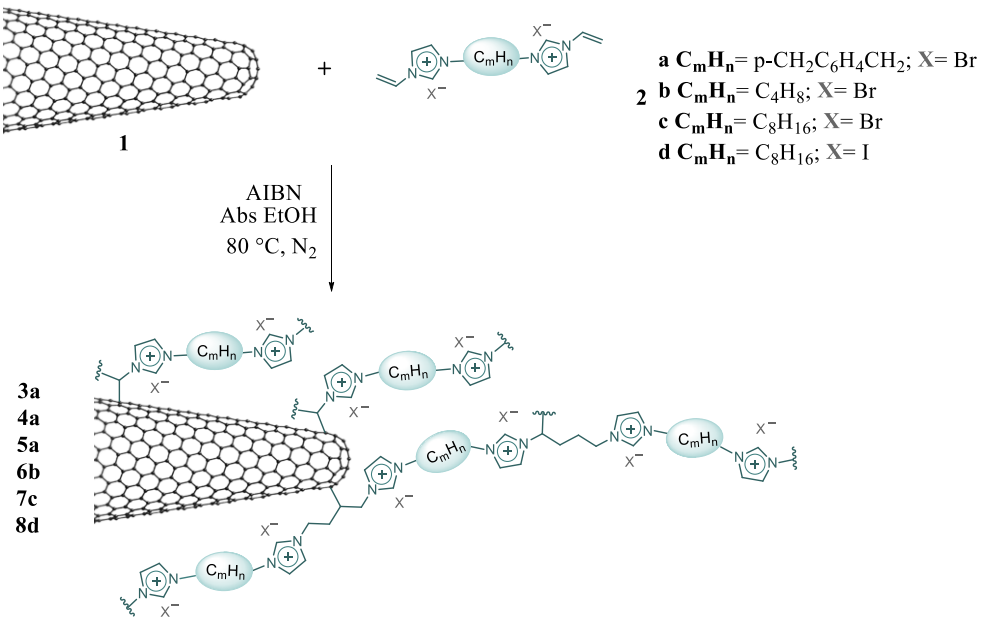

Scheme 1. Synthesis of imidazolium-functionalized CNHs.

The formation of an imidazolium cross-linked network was achieved by using 2,2′-azobis(2-methylpropionitrile) (AIBN) as a radical initiator. To obtain a series of functionalized CNHs with different catalyst loadings, some reaction parameters were modified including the amount of solvent, CNHs to bis-vinylimidazolium salt ratio, and the reaction time. The bis-vinylimidazolium salt (**2a**) containing a *p*-xylyl group as a linker connecting the two imidazolium units was selected for this screening (Table 1, catalysts **3a**, **4a**, **5a**).

Table 1. Synthesis conditions and catalyst loading of **3a**, **4a**, and **5a**.

Catalyst	CNHs [mg]	bVImi$^+$X$^-$ [mmol]	EtOH [mL]	AIBN [mmol]	Time [h]	X$^-$ loading [mmol g^{-1}]
3a	130	1.07	100	0.14	45	1.052
4a	130	1.98	140	0.14	45	1.933
5a	50	1.88	29	0.14	6	2.928

The degree of functionalization of the supported CNHs was evaluated by thermogravimetric analysis (TGA). In particular, the catalyst loadings reported in Table 1 were calculated from the net weight losses at 700 °C. TGA profiles of **3a**, **4a**, and **5a** are showed in Figure 1. Notably, the polymeric networks displayed good thermal stability as their degradation started in the 210–240 °C range, which is promising for their possible repeated use under heating regimes.

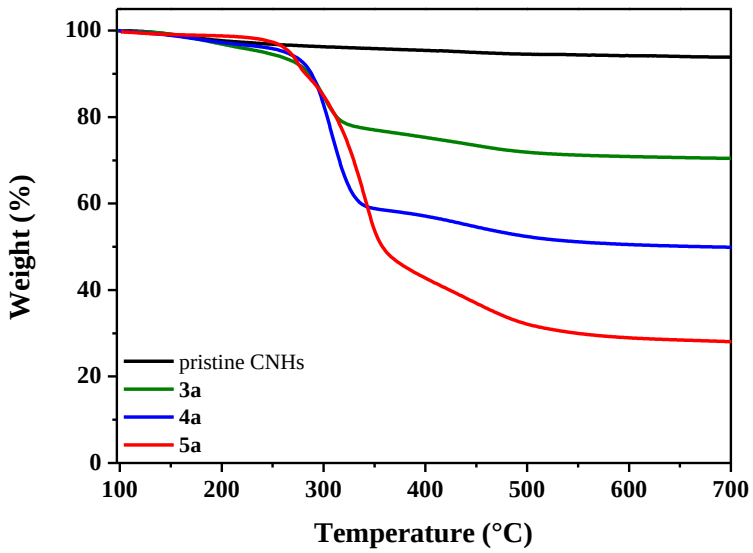

Figure 1. TGA analysis of pristine and functionalized CNHs (**3a**, **4a**, **5a**).

Transmission electron microscopy (TEM) was performed to provide morphological information of the CNHs based materials (**3a**, **4a**, **5a**, Figure 2). TEM images of the functionalized CNHs revealed the presence of different assemblies of spherical aggregates. In particular, the typical dahlia-like structure of the CNHs was wrapped in the cross-linked polymeric network. It is interesting to observe how the spherical structure of the starting CNHs can be distinguished even in the most functionalized material **5a**.

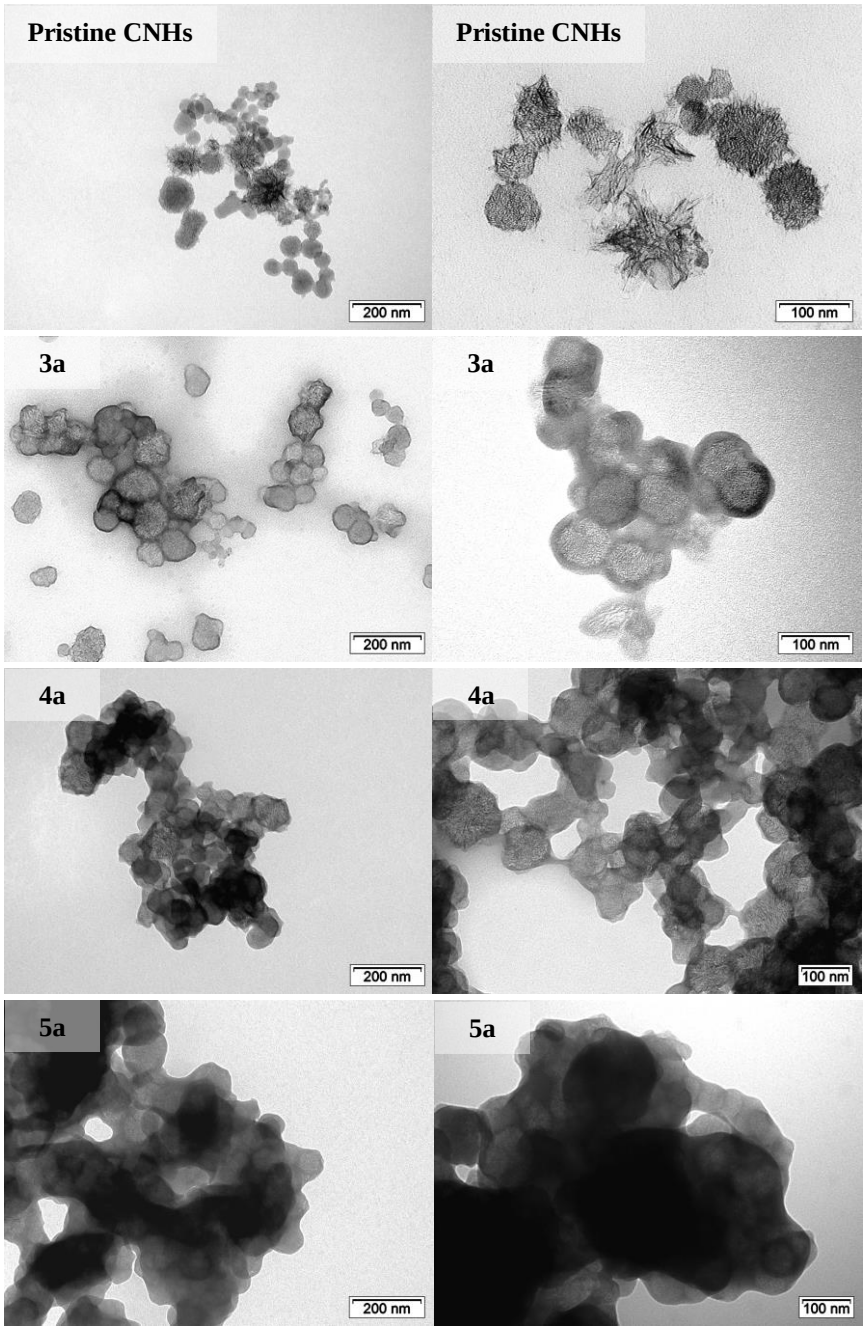

Figure 2. TEM images of pristine and functionalized CNHs (**3a**, **4a**, **5a**).

Then, imidazolium-functionalized CNHs were tested as catalysts for the conversion of CO_2 into cyclic carbonates under solvent-free reaction conditions and without adding salts with Lewis acid properties as co-catalytic species. Owing to the different imidazolium loading, the activity of the solids was compared in terms of turnover number (TON, calculated as moles of epoxide converted/moles of supported imidazolium halide). Moreover, the productivity (P, defined as grams of cyclic carbonates per gram of catalyst) for each catalytic test was determined. The conversion and the selectivity were calculated by ^{1}H NMR analysis of the reaction mixture. From the results reported in Table 2, **4a** was more active than **3a** in the reaction between CO_2 and epichlorohydrin. When the less reactive styrene oxide was used as the starting epoxide, **5a** showed slightly higher catalytic performance compared with **4a**. Interestingly, both **4a** and **5a** revealed improved performances than the self-condensed polymer.[3] Furthermore, imidazolium functionalized CNHs **5a** proved to be more active, in terms of both TON and productivity, than analogous imidazolium-based solids reported in the literature.[3-4]

Table 2. Synthesis of cyclic carbonates catalyzed by **3a**, **4a**, and **5a**.[a]

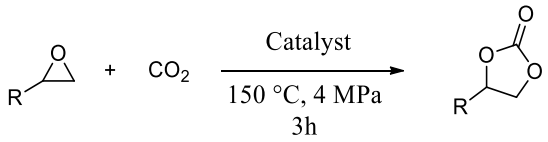

Entry	Substrate		Catalyst		Conv.[a]	S[a]	TON	P[a]
			[mg]	[mol%]	[%]	[%]		
1[b]	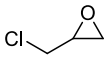	CNHs	–	–	0	0	–	0
2[c]	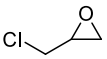	**3a**	60	0.021	34	>95	1636	223
3[c]	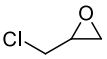	**4a**	60	0.038	72	>95	1886	473
4[d]		**4a**	240	0.227	23	>95	101	31
5[d]		**5a**	240	0.341	36	>95	106	48

[a] Conversion (Conv.), Selectivity (S), Productivity (P). [b] Reaction condition: epichlorohydrin (303.8 mmol), Pristine CNHs (60 mg), CO_2 (4 MPa), 150 °C, 3 h. [c] Reaction condition: epichlorohydrin (303.8 mmol), CO_2 (4 MPa), 150 °C, 3 h. [d] Reaction condition: styrene oxide (206.3 mmol), CO_2 (4 MPa), 150 °C, 3 h.

From this preliminary investigation, the solids **4a** and **5a** emerged as the most promising materials. Then, styrene oxide was selected as the target reagent to check their recyclability. At the end of each catalytic cycle, the catalyst was easily recovered from the reaction mixture by centrifugation, washed, and reused for the next cycle. Catalysts **4a** and **5a** were used for six consecutive runs (Figure 3). Interestingly, both materials displayed an unprecedented increase in the catalytic activity from the first to the sixth cycle. This behavior was not observed in the recycling test if carbon nanotubes were employed as a catalytic support.[3] Furthermore, a gradual increase in the catalyst performances for three consecutive runs, followed by a stabilization of the activity, was achieved when the same imidazolium cross-linked network was supported on silica.[5] Therefore, it can be assumed that for the above heterogeneous catalysts, the nature of the support plays an important role in the catalytic performances.

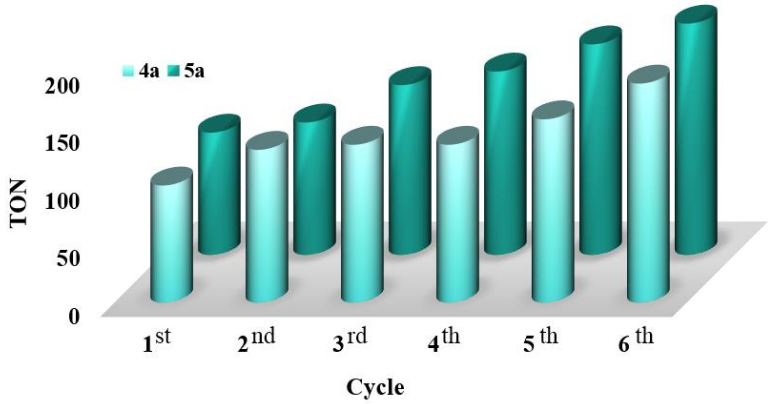

Figure 3. Recycling tests of **4a** and **5a**. Reaction conditions: styrene oxide (206.3 mmol), CO_2 (4 MPa), catalyst (240 mg, 0.464 mmol of **4a**, 0.703 mmol of **5a**), 150°C, 3h.

To shed light on these particular trends, TGA was carried out on the reused catalysts after the sixth cycle (Figure 4). TGA profiles of **4a** and **5a** reused for six cycles compared to those of the as-synthesized catalysts show a very low loss in weight (≈3% and 2.6% for **4a** and **5a**, respectively). The different TGA profile of the reused catalysts can be attributed to the different CNHs/bVImiX ratio (Table 1). These results confirmed that there was negligible leaching of the catalysts from the support with increasing catalytic cycles. The specific trends of the catalytic activity could be ascribed to some modifications of the polymeric network depending on the reaction conditions. It is well known that the solubility of carbon dioxide in ionic liquid phases plays a crucial role.[6]

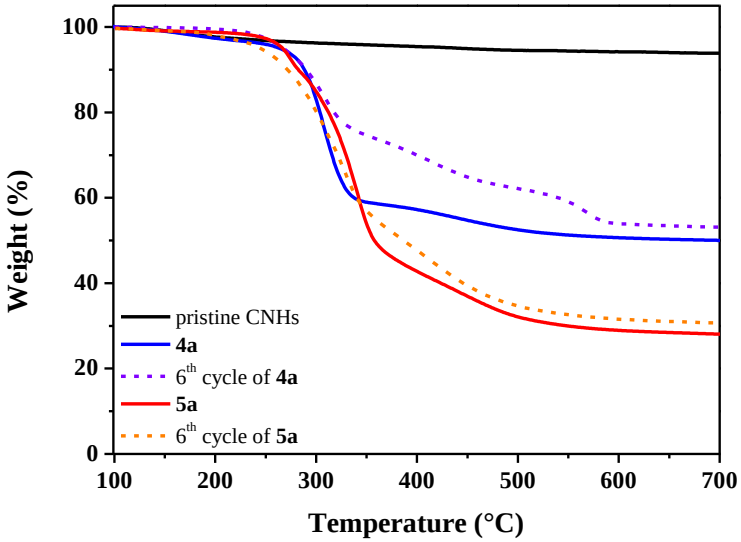

Figure 4. TGA analysis of as-synthesized and reused **4a** and **5a**.

In our case, CO_2 probably induced a swelling of the imidazolium polymeric network,[7] enhancing the diffusion of the reagents and improving the accessibility of the active sites. To further clarify the nature of the catalytic behavior, mercury porosimetry analysis was performed. The measurements of differential intrusion versus pore diameter, carried out on both fresh and reused **4a** catalyst, showed a similar trend with a broad pore size distribution (psd) centered in the macroporous region owing to the presence of the irregular polymeric network (Figure 5).

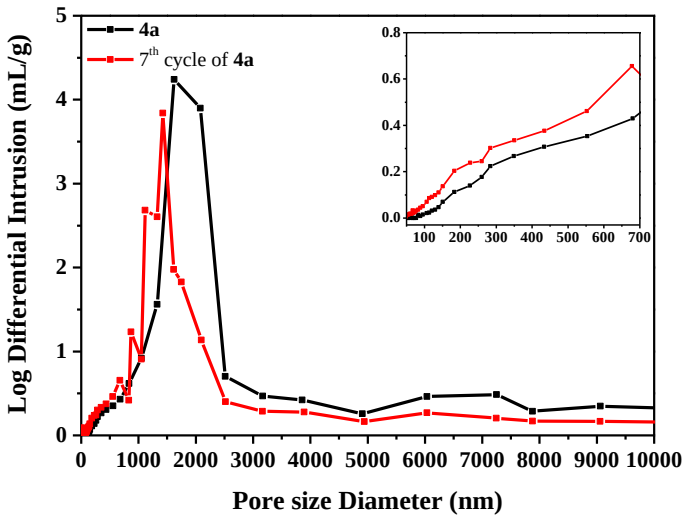

Figure 5. Differential intrusion *vs* pore diameter determined *via* mercury porosimetry of fresh (black line) and after 7th cycle (red line) **4a** solid.

However, a clear shift of the psd profile to lower values was observed for the reused catalyst. The reused solid also displayed a higher percentage of porosity. The results of this investigation support the hypothesis of the possible modification of the cross-linked network during the catalytic reaction.

Furthermore, materials **4a** and **5a** were characterized by TEM after the sixth cycle (Figure 6) without showing any important morphological variation compared to the fresh catalysts.

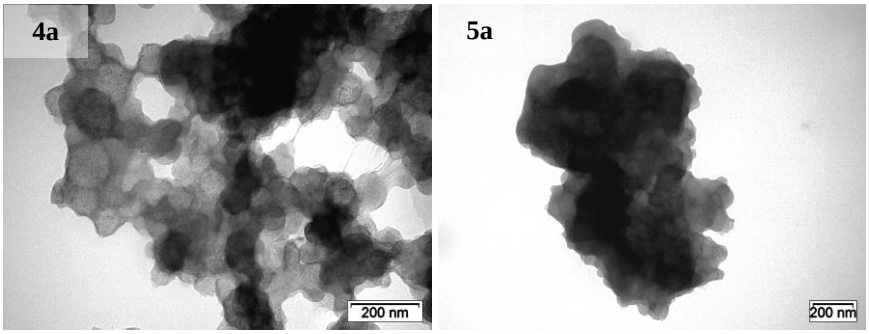

Figure 6. TEM images of catalytic materials **4a** and **5a** after the sixth cycle.

The hybrid material **5a** was employed for an additional investigation. The CO_2 fixation into epichlorohydrin was selected for this purpose. Two catalytic tests were carried out. In the first case, the as-synthesized solid **5a** was used with a catalytic loading of 0.014 mol% allowing to obtain a 32% of conversion corresponding to a TON value of 2214. Then, the catalytic activity of the reused **5a**, previously recovered from the 6th cycle presented in Figure 3, was checked.

Table 3. Catalytic tests performed with **5a** (1st and 7th cycle).[a]

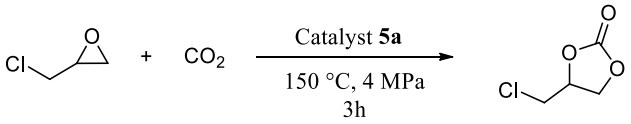

Entry	Catalyst			Conv.[a]	S[a]	TON	P[a]
	Cycle	[mg]	[mol%]	[%]	[%]		
1	1	15	0.014	32	>95	2214	841
2	7[b]	15	0.014	40	>95	2767	1051

[a] Conversion (Conv.), Selectivity (S), Productivity (P). Reaction condition: epichlorohydrin (303.8 mmol), CO_2 (4 MPa), catalyst **5a** (0.044 mmol), 150 °C, 3h. [b] **5a** was taken from the 6th cycle presented in **Figure 3**.

The results reported in Table 3 show that the reused catalyst was still more active than the fresh one in terms of TON (2767) and productivity (1051 *vs* 841), even with a different substrate. Based on the results reached with **5a**, bis-vinylimidazolium bromide salts with butyl or octyl linkers between imidazolium units were used for the synthesis of additional functionalized CNHs (Scheme 1, catalysts **6b** and **7c**). In order to study the influence of the nucleophile, a bis-vinylimidazolium iodide salt with octyl as the linker was employed for the synthesis of catalyst **8d**. The materials were prepared using the same amount of pristine CNHs and the selected imidazolium salt according to the reaction conditions adopted for **5a** (Table 4).

Table 4. Synthesis conditions and catalyst loading of **5a**, **6b**, **7c**, and **8d**.

Catalyst	CNHs [mg]	bVImi$^+$X$^-$ [mmol]	EtOH [mL]	AIBN [mmol]	Time [h]	X$^-$ loading [mmol g^{-1}]
5a	50	1.88	29	0.14	6	2.928
6b	50	1.88	29	0.14	6	3.822
7c	50	1.88	7	0.14	6	3.520
8d	50	1.88	19	0.14	6	2.951

The imidazolium-modified CNHs (**6b**, **7c**, **8d**) were characterized by TGA to estimate the catalyst loading. Similar to the previous materials, the catalysts **6b**, **7c**, and **8d** displayed good thermal stability as evidenced in Figure 7.

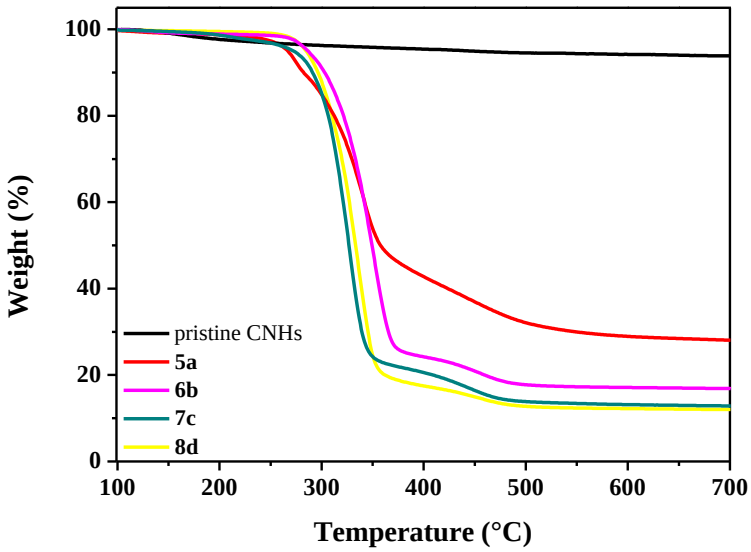

Figure 7. TGA analysis of **5a**, **6b**, **7c**, and **8d**.

TEM images of **6b**,**7c**, **8d** showed the presence of large irregular aggregates in which the quasi-spherical shapes of the CNHs embedded in the polymeric network were still clearly discernable (Figure 8).

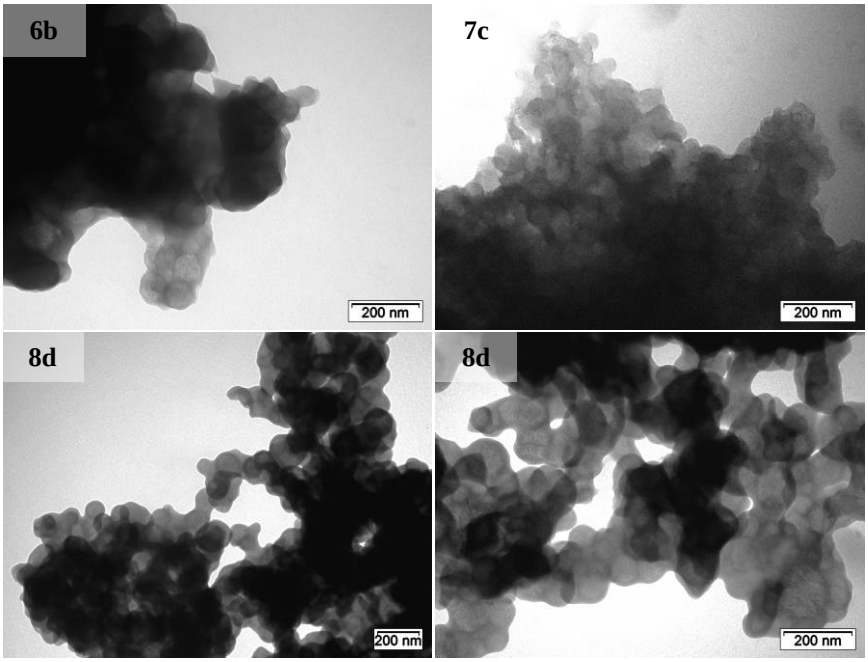

Figure 8. TEM images of **6b**, **7c**, and **8d**.

The reaction between CO_2 and styrene oxide was selected as benchmark process to identify the best catalyst among **5a**, **6b**, **7c**, and **8d**. A trend in the catalytic performances was observed based on the nature of the linker.

From the results reported in Table 5, imidazolium-based catalysts prepared using the octyl chain as a linker emerged as the best performing material.

As expected, the functionalized CNHs **8d** with iodide as a nucleophile led to higher conversion, turnover number, and productivity than the analogous material with a bromide as a counterion. The recyclability of **7c** and **8d** was successfully verified for three consecutive runs of the fixation of CO_2 into styrene oxide (Figure 9). Both materials were recycled without any loss of catalytic activity. TGA of the reused catalysts **7c** and **8d** (Figure 10) confirmed the stability of the materials, especially in the case of the bromide-based catalyst **7c**; in the case of the iodide-based catalyst **8d**, a loss in weight of 5.7% was observed after three cycles.

Table 5. Synthesis of cyclic carbonates catalyzed by **5a**, **6b**, **7c**, and **8d**.[a]

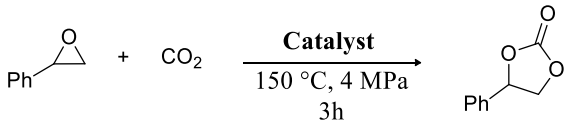

Entry	Catalyst	[mol%]	Conv.[a] [%]	S[a] [%]	TON	P[a]
1	**5a**	0.227	36	>95	106	48
2	**6b**	0.445	20	>95	45	27
3	**7c**	0.409	46	>95	112	62
4	**8d**	0.343	63	>95	184	84

[a] Conversion (Conv.), Selectivity (S), Productivity (P). Reaction condition: styrene oxide (206.3 mmol), CO_2 (4 MPa), 240 mg of **5a**, **6b**, **7c**, **8d**, 150 °C, 3 h.

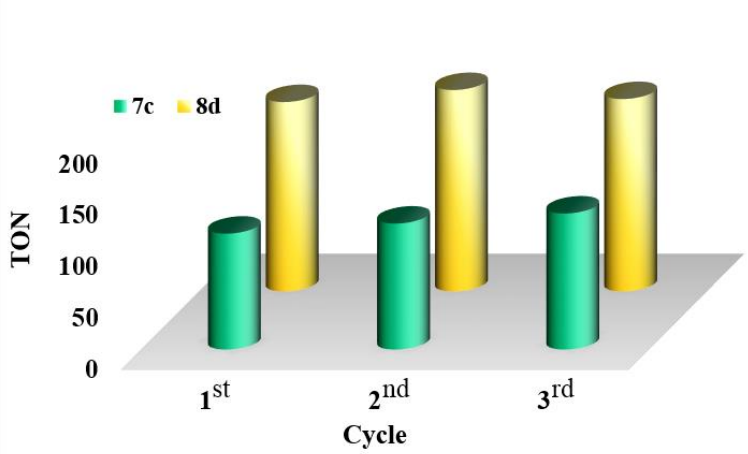

Figure 9. Recycling tests of **7c** and **8d**. Reaction conditions: styrene oxide (206.3 mmol), CO_2 (4 MPa), catalyst (240 mg, 0.845 mmol of **7c**, 0.711 mmol of **8d**), 150 °C, 3h.

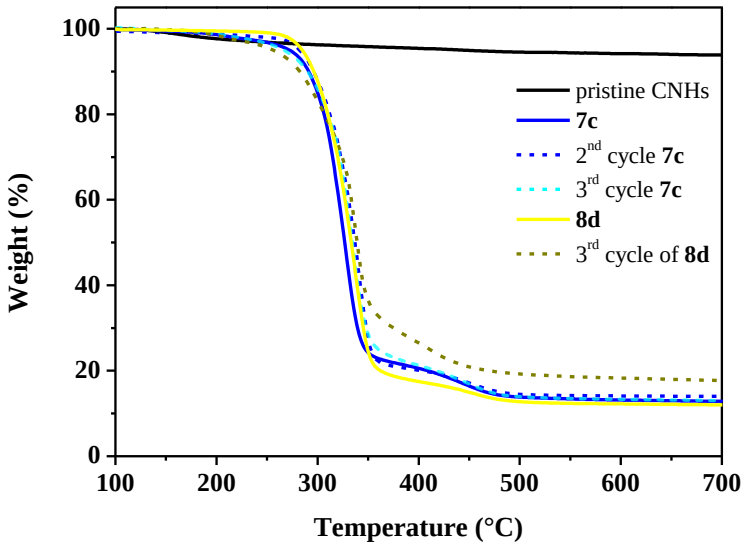

Figure 10. TGA profile of as synthesized and reused **7c** and **8d**.

Moreover, TEM analysis performed on the reused solid **8d** did not show any appreciable difference to the as-synthesized catalyst (Figure 11).

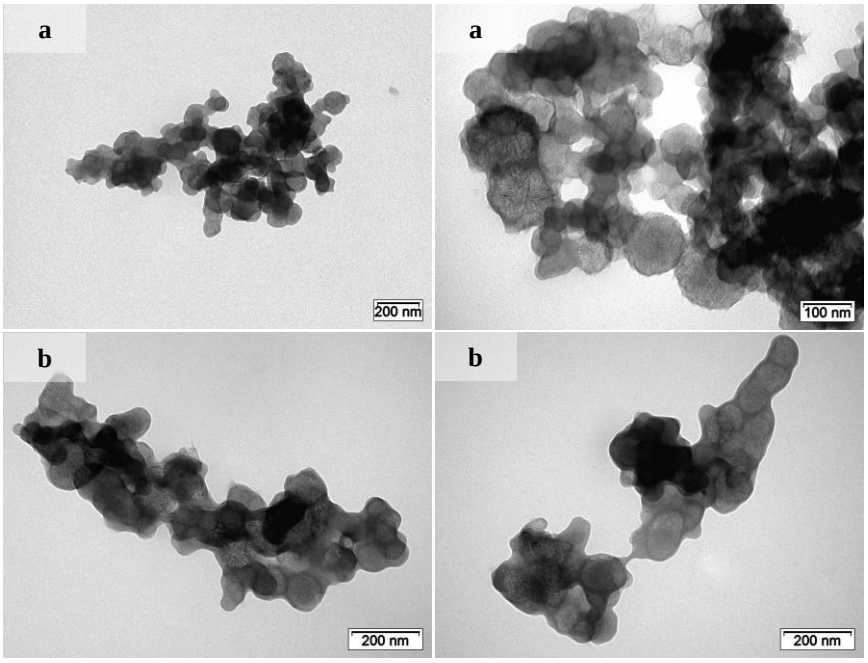

Figure 11. TEM images of as synthesized (a) and reused (b) **8d**.

The results presented in Table 5 indicated that the linker between imidazolium units influences the catalytic activity of the final solid. Catalyst **7c** displayed improved catalytic performance if compared with the analogous solids bearing the same counterion and different linkers (**5a** and **6b**).

A deeper investigation of the nature of the interaction between the imidazolium-based functionalization and the CNHs was carried out on the solid **7c**. For doing so, the Raman spectra of both pristine and functionalized CNHs were recorded. The collected results showed the presence of two prominent bands: the D-band centered at around 1350 cm^{-1} and the G-band at 1590 cm^{-1} (Figure 12).

As known for carbon nanostructures, the G-band is assigned to the vibration of the sp^2 hybridized carbon atoms, whereas the D-band is ascribed to sp^3 single-bonding carbon atoms and corresponds to the defect sites of the nanostructure arising from the loss of the basal symmetry. The covalent functionalization of CNHs allows a higher number of defect sites, and thus an increase in the D band intensity.

Herein, Raman spectra were normalized with respect to the G-band revealing the covalent nature of the functionalization, as evidenced by the increased contribution of the D band in the imidazolium-supported CNHs (Figure 12).[2]

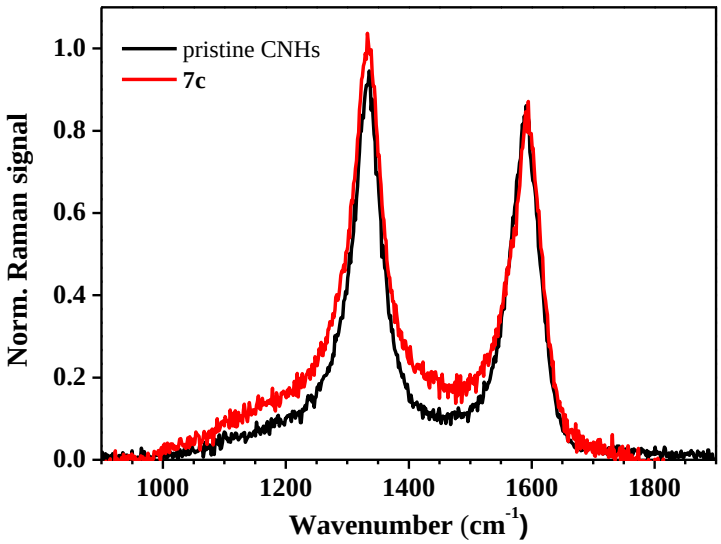

Figure 12. Raman spectra of pristine CNHs (black), and catalyst **7c** (red), recorded with excitation at λ_{exc} = 532 nm.

Considering the catalytic influence of the linker between the imidazolium units and the thermal stability of the solids after recycling, hybrid material **7c** was also chosen for deeper investigations (Table 6). A first screening of the catalyst amount was performed by using epichlorohydrin as the starting epoxide (Table 6, entries 1–3). In this context, the TON and productivity of **7c** increased when the amount of the catalyst was reduced. This behavior was ascribed to a better dispersion of the solid in the reaction mixture with the decreased amount of catalyst.

A second screening was carried out for the same reaction in order to study the effect of CO_2 pressure (Table 6, entries 3–5). The activity of the catalyst remained almost the same at a working pressure of 4 and 8 MPa, whereas a slightly increased activity was recorded at 5 MPa. This behavior was previously observed for imidazolium based polymeric networks supported on silica.[4a, 5] Then, the versatility of **7c** was further verified with glycidol and propylene oxide as starting epoxides (Table 6, entry 3, 6–8).

Table 6. Synthesis of cyclic carbonates catalyzed by **7c**.[a]

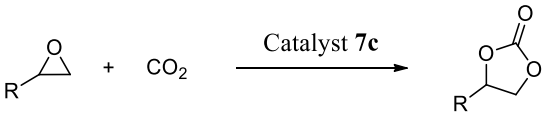

Entry	Substrate	Catalyst		Conv.[a]	S [b]	TON [c]	P[d]
		[mg]	[mol%]	[%]	[%]		
1	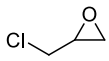	60	0.070	95	>95	1367	624
2	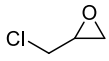	30	0.035	76	>95	2186	998
3	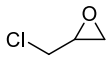	15	0.017	44	>95	2532	1156
4[b]	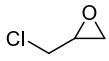	15	0.017	49	>95	2819	1287
5[c]	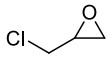	15	0.017	44	>95	2532	1156
6[d]	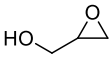	15	0.017	44	>95	2532	1000
7		15	0.017	44	>95	2532	865
8[e]		240	0.409	36	>95	112	62

[a] Conversion (Conv.), Selectivity (S), Productivity (P). Reaction conditions: epoxide (303.8 mmol), CO_2 (4 MPa), **7c** as catalyst, 150 °C, 3 h. [b] Reaction conditions: epichlorohydrin (303.8 mmol), CO_2 (5 MPa), **7c** as catalyst, 150 °C, 3 h. [c] Reaction conditions: epichlorohydrin (303.8 mmol), CO_2 (8 MPa), **7c** as catalyst, 150 °C, 3 h. [d] Reaction conditions: glycidol (303.8 mmol), CO_2 (4 MPa), **7c** as catalyst, 100 °C, 3 h. [e] Reaction conditions: styrene oxide (206.3 mmol), CO_2 (4 MPa), **7c** as catalyst, 150 °C, 3 h.

CNHs functionalized with imidazolium iodide networks **8d** were tested using a catalytic loading down to 0.015 mol% in the reaction of CO_2 with epichlorohydrin. As showed in Scheme 2, excellent results were achieved in terms of TON and productivity up to 3226 and 1235, respectively (Scheme 2).

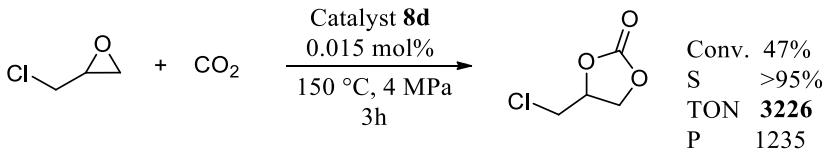

Scheme 2. Synthesis of cyclic carbonate from CO_2 and epichlorohydrin catalyzed by **8d**.

3.3 Conclusions

In conclusion, several CNHs/cross-linked imidazolium salt hybrid materials were prepared *via* a straightforward one-step procedure by radical polymerization of various bis-vinylimidazolium salts in the presence of pristine CNHs. Materials were characterized by TGA and TEM. The as-synthesized hybrids were employed as catalysts for the conversion of epoxides into cyclic carbonates by reaction with CO_2 without the presence of any co-catalysts. The reactions were performed using catalytic materials prepared with different CNHs/bVImiX ratios, different linkers, and by modifying the reaction conditions. Moreover, several epoxides were tested. Cyclic carbonates were obtained with high TON and productivity values. Four catalytic materials were also tested in recycling experiments with styrene oxide.

Two materials, **7c** and **8d**, possess the same linker between the imidazolium moiety (octyl) and different anion (Br^- and I^-, respectively). Two materials, **4a** and **5a**, possess the same linker between theimidazolium moiety (*p*-xylyl) and the same anion (Br^-) and different CNHs/bVImiX ratios. Catalysts **7c** and **8d** were both used in three consecutive runs without loss of catalytic activity. Catalysts **4a** and **5a** displayed an unprecedented increase of the catalytic activity from the first to the sixth cycle. Moreover, catalyst **5a** was tested in a seventh cycle with epichlorohydrin, showing an increased catalytic activity with respect to the first cycle with the same epoxide. TGA of the recycled catalysts evidenced the good thermal stability of the materials. The trends of the catalytic activity could be ascribed to some local modifications of the polymeric network with consequent generation of a more stable cross-linked structure with an increased percentage of porosity.

3.4 Experimental Section

Spectroscopic and analytical methods

CNHs were purchased from Carbonium Srl. 1-vinylimidazole, 1,4-dibromobutane, 1,8-dibromooctane, 1,8-diiodooctane, and styrene oxide (SO) were purchased from TCI. Epichlorohydrin (ECH), propylene oxide (PO), glycidol (GLY), and 2,2′-Azobis(2-methylpropionitrile) (AIBN) were purchased from Sigma–Aldrich. 1,4-dibromo-*p*-xylene and absolute ethanol were purchased from Fisher (ACROS Organics). Chloroform was purchased from Roth. All the solvents were used without further purification. ^{1}H NMR spectra were recorded on a JEOL 400 spectrometer. TEM images were recorded on a Philips TECNAI 10 at 80–100 kV. TGA was performed under nitrogen flow from 100 to 1000 °C with a heating rate of 10 °C min^{-1} in a Mettler Toledo TGA STAR system. Mercury intrusion porosimetry tests were performed on a Micromeritics Autopore IV 9500. The maximum pressure applied was 33 000 psi. Raman measurements were carried out with a HORIBA Scientific LabRAM HR Evolution spectrometer featuring a laser diode source at 532 nm.

Synthesis of bis-vinylimidazolium salts

The synthesis of bis-vinylimidazolium salts **2a-d** was performed according to the procedure reported in the literature.[4a, 5]

Synthesis of imidazolium functionalized CNHs

Pristine CNHs (130 or 50 mg, see Table 1 or 4) were transferred to a two-necked round bottom flask. Bis-vinylimidazolium salt **2**, previously dissolved in absolute ethanol, was added to the pristine CNHs (see Table 1 or 4). The dispersion was sonicated for 20 min. Nitrogen was bubbled into the mixture for 10 min. AIBN (0.14 mmol) was added to the reaction mixture, which was then refluxed and stirred at 80 °C for the time indicated in Table 1 or 4. The reaction mixture was allowed to cool down to room temperature and sonicated for 30 min. The hybrid solid material was recovered by filtration through a 0.1 mm

membrane filter (materials **3a**, **4a**). Functionalized CNHs (**3a**, **4a**) were washed with hot methanol, recovered from the filter, sonicated in methanol for 10 min, and filtered. This procedure was repeated several times. The catalysts **5a**, **6b**, **7c**, and **8d** were recovered by centrifugation and washed several times with ethanol. Before each centrifugation, the catalyst was sonicated for 15 min in the washing solvent. The last washing was done with diethyl ether. The catalyst was dried under vacuum at 60 °C overnight.

Catalytic tests

The catalytic tests were performed in a Cambridge Design Bullfrog batch reactor with temperature control and mechanical stirring, designed to operate at high temperature and pressure. In a typical experiment, the catalyst was highly dispersed into the epoxide by sonication for 15 min. The above dispersion was placed inside the reactor. Once the reactor was closed, the mechanical stirring speed was set at 500 rpm. The system was purged with N_2 for 10 min (P = 0.4 MPa) and then pressurized with CO_2. The temperature was increased to 150 °C with a rate of 1 °C min^{-1}. The reaction mixture was stirred at 150 °C for 3 h. The reaction mixture was allowed to cool down to room temperature and a slow depressurization of the reactor was performed. The reaction mixture was recovered and centrifuged at 4500 rpm for 10 min to separate the solid catalyst from the reaction mixture. The supernatant solution was analyzed by ^{1}H NMR spectroscopy.

Imidazolium-functionalized CNHs recycling tests

The recyclability of the catalyst was tested for the reaction between styrene oxide and CO_2. The catalyst was recovered by centrifugation and washed several times with toluene. Before each centrifugation, it was sonicated for 15 min in the washing solvent. The last washing was performed with diethyl ether. The catalyst was dried under vacuum at 60 °C. Once dried, it was used for the next cycle. All the conversions of the substrate were estimated by ^{1}H NMR analysis.

3.5 References

[1] N. Karousis, I. Suarez-Martinez, C. P. Ewels, N. Tagmatarchis, *Chemical Reviews* **2016**, *116*, 4850-4883.

[2] G. Mountrichas, S. Pispas, T. Ichihasi, M. Yudasaka, S. Iijima, N. Tagmatarchis, *Chemistry – A European Journal* **2010**, *16*, 5927-5933.

[3] M. Buaki-Sogó, A. Vivian, L. A. Bivona, H. García, M. Gruttadauria, C. Aprile, *Catalysis Science & Technology* **2016**, *6*, 8418-8427.

[4] a) P. Agrigento, S. M. Al-Amsyar, B. Sorée, M. Taherimehr, M. Gruttadauria, C. Aprile, P. P. Pescarmona, *Catalysis Science & Technology* **2014**, *4*, 1598-1607; b) J.-Q. Wang, X.-D. Yue, F. Cai, L.-N. He, *Catalysis Communications* **2007**, *8*, 167-172.

[5] C. Aprile, F. Giacalone, P. Agrigento, L. F. Liotta, J. A. Martens, P. P. Pescarmona, M. Gruttadauria, *ChemSusChem* **2011**, *4*, 1830-1837.

[6] F. Jutz, J.-M. Andanson, A. Baiker, *Chemical Reviews* **2011**, *111*, 322-353.

[7] a) W. Wang, C. Li, L. Yan, Y. Wang, M. Jiang, Y. Ding, *ACS Catalysis* **2016**, *6*, 6091-6100; b) Q. Sun, Z. Dai, X. Liu, N. Sheng, F. Deng, X. Meng, F.-S. Xiao, *Journal of the American Chemical Society* **2015**, *137*, 5204-5209.

CHAPTER IV

Supported Imidazolium Modified POSS Hybrids for the Conversion of Carbon Dioxide into Cyclic Carbonates

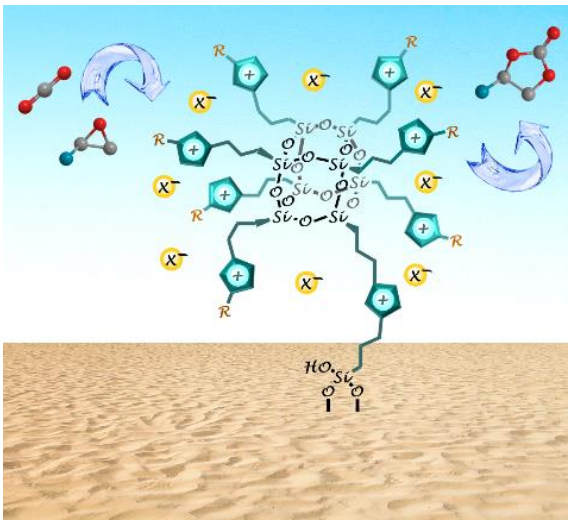

This chapter is based on:

ChemCatChem, **2019**, *11*, 560–567

CHAPTER IV

Supported Imidazolium Modified POSS Hybrids for the Conversion of Carbon Dioxide into Cyclic Carbonates

4.1 Abstract

Very high turnover numbers (TON) and productivity values up to 7875 and 740 respectively have been obtained for the conversion of CO_2 into cyclic carbonates by using hybrid materials based on imidazolium modified polyhedral oligomeric silsesquioxanes (POSS-Imi) grafted on amorphous silica (SiO_2) and mesostructured SBA-15. The heterogeneous organocatalysts were easily prepared *via* a straightforward synthetic procedure allowing to generate high local concentration spots of imidazolium active sites surrounding the POSS core. This synthetic procedure is also a promising approach for the design of a wide library of hybrid functional materials. The materials do not possess other co-catalytic species with Lewis or Brønsted acid functionalities which still represents a challenging aspect for the outcome of the process. The recyclability of the catalysts was successfully verified for four consecutive runs. The catalytic versatility was proved with a wide range of epoxides and with the most challenging oxetane on large scale (105–210 mmol) showing higher performances in comparison with other unmodified imidazolium-based catalytic systems. The new hybrids based on supported POSS nanostructures allowed the sustainable conversion of carbon dioxide under solvents- and metal-free reaction conditions with a full selectivity toward cyclic carbonates.

4.2 Results and Discussion

A novel series of imidazolium modified POSS hybrids was designed and prepared to be applied as heterogeneous catalytic systems for the synthesis of cyclic carbonates from carbon dioxide and epoxides. In order to combine the proximity effect of imidazolium moieties surrounding the inorganic nanocage structure[1] together with the benefits of heterogeneous catalysis, functionalized POSS units were covalently grafted onto different solid supports, namely amorphous silica and mesostructured SBA-15.

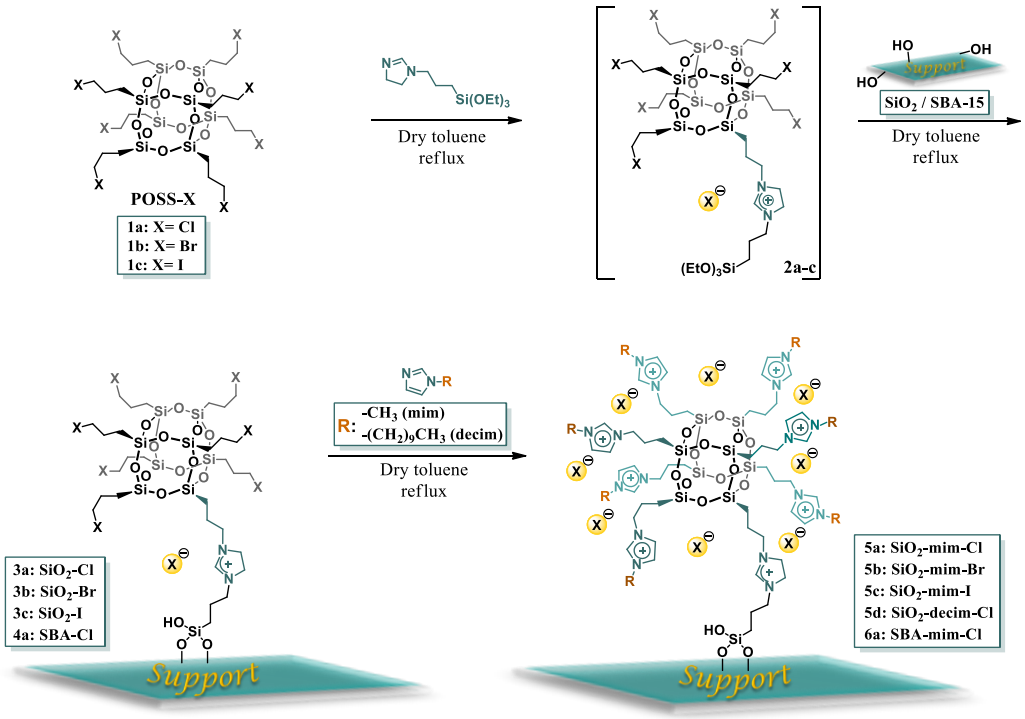

Scheme 1. Synthesis of imidazolium functionalized POSS hybrids.

A straightforward modular synthesis was developed using triethoxy-3-(2-imidazolin-1-yl)propylsilane as linker to connect POSS units to the solid support allowing to obtain dangling imidazolium modified supported nanostructures.

In particular, the general synthetic route of these hybrids, reported in Scheme 1, started from the reaction between triethoxy-3-(2-imidazolin-1-yl)propylsilane and octakis(3-chloropropyl)-octasilsesquioxane (compounds **1a**, POSS-Cl) to give compound **2a** which was directly used for the grafting reaction onto two different

supports to give materials **3a** (SiO_2-Cl) and **4a** (SBA-Cl). In this context, it is worth to observe that the above synthetic strategy represents a promising approach for the design of a wide library of hybrid functional materials. The latter materials were in turn reacted with 1-methylimidazole allowing to obtain the corresponding **5a** and **6a**. Materials **5a** and **6a**, endowed with chloride as counterion, were employed to study the effect of the solid supports on the catalytic performances. Then, amorphous silica was used, as support, to investigate the influence of the nucleophilic species in the final catalytic materials. For doing so, octakis(3-bromopropyl)-octasilsesquioxane (**1b**, POSS-Br) and octakis(3-iodopropyl)-octasilsesquioxane (**1c**, POSS-I) were prepared by halogen exchange reactions starting from POSS-Cl.[2] Then, both POSS-Br and POSS-I were grafted into amorphous silica to obtain the final imidazolium hybrids **5b** and **5c**. Moreover, in order to investigate the effect of the length of imidazolium alkyl side chain, a further hybrid was prepared *via* reaction between solid **3a** and 1-decylimidazole to give material SiO_2-decim-Cl (**5d**).

The grafting of imidazolium modified POSS units into the solid support was proved by means of solid state NMR. Solid state ^{13}C and ^{29}Si cross polarization - magic angle spinning (CP-MAS) NMR experiments were carried out to characterize all the final hybrids (Figure 1).

All the solid state ^{13}C CP-MAS NMR experiments were performed using the TOSS (total suppression side band) pulse sequence to remove the spinning side bands while leaving the isotropic signals. In CP-MAS ^{13}C NMR spectra the characteristic signals of the carbon atoms of imidazolium ring were observed in the range δ = 122–137 ppm, whereas the aliphatic ones resonated in the range δ = 10–52 ppm. The weak signal located at δ = ~158 ppm can be attributed to the C2 imidazolidinium carbon atom. CP-MAS ^{29}Si NMR spectra showed the presence of $Q^4[(SiO)_4Si]$ (δ = -118 ppm) and $Q^3[(SiO)_3SiOH]$ (δ = -110 ppm) units. The signal at δ = -75 ppm corresponded to the completely condensed T^3 silicon units [R-Si$(OSi)_3$] of both POSS nanocage and the organosilane silicon acting as linker between the solid support and the POSS itself, whereas the signal at δ = -67 ppm was ascribed to T^2 [R-Si$(OSi)_2$OR] silicon atoms bridging bulky silica to POSS units.

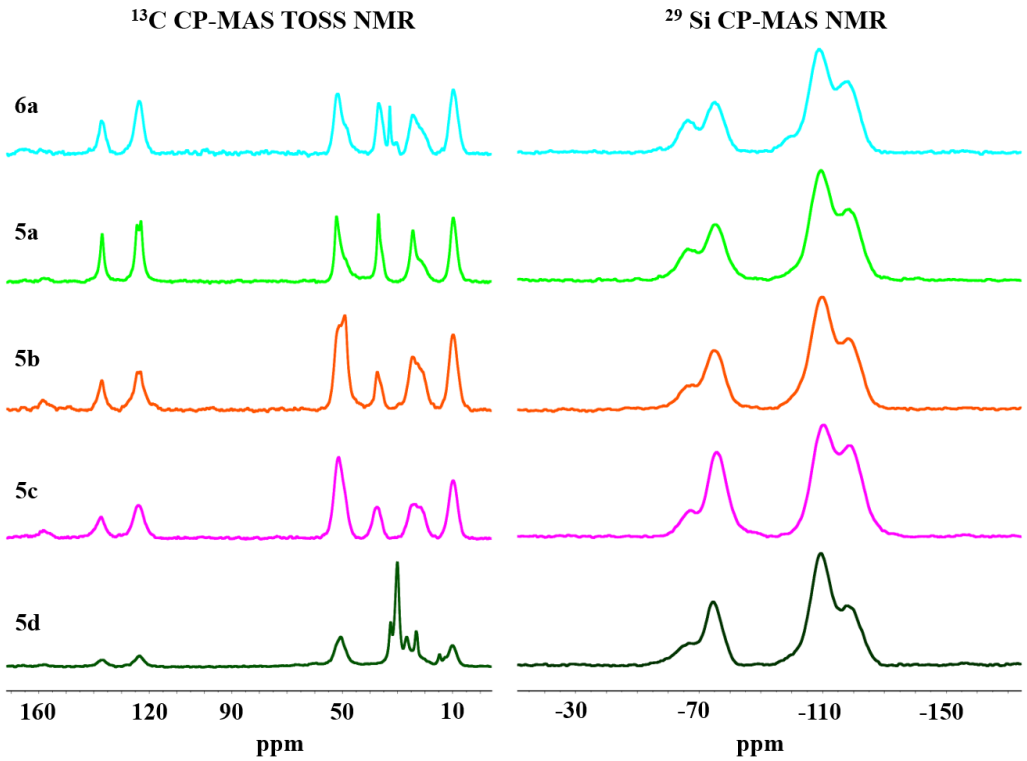

Figure 1. Solid state ^{13}C CP-MAS TOSS (on the left) ^{29}Si CP-MAS (on the right) NMR spectra of imidazolium functionalized POSS hybrids.

Combustion chemical analysis (C, H, N) allowed to estimate the catalyst loadings of all the solids, as showed in Table 1.

Table 1. Combustion chemical analysis and catalyst loadings of imidazolium hybrids.

Catalyst	**C** [%]	**H** [%]	**N** [%]	**X$^-$ Loading** [mmol/g]
5a SiO_2-mim-Cl	11.05	2.41	2.32	0.830
5b SiO_2-mim-Br	9.79	2.04	1.96	0.700
5c SiO_2-mim-I	10.26	1.93	2.02	0.721
5d SiO_2-decim-Cl	14.74	2.89	2.55	0.911
6a SBA-mim-Cl	11.12	2.27	2.28	0.814

Thermogravimetric analysis (TGA) evidenced the thermal stability of the hybrid materials (Figure 2). Moreover, from TGA data it is interesting to observe that the degradation of organic moieties starts at around 250 °C. On this ground, the good thermal stability of the solids emerged as promising feature for their repeated use under heating conditions.

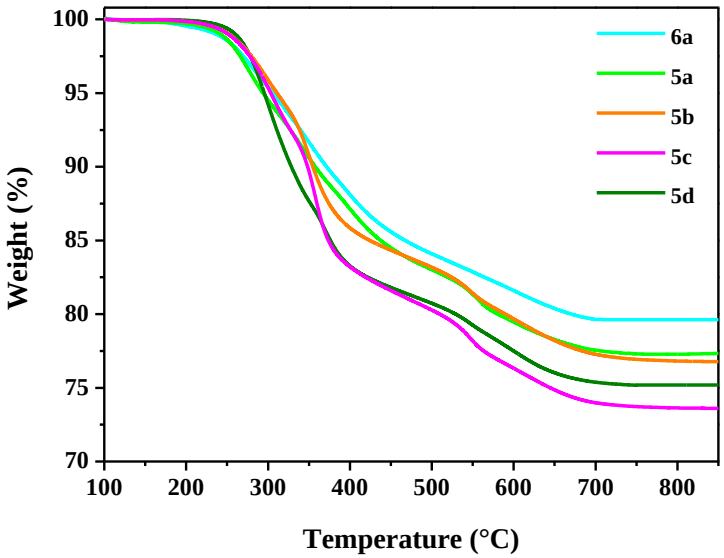

Figure 2. TGA profiles of imidazolium functionalized POSS hybrids.

Surface textural properties of the materials were investigated by means of N_2 adsorption/desorption measurements (Table 2). In particular, the specific surface area (SSA) was analyzed by Brunauer-Emmett-Teller (BET) method,[3] whereas pore volumes and pore size distributions (PSD) were estimated by applying Barrett-Joyner-Halenda (BJH) method[4] using the adsorption isotherms.

Table 2. Textural properties of silica oxide and supported POSS hybrids.

Material	BET[a] [m^2/g]	Pore Volume [cm^3/g]	PSD[b] [nm]
SiO_2	424	0.60	4.6
5a	250	0.28	3.7
5b	285	0.38	3.9
5c	279	0.37	3.5
5d	203	0.22	3.6
SBA-15	634	1.39	15.6
6a	272	0.87	14.3

[a] BET p/p^0 range: 0.05-0.3. [b] PSD calculated on the adsorption curve.

A clear decrease in surface area and cumulative pore volume of amorphous silica and mesostructured SBA was observed after the grafting of imidazolium

modified POSS units. All the supported POSS hybrids displayed a type IV isotherm (Figure 3) according to the IUPAC classification with a H_2 hysteresis loop.

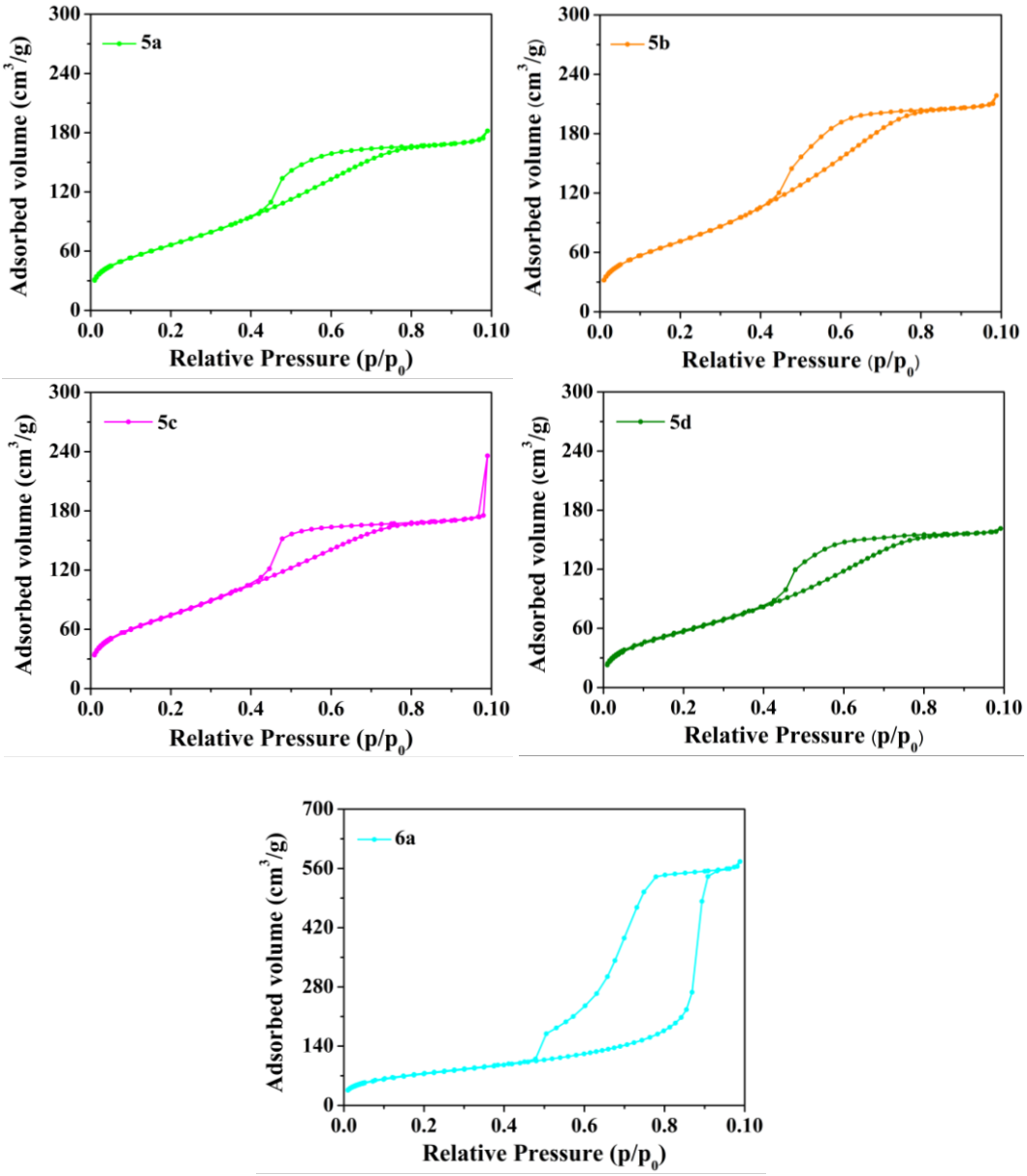

Figure 3. N_2 adsorption/desorption isotherms of **5a-d** and **6a**.

Materials **5a** and **6a** were analyzed by means of transmission electron microscopy (TEM) in order to collect morphological information. However, TEM pictures (Figure 4) did not reveal any appreciable difference compared to pristine solid supports. The amorphous morphology of SiO_2 and the bidimensional hexagonal mesostructure of SBA-15 were further observed for **5a** and **6a**, respectively.

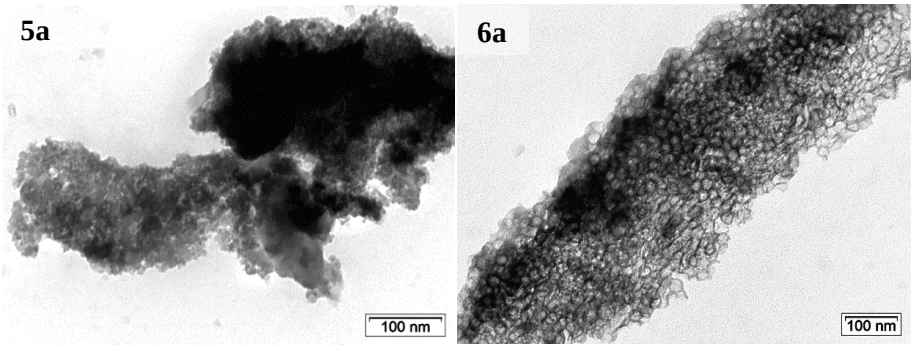

Figure 4. TEM pictures of **5a** (on the left) and **6a** (on the right).

Once characterized, imidazolium modified POSS hybrids were tested as catalysts for the synthesis of cyclic carbonates *via* reaction of CO_2 with epoxides under solvent free conditions, at 150 °C, and without using any co-catalytic species with Lewis acid properties. It is worth to mention that such reaction is highly exothermic. In this context, from an industrial point of view a reaction temperature around 150 °C could be evaluated as a beneficial condition allowing to recover the reaction heat as steam.[5] To minimize the energy consumption, reaction temperatures <100 °C display indeed lower heat exchange efficiencies. The catalytic performances of the solids were evaluated in terms of turnover number (TON, defined as moles of epoxide converted/moles of of supported imidazolium halide), productivity (P, calculated as grams of cyclic carbonates per grams of catalyst), recyclability and versatility. In order to study the effect of the solid support, two catalytic tests were carried out with materials **5a** and **6a** in the reaction between carbon dioxide and styrene oxide (Table 3, entries 1, 2). From this preliminary investigation, imidazolium modified POSS grafted into amorphous silica (**SiO_2-mim-Cl 5a**) resulted more active than the analogous material prepared by supporting POSS into SBA-15 (**SBA-mim-Cl 6a**). This behavior can be accounted to the specific textural properties of the final materials (Table 2). By comparison with **6a**, the solid **5a** displayed lower values in terms of both pore volume and pore size distribution, whereas it presented a similar catalyst loading (0.830 *vs* 0.814 mmol/g, Table 1). On this basis, the better catalytic activity of **5a** could be explained by a higher local concentration of imidazolium modified POSS units which resulted in improved intermolecular interactions. Both **5a** and **6a** showed competitive and higher performances in

comparison with other catalytic systems recently reported in literature (Table 3) such as 1-butyl-3-methylimidazolium chloride (BmImCl)[1, 6] or pyrazolium bromide (HEPzBr)[7] unsupported ionic liquids (entries 3,4), and heterogeneous catalysts based on polymer supported ammonium chloride salts (PSCQNCl),[8] imidazolium chloride[9] and tetrafluoroborate[10] active sites supported onto silica (SiO_2ImCl, SiO_2ImBF_4), or imidazolium salts bearing bromide as counterion grafted onto carbon nanohorns (CNHsImBr),[11] and benzyl chloride polymer (BCPImBr)[12] (entries 5–9). The above catalytic systems do not present other co-catalytic species with Brønsted or Lewis acid functionalities. High catalytic activity under such conditions is still challenging. On the other hand, much better performances can be obtained when co-catalytic species are present.[13]

Table 3. Conversion of styrene oxide into cyclic carbonate.[a]

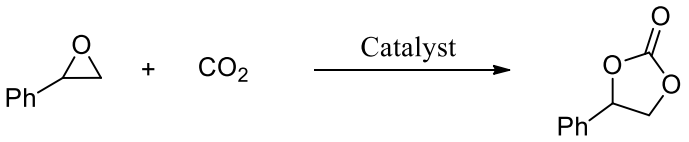

Entry	Catalyst	T [°C]	Time [h]	TON	TOF[a] [h^{-1}]	Reference
1[b]	**5a**	150	3	477	159	This work
2[b]	**6a**	150	3	306	102	This work
3	BmImCl	150	3	326	109	Ref[1]
4	HEPzBr	140	4	68	17	Ref[7]
5	SiO_2ImCl	150	3	28	9	Ref[9]
6	PSCQNCl	150	5	75	15	Ref[8]
7	SiO_2ImBF_4	160	4	53	13	Ref[10]
8	CNHsImBr	150	3	106	35	Ref[11]
9	BCPImBr	140	5	323	65	Ref[12]

[a] Turnover frequency (TOF, calculated as TON/reaction time). [b] Reaction conditions: styrene oxide (172 mmol), CO_2 (P_i 4 MPa), catalyst **5a** and **6a**, 150 °C, 3 h.

The higher catalytic activity of **5a** and **6a** can be ascribed to the proximity effect due to the increased local concentration of imidazolium moieties surrounding POSS nanocage skeleton. It is worth to note that supported POSS materials allowed to a good combination between the positive features of POSS nanostructures and the intrinsic advantages of heterogeneous catalytic systems such as their easy recovery

from the reaction mixture together with the possibility to reuse them for consecutive runs.

As a result of the higher activity of **5a** compared to **6a**, amorphous silica was selected as solid support in order to study the effect of the nucleophilic species. For doing so, materials **5b** and **5c**, bearing imidazolium bromide and iodide moieties respectively, were synthesized and tested. In order to compare the catalytic performances and investigate the recyclability of the solids **5a-c**, styrene oxide was selected as target substrate (Figure 5). The effect of the nucleophilic species led to the overall order of activity $I^- > Br^- > Cl^-$ corresponding to **5c** > **5b** > **5a** hybrids. All the solid displayed promising turnover number and excellent selectivity. The recyclability of **5a**, **5b**, **5c** was studied for four consecutive runs without showing, in the case of **5a** and **5b**, any significant decrease in the catalytic activity. However, a progressive decrease was observed in the case of the most active **5c**.

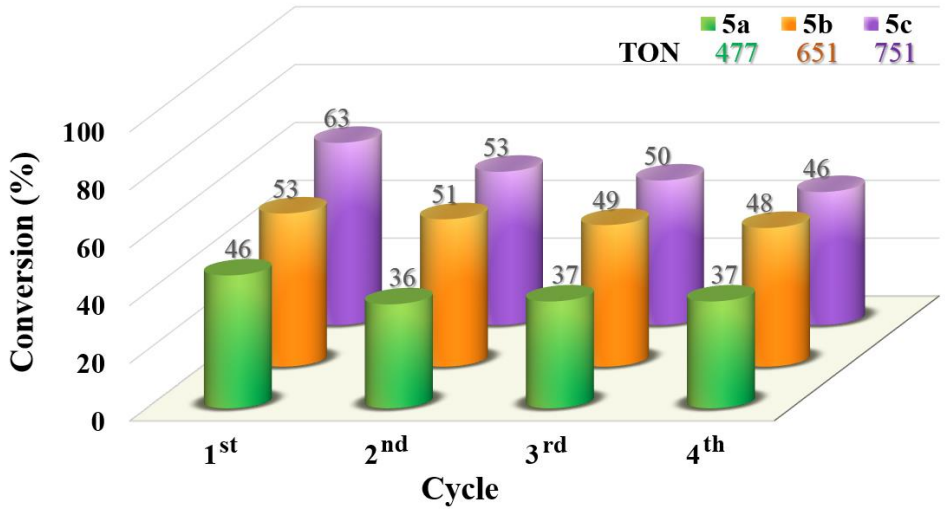

Figure 5. Recycling tests of materials **5a**, **5b**, **5c**. Reaction conditions: styrene oxide (172 mmol), CO_2 (P_i 4 MPa), 200 mg of catalyst (0.166 mmol of **5a**, 0.140 mmol of **5b**, 0.144 mmol of **5c**), 150 °C, 3 h. TON calculated on the first cycle.

In order to check the thermal stability and the catalyst loading of reused solids, TGA measurements were performed on **5a-c** after the fourth catalytic cycle. Thermogravimetric analysis of reused catalysts confirmed the good robustness of materials **5a-b**. Indeed, TGA profiles of reused **5a-b** displayed the same weight loss compared to those of the as synthesized materials (Figure 6) leading to rule out the possibility of any leaching phenomena during the catalytic

tests. Conversely, TGA profile of **5c** reused for four cycles compared to that of the as-synthesized catalyst showed a loss in weight (~2.7%) allowing to justify the decrease in the catalytic activity during recycling experiments. Although the material **5c** proved to be the most active catalyst, the solid **5b** was selected for further investigations (Table 4) because of its higher stability after recycling compared to **5c** (Figure 5).

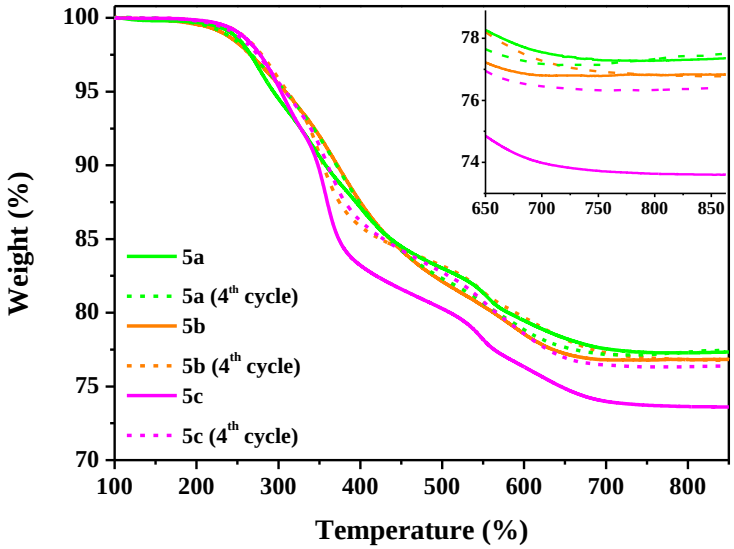

Figure 6. TGA profiles of as-synthesized and reused **5a-c**. Magnification of TGA curves (inset).

Firstly, the potential influence of catalyst amount was evaluated by using epichlorohydrin as target epoxide (entries 1–3). Material **5b**, tested at 0.020 mol%, displayed appealing performances in terms of TON, productivity and selectivity leading to 85% conversion into the desired product after 3 h. Furthermore, when the catalyst loading was scaled down to 0.005 mol%, **5b** showed an outstanding increased activity resulting in a turnover number of 7875 (entries 1–3). Such catalytic behavior could be ascribed to a better dispersion of the solid in the reaction medium when a decreased amount of **5b** was utilized.

Furthermore, the overall versatility of **5b** was evaluated with a broad range of epoxides such as epichlorohydrin, propylene oxide, glycidol, 1,4-butanediol diglycidyl ether, and the less reactive cyclohexene oxide (entries 1–9). In all the catalytic tests, a full selectivity toward the corresponding cyclic carbonates was reached together with excellent TON and productivity. In particular, the reaction

between CO_2 and 1,4-butanediol diglycidyl ether using 0.133 mol% of catalyst (entry 7) gave rise to a quantitative conversion. An additional catalytic test of **5b** was performed using the most challenging oxetane as substrate (entry 10).

Table 4. Synthesis of cyclic carbonates catalyzed by **5b**[a].

Entry	Substrate	Catalyst		Conv.	S	Time	TON	P
		[mg]	[mol%]	[%]	[%]	[h]		
1		60	0.020	85	>99	3	4250	402
2		40	0.013	61	>99	3	4575	433
3		16	0.005	42	>99	3	7875	745
4		40	0.013	55	>99	3	4125	292
5[b]		40	0.013	51	>99	3	3825	313
6[c]	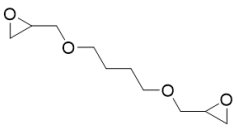	40	0.013	41	>99	16	3075	309
7[c]	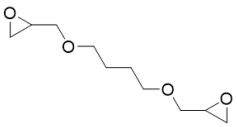	200	0.067	99	>99	16	1485	149
8[d]		200	0.081	53	>99	3	651	74
9[e]		200	0.093	30	>99	16	321	32
10[f]		200	0.067	16	>99	16	240	19

[a] Conversion (Conv.), Selectivity (S), reaction time (t), Productivity (P, calculated as grams of cyclic carbonate/grams of catalyst). Reaction conditions: epoxide (210 mmol), CO_2 (P_i 4 MPa), catalyst **5b**, 150 °C. [b] Reaction conditions: glycidol (210 mmol), CO_2 (P_i 4 MPa), catalyst **5b**, 100°C. [c] Reaction conditions: 1,4-butanediol diglycidyl ether (105 mmol), CO_2 (P_i 4 MPa), catalyst **5b**, 150 °C. [d] Reaction conditions: styrene oxide (172 mmol), CO_2 (P_i 4 MPa), catalyst **5b**, 150 °C. [e] Reaction conditions: epoxide (150 mmol), CO_2 (P_i 4 MPa), catalyst **5b**, 150 °C. [f] Reaction conditions: oxetane (210 mmol), CO_2 (P_i 4 MPa), catalyst **5b**, 150 °C.

The synthesis of six membered cyclic carbonates by coupling of CO_2 and oxetane is challenging because of *i*) the lower reactivity of four membered ether rings compared to epoxides, and *ii*) a poor reaction selectivity as the six-membered cyclic carbonates is thermodynamically less stable than its corresponding co-polymer. Therefore, in the reaction with CO_2, oxetane ring opening step usually requires the use of an organometallic catalyst[14] or bicomponent catalysts composed of organometallic catalyst and ammonium salts[15]. A simple organocatalytic approach has been used only twice, using 2 mol% of tetraphenylstibonium iodide[16] or 3 mol% of TBAI and a hydrogen bond donor as co-catalyst[17]. In the latter case a mixture of oligocarbonate and six membered cyclic carbonate was formed. Nevertheless, in the reaction between carbon dioxide and oxetane ring, the catalytic performances of **5b** stand out from literature data in terms of TON.

Then, the conversion of CO_2 and styrene oxide into styrene carbonate was chosen as benchmark reaction to check the influence of imidazolium alkyl chain length by comparison between the solids bearing imidazolium moieties with methyl and decyl alkyl side chain (**5a** and **5d**). Hybrid **5d** was tested for four consecutive runs and results compared with those of hybrid **5a** (Figure 7). Catalyst **5d** proved to be slightly less active than **5a** in terms of TON, indicating that the major role in the catalytic activity is probably played by the local arrangement due to the presence of the nanocage.

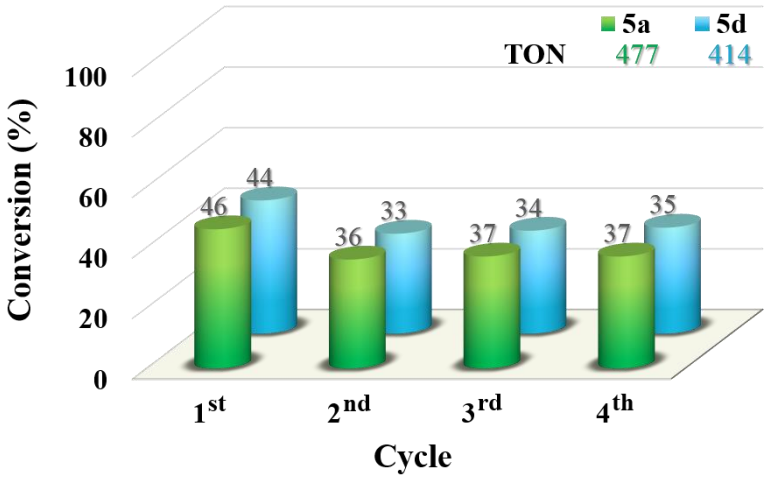

Figure 7. Recycling tests of materials **5a** and **5d**. Reaction conditions: styrene oxide (172 mmol), CO_2 (P_i 4 MPa), 200 mg of catalyst (0.166 mmol of **5a**, 0.183 mmol of **5d**), 150 °C, 3 h. TON calculated on the first cycle.

In both **5a** and **5d** catalytic tests, the activity of the solid displayed a decreasing from the first to the second cycle followed by a stabilization in the next cycle. This behavior is probably due to thermal condensation phenomena that took place during the catalytic cycle. In order to verify such hypothesis, a ^{29}Si CP-MAS NMR experiment was carried out on the reused catalyst **5a** after the fourth cycle (Figure 6). The ^{29}Si spectrum of **5a** reused for four cycles compared to that of the as-synthesized catalyst showed a clear increase in the Q^4/Q^3 ratio allowing to confirm a structural modification during the reaction.

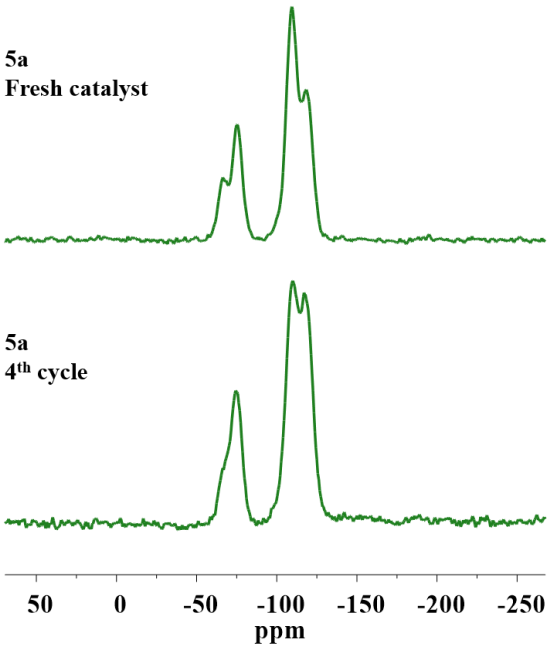

Figure 8. Solid state ^{29}Si CP-MAS NMR spectra of as synthesized and reused **5a**.

4.3 Conclusions

In conclusion, we have prepared and characterized a series of hybrid materials based on imidazolium modified polyhedral oligomeric silsesquioxanes (POSS-Imi) in order to be employed as heterogeneous organocatalysts for the conversion of epoxides and CO_2 into cyclic carbonates in solvent-free reaction conditions. The main goal of this research was to maintain the high catalytic activity of unsupported imidazolium modified POSS, due to the proximity effect of the imidazolium units linked to the POSS nanocage, with the benefits of heterogeneous catalysis, in terms of recyclability, without the need of other co-catalytic species with Brønsted or Lewis acid functionalities. All the solids were easily prepared following tailored procedures designed to study the influence of the solid support (SiO_2 *vs* SBA-15) and the effect of both nucleophilic species (Cl^-, Br^-, I^-) and imidazolium alkyl side chain length. Such new hybrid materials were easily recyclable as well as highly active toward the formation of cyclic carbonates even with the less reactive oxetane, showing higher performances in terms of turnover number, productivity and selectivity in comparison with other unmodified imidazolium-based catalytic systems described in literature.[18] The combined features due to the good thermal stability of the solids and the local arrangement of the imidazolium units are, probably, the main reasons of the recyclability and high activity of such catalytic materials.

4.4 Experimental Section

Spectroscopic and analytical methods

Chemicals and solvents were purchased from commercial suppliers to be used without further purification. Combustion chemical analysis was carried out on a PerkinElmer 2400 Series II Elemental Analyzer. Thermogravimetric analysis was performed under oxygen flow from 100 to 1000 °C with a heating rate of 10 °C min^{-1} in a Mettler Toledo TGA STAR system. Solid state CP-MAS-TOSS ^{13}C-NMR spectra were recorded at room temperature, on a Bruker Avance 500 Spectrometer operating at 11.7 T, using a contact time of 2 ms, a spinning rate of 5 KHz and a Bruker probe of 4mm. CP-MAS ^{29}Si-NMR spectra were recorded at room temperature, on a Bruker Avance 500 Spectrometer operating at 11.7 T, using a contact time of 2 ms, a spinning rate of 8 KHz and a Bruker probe of 4mm. Liquid state ^{1}H-NMR spectra were collected on a JEOL 400 spectrometer. TEM micrographs were taken on a Philips TECNAI 10 at 80-100 kV. N_2 adsorption–desorption measurements were carried out at 77 K by using a volumetric adsorption analyzer (Micromeritics Tristar 3000). Before the analysis, the samples were pretreated at 150°C for 16 h under reduced pressure (0.1 mbar). The BET method was applied in the p/p^0 = 0.05–0.30 range to calculate the specific surface area, whereas the pore size distributions were estimated from the adsorption isotherm using the BJH method.

Preparation of SBA-15

Mesoporous SBA-15 was prepared starting from tetraethyl orthosilicate (TEOS) as silica source, Pluronic P123 ($EO_{20}PO_{70}EO_{20}$) as template, and mesitylene as swelling agent, according to a published procedure.[19]

Synthesis of POSS 1a-c

POSS-Cl,[20] POSS-Br and POSS-I[2] were synthesized according to literature procedures.

Synthesis of materials 3a-c, 4a

A selected polyhedral oligomeric silsesquioxane (1 eq., 0.675 mmol of **1a-c**) was transferred in a two-necked round bottom flask. Anhydrous toluene (10 mL) and trethoxy-3-(2-imidazolin-1-yl)propylsilane (1.5 eq.) were added to POSS. The reaction mixture was refluxed under Argon atmosphere for 24 h. Then, the support (1.8 g of SiO_2 or SBA-15) was added to the reaction mixture without a prior isolation of intermediates **2a-c**. The obtained suspension was refluxed under Argon atmosphere for 72 h. The solids were recovered by centrifugation and washed with toluene, dichloromethane, and diethyl ether. The obtained materials (**3a-c**, **4a**) were dried at 60 °C under vacuum.

Synthesis of materials 5a-d, 6a

1-methylimidazole or 1-decylimidazole (15 eq. respect to halopropyl moieties of **3a-c** and **4a**) were added to a suspension of materials **3a-c** and **4a** (2.4 g) in toluene (25 mL). The reaction mixtures were refluxed for 72 h. The final solids **5a-d** and **6a** were recovered by centrifugation and washed with toluene, dichloromethane, hot methanol and diethyl ether. The final materials were dried at 60°C under vacuum.

Catalytic tests

The catalytic tests were carried out in a Cambridge Design Bullfrog batch reactor with temperature control and mechanical stirring, designed to operate at high temperature and pressures. A fine dispersion of the catalyst into the selected epoxide was transferred inside the reactor. Then, the reactor was closed and the mechanical stirring speed set at 500 rpm. The system was purged with N_2 for 10 min (0.4 MPa) and then, pressurized with CO_2. The temperature was increased to 150 °C with a rate of 5 °C min^{-1}. The reaction mixture was stirred at 150 °C for 3 h. Then, the reaction mixture was cooled down to room temperature and a slow depressurization of the reactor was carried out. The separation of the catalyst from the reaction mixture was easily performed by centrifugation (10 min at 4500 rpm). The supernatant solution was sampled and analyzed by ^{1}H-NMR.

Recycling tests

The recyclability of the materials was checked in the reaction between styrene oxide and CO_2. At the end of each catalytic test, the solids were recovered by centrifugation and washed with toluene (3x35 mL), methanol (30 mL) and diethyl ether. Moreover, the catalysts were previously sonicated in the washing solvent up to get a good dispersion. Then, the solids were dried under vacuum at 60 °C. Once dried, the materials were reused for the next cycle by tailoring epoxide amount in function of the recovered catalyst in order to maintain the ratio between moles of catalyst and moles of epoxides. The conversions of styrene oxide into cyclic carbonate was calculated by ^{1}H-NMR analysis.

4.5 References

[1] L. A. Bivona, O. Fichera, L. Fusaro, F. Giacalone, M. Buaki-Sogo, M. Gruttadauria, C. Aprile, *Catalysis Science & Technology* **2015**, *5*, 5000-5007.

[2] V. Ervithayasuporn, N. Pornsamutsin, P. Prangyoo, K. Sammawutthichai, T. Jaroentomeechai, C. Phurat, T. Teerawatananond, *Dalton Transactions* **2013**, *42*, 13747-13753.

[3] S. Brunauer, P. H. Emmett, E. Teller, *Journal of the American Chemical Society* **1938**, *60*, 309-319.

[4] E. P. Barrett, L. G. Joyner, P. P. Halenda, *Journal of the American Chemical Society* **1951**, *73*, 373-380.

[5] T. Sakakura, J.-C. Choi, H. Yasuda, *Chemical Reviews* **2007**, *107*, 2365-2387.

[6] A.-L. Girard, N. Simon, M. Zanatta, S. Marmitt, P. Goncalves, J. Dupont, *Green Chemistry* **2014**, *16*, 2815-2825.

[7] T. Wang, D. Zheng, J. Zhang, B. Fan, Y. Ma, T. Ren, L. Wang, J. Zhang, *ACS Sustainable Chemistry & Engineering* **2018**, *6*, 2574-2582.

[8] Y.-Y. Zhang, L. Chen, S.-F. Yin, S.-L. Luo, C.-T. Au, *Catalysis Letters* **2012**, *142*, 1376-1381.

[9] C. Aprile, F. Giacalone, P. Agrigento, L. F. Liotta, J. A. Martens, P. P. Pescarmona, M. Gruttadauria, *ChemSusChem* **2011**, *4*, 1830-1837.

[10] J.-Q. Wang, X.-D. Yue, F. Cai, L.-N. He, *Catalysis Communications* **2007**, *8*, 167-172.

[11] C. Calabrese, L. F. Liotta, E. Carbonell, F. Giacalone, M. Gruttadauria, C. Aprile, *ChemSusChem* **2017**, *10*, 1202-1209.

[12] D. Xing, B. Lu, H. Wang, J. Zhao, Q. Cai, *New Journal of Chemistry* **2017**, *41*, 387-392.

[13] Q. He, J. W. O'Brien, K. A. Kitselman, L. E. Tompkins, G. C. T. Curtis, F. M. Kerton, *Catalysis Science & Technology* **2014**, *4*, 1513-1528.

[14] H. Koinuma, H. Hirai, *Die Makromolekulare Chemie* **1977**, *178*, 241-246.

[15] a) D. J. Darensbourg, W. Choi, P. Ganguly, C. P. Richers, *Macromolecules* **2006**, *39*, 4374-4379; b) D. J. Darensbourg, A. I. Moncada, *Macromolecules* **2009**, *42*, 4063-4070; c) D. J. Darensbourg, A. I. Moncada, *Macromolecules* **2010**, *43*, 5996-6003; d) F. Chen, N. Liu, B. Dai, *ACS Sustainable Chemistry & Engineering* **2017**, *5*, 9065-9075; e) J. Rintjema, W. Guo, E. Martin, E. C. Escudero-Adán, A. W. Kleij, *Chemistry – A European Journal* **2015**, *21*, 10754-10762; f) M. Taherimehr, J. P. C. C. Sertã, A. W. Kleij, C. J. Whiteoak, P. P. Pescarmona, *ChemSusChem* **2015**, *8*, 1034-1042; g) C. J. Whiteoak, E. Martin, M. M. Belmonte, J. Benet-Buchholz, A. W. Kleij,

Advanced Synthesis & Catalysis **2012**, *354*, 469-476; h) D. J. Darensbourg, A. Horn Jr, A. I. Moncada, *Green Chemistry* **2010**, *12*, 1376-1379.

[16] M. Fujiwara, A. Baba, H. Matsuda, *Journal of Heterocyclic Chemistry* **1989**, *26*, 1659-1663.

[17] M. Alves, B. Grignard, A. Boyaval, R. Méreau, J. De Winter, P. Gerbaux, C. Detrembleur, T. Tassaing, C. Jérôme, *ChemSusChem* **2017**, *10*, 1128-1138.

[18] a) M. Cokoja, M. E. Wilhelm, M. H. Anthofer, W. A. Herrmann, F. E. Kühn, *ChemSusChem* **2015**, *8*, 2436-2454; b) A. A. Chaugule, A. H. Tamboli, H. Kim, *Fuel* **2017**, *200*, 316-332.

[19] L. Wang, T. Qi, Y. Zhang, J. Chu, *Microporous and Mesoporous Materials* **2006**, *91*, 156-160.

[20] W. Zhang, Z.-S. Wang, *ACS Applied Materials & Interfaces* **2014**, *6*, 10714-10721.

CHAPTER V

Imidazolium Based Cross-Linked Nanostructures from POSS Molecular Bricks for the Efficient Conversion of Carbon Dioxide

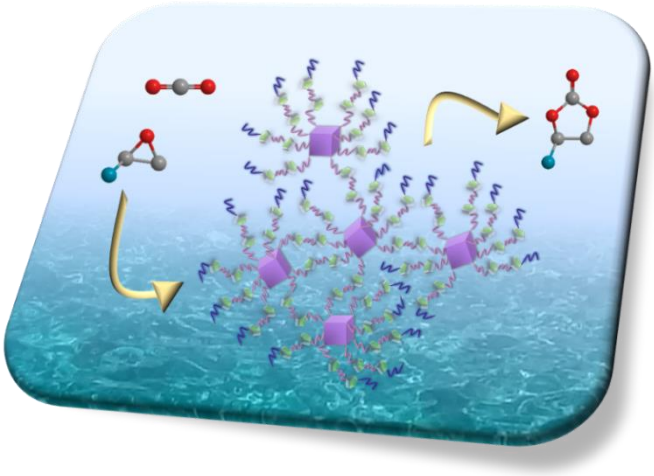

This chapter is based on a *manuscript in preparation*

CHAPTER V

Imidazolium Based Cross-Linked Nanostructures from POSS Molecular Bricks for the Efficient Conversion of Carbon Dioxide

5.1 Abstract

Polyhedral oligomeric silsesquioxanes (POSS) have been employed as molecular bricks for the synthesis of imidazolium cross-linked networks as heterogeneous catalyst for the conversion of carbon dioxide into cyclic carbonates *via* reaction with epoxides. Two hybrid materials with different nucleophilic species (bromide and iodide) have been prepared and characterized by means of elemental analysis, ^{13}C and ^{29}Si solid state NMR, thermogravimetric analysis and IR spectroscopy. The solids were tested as the sole catalyst under metal- and solvent-free reaction conditions showing full selectivity toward the formation of cyclic carbonates and outstanding productivity values. Several epoxides were reacted with CO_2 proving a good catalytic versatility. The recyclability of the materials was successfully verified for four consecutive runs allowing to consider them as promising candidates for continuous flow technologies.

5.2 Results and Discussion

Imidazolium based cross-linked POSS nanohybrids were prepared by using a simple one-pot procedure. As reported in Scheme 1, the synthesis of the materials was performed by reacting octakis(3-bromopropyl)-octasilsesquioxane (compound **1a**, POSS-Br) or octakis(3-iodoopropyl)-octasilsesquioxane (compound **1b**, POSS-I) with 1,4-bis(imidazol-1-yl)-butane (compound **2**) to give the solids **3a** and **3b**, respectively.

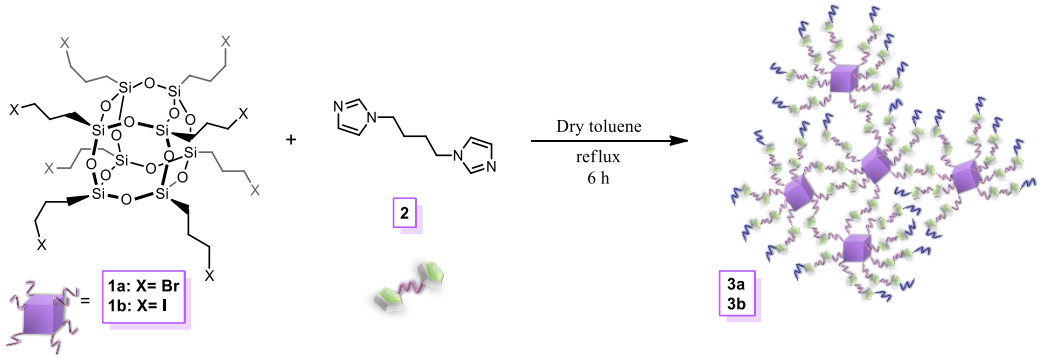

Scheme 1. Synthesis of imidazolium cross-linked POSS nanohybrids.

Thermogravimetric analysis (TGA) was performed on the starting POSS molecules (**1a**, **1b**) and on the final imidazolium based cross-linked networks (**3a**, **3b**) in order to study their thermal behavior (Figure 1).

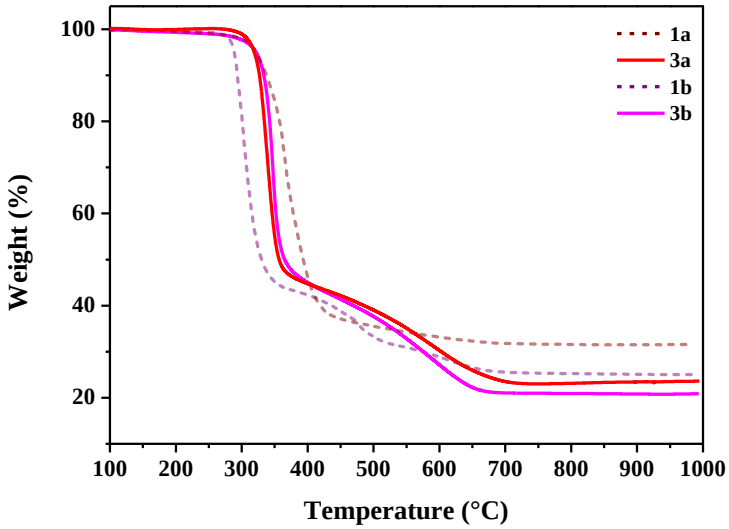

Figure 1. TGA profiles of POSS molecules (**1a**, **1b**) and imidazolium cross-linked networks (**3a**, **3b**).

TGA thermograms evidenced the good thermal stability of all the solids, as the degradation of organic moieties started in 250–300 °C range. In this respect, the thermal behavior of the imidazolium cross-linked nanohybrids is of paramount importance for their possible cyclic use under heating regimes. Furthermore, the catalytic loading of materials **3a** and **3b** was firstly determined by considering their residual weight at 800 °C associated to the POSS inorganic core. In agreement with these calculations, data collected from combustion chemical analysis (C, H, N) allowed to estimate the imidazolium halide catalytic loadings of 2.62 and 1.68 mmol/g for material **3a** and **3b**, respectively. The specific surface area of the cross-linked materials was determined by N_2 physisorption to be lower than 20 m^2 g^{-1}. ^{13}C and ^{29}Si magic angle spinning (MAS) solid state NMR measurements were carried out to gain insight into the structure of our materials. ^{29}Si MAS NMR spectra were recorded by the direct excitation (DE) of ^{29}Si (Figure 2).

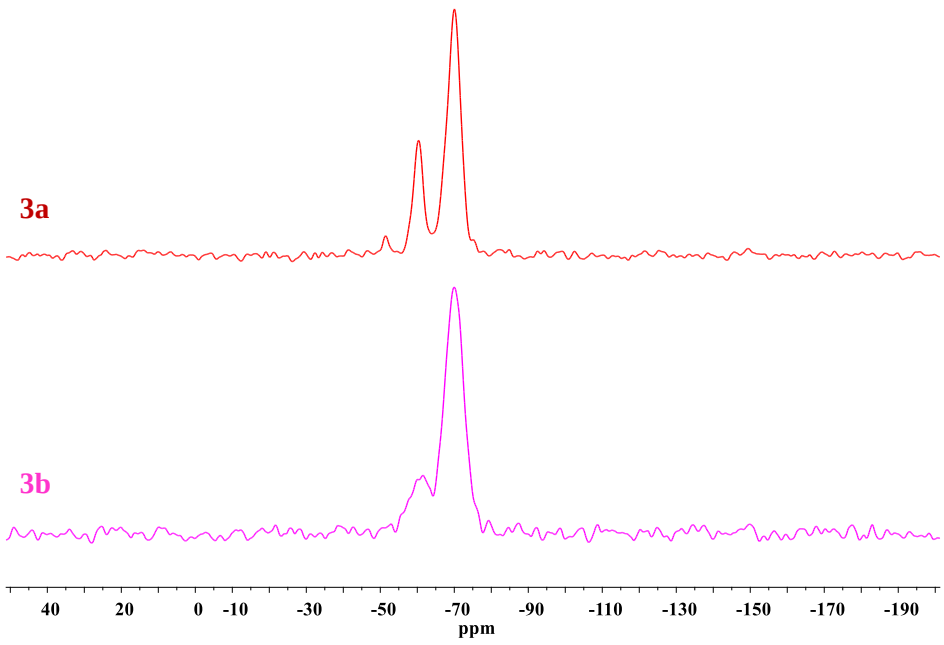

Figure 2. Solid state ^{29}Si DE MAS NMR spectra of **3a** and **3b**.

^{29}Si NMR spectra of **3a** and **3b** revealed the presence of the completely condensed T^3 silicon units [R-Si$(OSi)_3$] of POSS nanocages at δ = -70 ppm. The peaks at δ = -60 ppm could be ascribed to a partial distortion and/or a partial opening of the POSS core. However, it is not easy to discriminate between these

possible contributions. The first hypothesis agrees with some studies reported in literature[1] concerning the influence of Si–O–Si angle on the ^{29}Si NMR chemical shift in imidazolium modified POSS nanostructures. In our polymeric networks silicon nuclei are bonded to 1-methyl-3-propylimidazolium cross-linked branches but also to some unreacted halopropyl chains. From the above, different silicon chemical surroundings could give rise to the signals at around δ = -60 or -51 ppm. On the other hand, the presence of such signals can be due to a partial opening of POSS nanocage generating T^2 structures [R-Si(OSi)$_2$OR] at δ = -60 ppm or, in the case of material **3a**, T^1 silicon units [R-Si(OSi)(OR)$_2$] from the peak observed at δ = -51 ppm. Solid state ^{13}C NMR measurements were performed by using the cross polarization (CP) MAS total suppression side band (TOSS) pulse sequence to further characterize the structure of the materials through the qualitative detection of the isotropic chemical shift of carbon signals by removing the spinning side bands (Figure 3). ^{13}C NMR spectra of both **3a** and **3b** showed the signals of the carbon atoms of imidazolium ring in the range δ = 123–144 ppm, whereas the aliphatic ones were located in the range δ = 10–51 ppm.

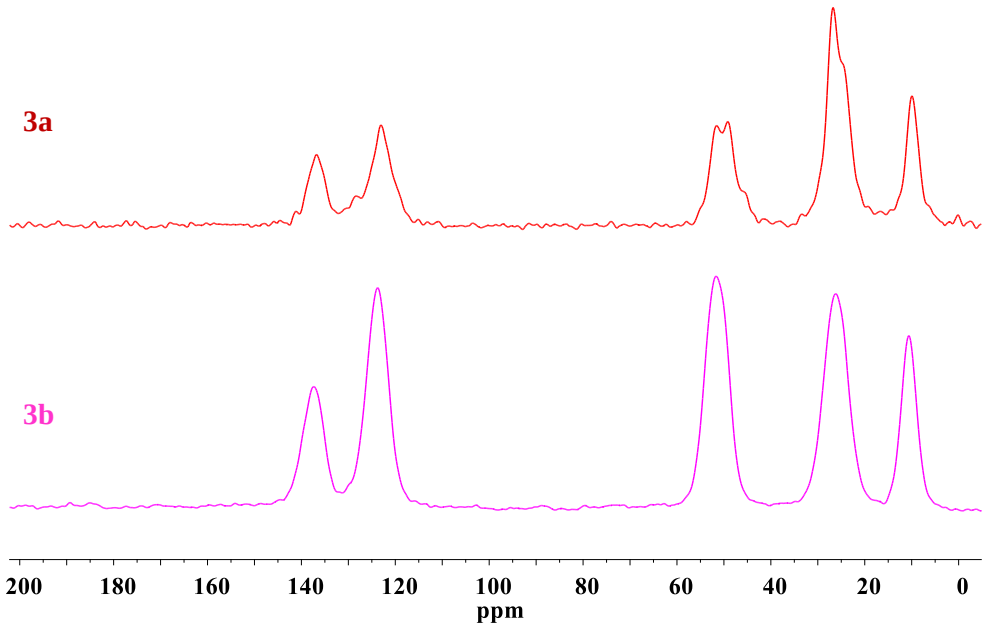

Figure 3. Solid state ^{13}C CP MAS TOS NMR spectra of **3a** and **3b**.

^{15}N CP MAS NMR analysis was also performed on material **3b**. ^{15}N CP MAS NMR spectrum was dominated by a prominent peak centered at δ = 181.8 ppm (Figure 4) and ascribed to nitrogen atoms of the imidazolium ring.

According to literature,[2] the absence of signals in the range δ = 230-260 ppm allowed us to rule out the presence of free dangling unreacted imidazole moieties.

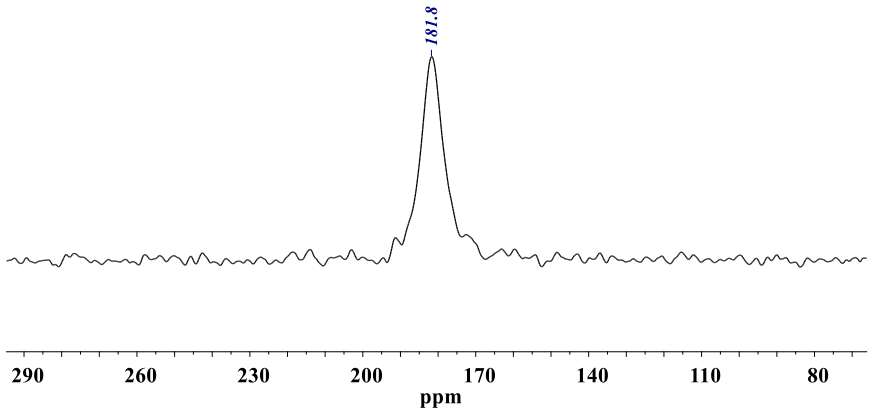

Figure 4. Solid state ^{15}N CP MAS NMR spectrum of **3b**.

Fourier transform infrared (FT IR) spectra of **3a** and **3b** and their POSS precursors (**1a** and **1b**) were recorded (Figure 5). All the materials displayed the typical Si–O–Si asymmetric stretching vibrations at around 1120 cm^{-1} whereas the deformational vibration of the silicon-oxygen framework is located in the region below 600 cm^{-1}. Si–C stretching can be observed at 750 cm^{-1}.

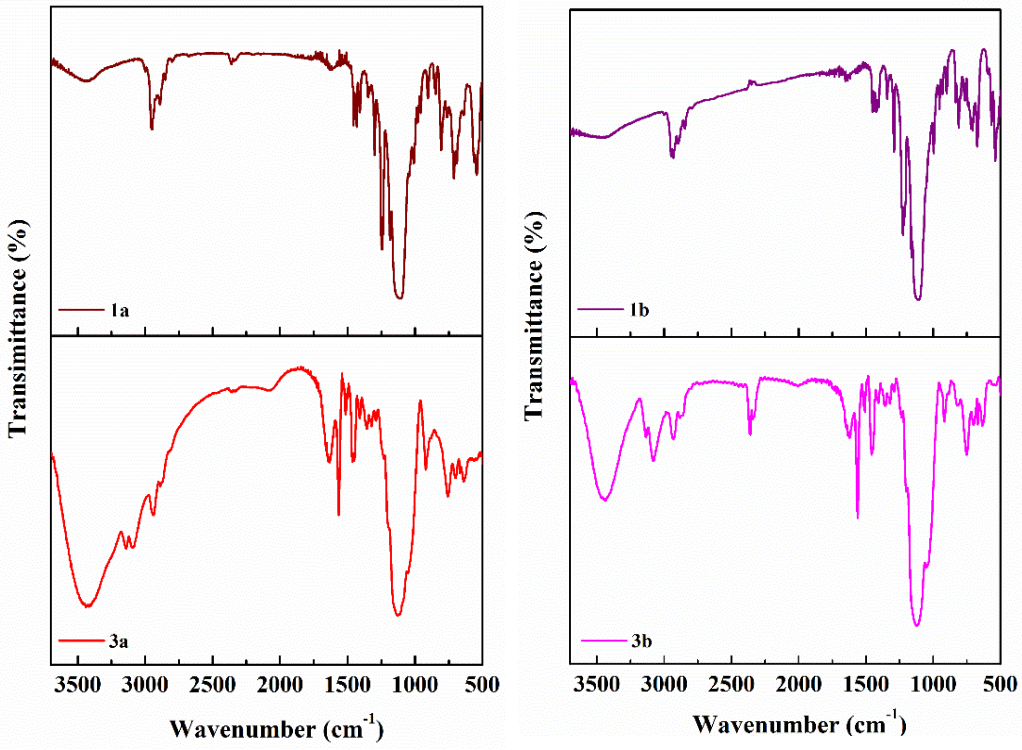

Figure 5. FT-IR spectra of **1a**, **1b**, **3a** and **3b**.

Moreover, IR spectra of hybrids **3a** and **3b** showed the presence of imidazolium moieties with stretching vibration of C=N at 1633 cm^{-1} and C–C stretching vibration at 1561 cm^{-1}. The bands at around 1450 cm^{-1} were ascribed to Si–CH_2 in plane deformation. In addition to the above, the bands in the range 2850–3140 cm^{-1} result from C–H stretching vibration of the methylene group and C–H stretching of imidazolium ring. Once characterized, both **3a** and **3b** were tested as heterogeneous organo-catalyst for the conversion of carbon dioxide into cyclic carbonates by reaction with epoxides. Their overall performance was deeply evaluated in terms of selectivity toward the formation of cyclic carbonates, recyclability, turnover number (TON calculated as moles of epoxide converted/moles of catalyst), versatility, and productivity (P calculated as grams of cyclic carbonates/grams of catalyst). The catalytic activity was studied under metal- and solvent free reaction conditions with an initial CO_2 pressure (P_i) of 4 MPa. The reaction between CO_2 and styrene oxide was selected with a dual purpose: to evaluate the effect of the anionic species and to check the recyclability of the materials. The recycling experiments were carried out to finely investigate the catalytic behavior and the robustness of the solids. For doing so, the catalytic tests were performed up to non-quantitative conversion of styrene oxide.

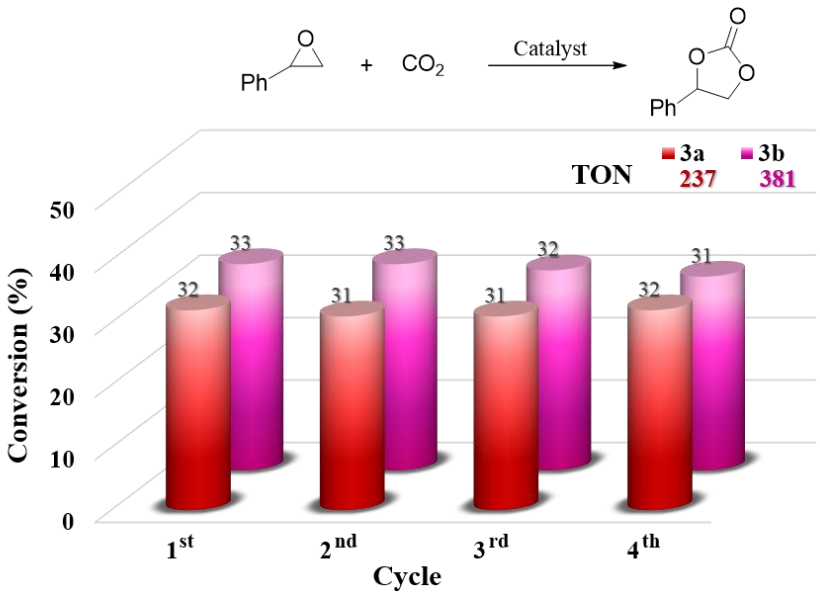

Figure 6. Recycling tests of materials **3a** and **3b**. Reaction conditions: styrene oxide (155 mmol), CO_2 (P_i 40 MPa), 80 mg of catalyst (0.210 mmol of **3a**, 0.135 mmol of **3b**), 150 °C, 3 h. TON calculated on the 1st cycle.

As illustrated in Figure 6, materials **3a** and **3b** were used for four consecutive runs at 150 °C without showing any considerable decrease of the catalytic performance. The conversion into styrene carbonate was almost the same for both catalysts. However, the solid **3b**, bearing imidazolium iodide moieties, reached a higher TON value (381 *vs* 237) than **3a** decorated with imidazolium bromide functionalities. This evaluation arises from the lower loading of active sites in **3b** by comparison with **3a**. Based on these preliminary results, our attention has been focused on the most active catalyst **3b** to proceed with deeper investigations. First of all, the reused catalyst from the fourth cycle was recovered to be characterized by means of TGA and ^{29}Si CP MAS NMR analysis. TGA analysis on **3b** after the fourth catalytic cycle was performed in order to check the thermal stability of the reused material. By comparison with the as-synthesized catalyst, the TGA thermogram of the reused solid showed a slightly different profile over the initial part of curve (Figure 7). In particular, for the reused **3b** the degradation of organic moieties started in 170–200 °C range, whereas for the fresh catalyst in 250–300 °C range. This behavior can be accounted to some local modifications of the imidazolium cross-linked network depending on the reaction conditions. This result could support the hypothesis that some reversible dealkylations of the organic salt[3] took place, generating novel arrangements of the cross-linked network.

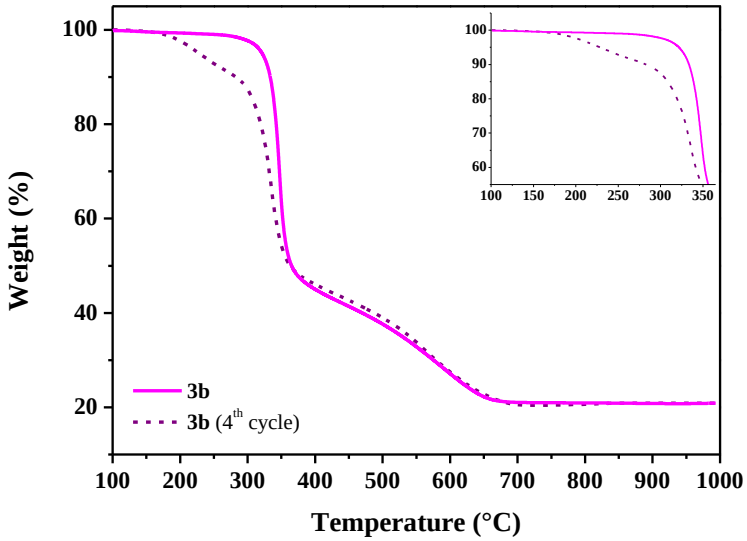

Figure 7. TGA profiles of as-synthesized and reused **3b**. Magnification of TGA curves (inset).

Furthermore, from the TGA thermogram of the reused material it is worth to note that, ranging from 368 °C until the end of the ramp (1000 °C), the curve of the reused catalyst matches perfectly to the profile of the as-synthesized **3b** showing the same weight loss. Then, ^{29}Si CP MAS NMR measurements were carried out on both the as-synthesized and the reused catalyst **3b**. The recorded spectra, reported in Figure 8, showed a similar profile being the silicon signals of the reused catalyst slightly shifted to higher frequencies compared to those of the as-synthesized solid. Analysis of data collected on the reused solid evidenced the good robustness of the material after recycling.

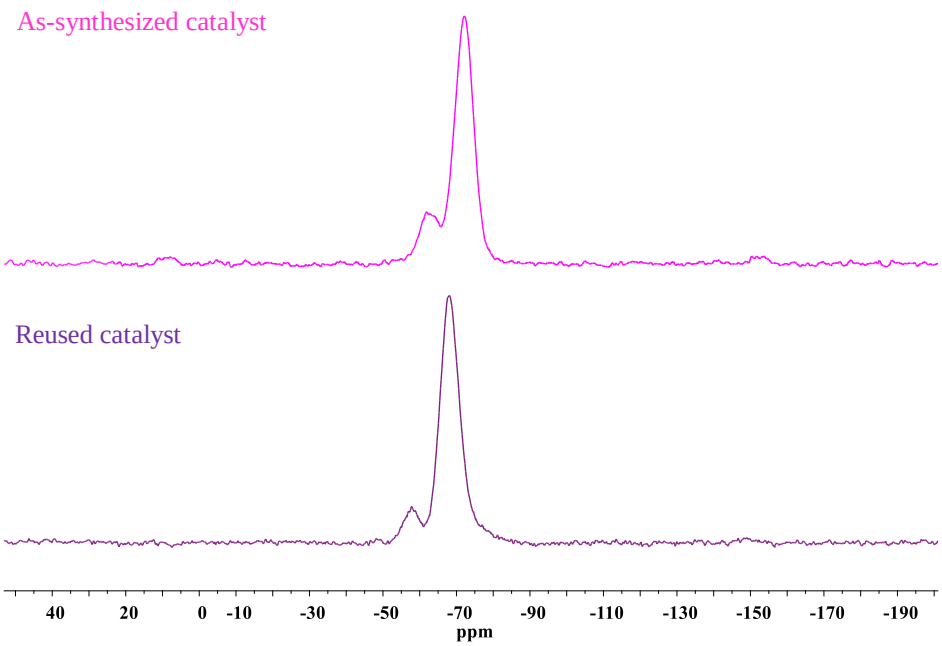

Figure 8. Solid state ^{29}Si CP MAS NMR spectra of as-synthesized and reused **3b**.

The catalytic versatility of **3b** was verified with several epoxides (Table 1). The coupling between epichlorohydrin and CO_2 was chosen for a general screening of the reaction conditions. A first catalytic test was run by using a catalytic loading of $2.2 \cdot 10^{-2}$ mol% at 150 °C for 3 h (Table 1, entry 1). The outstanding results in terms of conversion (93%), turnover number (4163) and productivity (945) directed to investigate the catalytic performance by working with a lower loading equal to $1.1 \cdot 10^{-2}$ mol%. In this case, a 53% conversion was reached together with improved TON and productivity values (4942 and 1122, respectively). The above coupling was carried out by using the catalyst recovered from the recycling test performed

with styrene oxide (Figure 6). The 5th catalytic cycle of **3b** led to the same epichlorohydrin conversion reached with the as synthesized **3b** (Table 1, entries 2–3). This result, once again, confirmed the good robustness and recyclability of the imidazolium cross-linked network.

Table 1. Synthesis of cyclic carbonates catalyzed by **3b**[a].

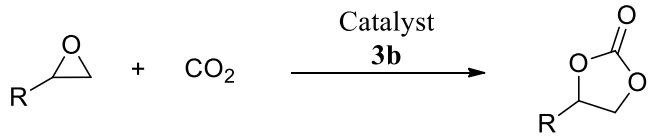

Entry	Substrate	Catalyst		Conv.	S	T	Time	TON	P
		[mg]	[mol%]	[%]	[%]	[°C]	[h]		
1	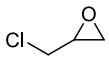	25	0.022	93	>99	150	3	4163	945
2	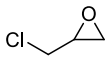	12	0.011	53	>99	150	3	4942	1122
3	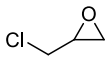	12[b]	0.011	53	>99	150	3	4942	1122
4	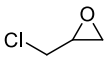	40	0.036	49	>99	100	16	1371	311
5		12	0.011	24	>99	150	3	2238	380
6	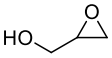	12	0.011	59	>99	100	3	5502	1081
7	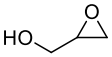	80	0.071	45	>99	50	16	630	124
8[c]		80	0.087	33	>99	150	3	381	104
9[c]		80	0.087	23	>99	150	16	265	63

[a] Conversion (Conv.), Selectivity (S), reaction time (t), Productivity. Reaction conditions: epoxide (188 mmol), CO_2 (P_i 4 MPa), catalyst **3b**, 150 °C. [b] Catalyst **3b** recovered from the 4th cycle showed in Figure 6. [c] Reaction conditions: epoxide (155 mmol), CO_2 (P_i 4 MPa), catalyst **3b**, 150 °C.

Furthermore, carbon dioxide fixation into epichlorohydrin was run at 100 °C affording 49% conversion into the corresponding cyclic carbonate in 16 h (entry

4). Next, the catalytic versatility was successfully proven with other epoxides such as propylene oxide, glycidol, and the less reactive cyclohexene oxide. The solid **3b** was employed at $1.1 \cdot 10^{-2}$ mol%, 100 °C for 3 h, leading to a 59% conversion into glycidol carbonate corresponding to remarkable TON and productivity values up to 5502 and 1081, respectively (Table 3, entry 6). Then, the catalyst, working at 0.071 mol%, was tested at 50 °C for 16 h giving 45% conversion into glycidol carbonate and still good TON and productivity values, 630 and 124, respectively (Table 3, entry 7).

5.3 Conclusions

Novel imidazolium cross-linked networks have been prepared by using polyhedral oligomeric silsesquioxanes as molecular bricks. A simple one-pot procedure has been followed for the synthesis of imidazolium nanohybrids bearing bromide (**3a**) or iodide (**3b**) as anionic species. The above materials have been characterized by means of elemental analysis, TGA, and IR spectroscopy. In order to get deeper insight on the structural properties, multinuclear (^{13}C, ^{29}Si, ^{15}N) solid state NMR investigation was carried out. The collected data evidenced the presence of POSS nanocages decorated with imidazolium salts. In the framework of our interest on carbon dioxide conversion, the catalytic ability of the above materials has been studied under both metal- and solvent-free reaction conditions. The catalyst performance assessment has been performed by considering some key criteria such as *i)* the selectivity toward the cyclic carbonate, *ii)* the recyclability of the catalysts, and *iii)* the achieved turnover number and productivity values. The robustness of materials **3a** and **3b** was successfully proven for four consecutive cycles in the reaction between CO_2 and styrene oxide. Furthermore, catalyst **3b** was chosen for deeper investigations showing high versatility with several epoxides, full selectivity combined with outstanding turnover number and productivity values up to 5502 and 1122, respectively. The very promising catalytic performance of both **3a** and **3b** paves the way to their possible use in continuous flow technologies.

5.4 Experimental Section

Spectroscopic and analytical methods

Chemicals and solvents were purchased from commercial suppliers to be used without further purification. Thermogravimetric analysis was carried out under oxygen flow from 100 to 1000 °C with a heating rate of 10 °C min^{-1} in a Mettler Toledo TGA STAR system. Elemental analysis was performed on a PerkinElmer 2400 Series II Elemental Analyzer. All the solid state MAS NMR experiments (^{13}C, ^{29}Si, ^{15}N) were performed at room temperature on a Bruker Avance 500 Spectrometer operating at 11.7 T, using a Bruker probe of 4 mm. CP-MAS-TOSS ^{13}C-NMR spectra were recorded using a contact time of 2 ms and a spinning rate of 5 KHz. The chemical shift scale was calibrated with respect to a sample of adamantane. DE-MAS ^{29}Si NMR spectra were recorded using 300 s relaxation delay, 3 μs (90 °) excitation pulse, 52 ms acquisition time and a spinning rate of 8 KHz. CP-MAS ^{29}Si NMR spectra were recorded, using a contact time of 2 ms, a spinning rate of 8 KHz. The chemical shift scale was calibrated with respect to a sample of solid 3-(trimethylsilyl)-1-propanesulfonic acid sodium salt. ^{15}N CP-MAS spectrum of **3b** was recorded using a contact time of 2 ms and a spinning rate of 10 KHz. The chemical shift scale was calibrated with respect to a sample of ammonium chloride.[4] IR spectra (KBr) were recorded on an Agilent Technologies Cary 630 FT-IR spectrometer. Specimens for these measurements were prepared by mixing 2 mg of the sample powder with 100 mg of KBr. Liquid state ^{1}H NMR spectra were collected on a JEOL ECA spectrometer operating at 9.4 T (400 MHz).

Synthesis of POSS 1a-b

POSS-Br[5] and POSS-I[6] were prepared according to literature procedures.

Synthesis of 1,4-bis(imidazol-1-yl)-butane (**2**)

1,4-bis(imidazol-1-yl)-butane was prepared according to a literature procedure by reaction between 1,4-dibromobutane and imidazole.[7]

Synthesis of materials 3a and 3b

A selected POSS nanostructure (0.284 mmol of **1a** or **b**) and 1,4-bis(imidazol-1-yl)-butane (1.136 mmol of **2**) were dissolved in toluene (3 mL) and stirred under reflux for 6 h. Then, the reaction mixture was cooled down to room temperature. The solid was recovered by centrifugation and washed with toluene, methanol, and diethyl ether to remove unreacted reactive or soluble oligomeric species. Before each centrifugation, the solid was sonicated for few min in the washing solvent. Materials **3a** and **3b** were obtained as white solids and dried at 60 °C under vacuum.

Catalytic tests

The catalytic tests were run in a Cambridge Design Bullfrog batch reactor with temperature control and mechanical stirring, designed to operate at high temperature and pressures. A fine dispersion of the catalyst into the selected epoxide was transferred inside the reactor. Then, the reactor was closed and the mechanical stirring speed set at 500 rpm. The system was purged with N_2 for 10 min (0.4 MPa) and then, pressurized with CO_2. The temperature was increased to 150 °C with a rate of 5 °C min^{-1}. The reaction mixture was stirred at 150 °C for 3 h. Then, the reaction mixture was cooled down to room temperature and a slow depressurization of the reactor was carried out. The separation of the catalyst from the reaction mixture was easily performed by centrifugation (10 min at 4500 rpm). The supernatant solution was sampled and analyzed by ^1H NMR spectroscopy.

Recycling tests

The recyclability of the materials **3a** and **3b** was verified in the coupling between styrene oxide and CO_2. At the end of each test, the catalyst was recovered by centrifugation and washed with toluene (3x35 mL) and diethyl ether. Before each centrifugation, the solid was previously sonicated in the washing solvent up to get a good dispersion. Then, the catalyst was dried under vacuum at 60 °C. Once dried, the materials were reused for the next cycle by

modulating epoxide amount in function of the recovered catalyst in order to keep the ratio between moles of catalyst and moles of epoxides. The conversions of styrene oxide into cyclic carbonate was estimated by ^{1}H NMR analysis.

5.5 References

[1] L. A. Bivona, O. Fichera, L. Fusaro, F. Giacalone, M. Buaki-Sogo, M. Gruttadauria, C. Aprile, *Catalysis Science & Technology* **2015**, *5*, 5000-5007.

[2] L. T. A. Sofia, A. Krishnan, M. Sankar, N. K. Kala Raj, P. Manikandan, P. R. Rajamohanan, T. G. Ajithkumar, *The Journal of Physical Chemistry C* **2009**, *113*, 21114-21122.

[3] F. D'Anna, H. Q. Nimal Gunaratne, G. Lazzara, R. Noto, C. Rizzo, K. R. Seddon, *Organic & Biomolecular Chemistry* **2013**, *11*, 5836-5846.

[4] P. Bertani, J. Raya, B. Bechinger, *Solid State Nuclear Magnetic Resonance* **2014**, *61-62*, 15-18.

[5] W. Zhang, Z.-S. Wang, *ACS Applied Materials & Interfaces* **2014**, *6*, 10714-10721.

[6] V. Ervithayasuporn, N. Pornsamutsin, P. Prangyoo, K. Sammawutthichai, T. Jaroentomeechai, C. Phurat, T. Teerawatananond, *Dalton Transactions* **2013**, *42*, 13747-13753.

[7] J. S. Parent, A. M. J. Porter, M. R. Kleczek, R. A. Whitney, *Polymer* **2011**, *52*, 5410-5418.

CHAPTER VI

Carbon–Carbon Cross Coupling Reactions Catalyzed by Supported Palladium Species

An Introduction to Chapters VII and VIII

CHAPTER VI

Carbon–Carbon Cross Coupling Reactions Catalyzed by Supported Palladium Species An Introduction to Chapters VII and VIII

6.1 Palladium Catalyzed C–C Couplings

The increasing demand of highly active and recyclable catalytic materials for C−C cross coupling reactions pushed the scientific research toward the design of performing heterogeneous hybrids. The importance of C−C bond formation process is well known in organic synthesis including the preparation of pharmaceuticals, drugs, agrochemicals, natural products, and the design of organic semiconductors. In particular, palladium catalyzed C−C couplings emerged as one of the most versatile tools as testified not only by the awarding of the Nobel Prize in Chemistry in 2010 to R. F. Heck, E.-C. Negishi and A. Suzuki, but also by the continuous growing publications on this field.[1] In order to improve the sustainability of such reactions, a broad spectrum of palladium based heterogeneous catalysts has been developed.[2] In this context, the reduction of waste generation is indeed connected to an easy recovery and reuse of the catalyst itself. Furthermore, a lower metal contamination of the final products is typically achieved with heterogeneous catalyst by comparison to the corresponding homogeneous reaction conditions. On this last point, it is worth to look at the strict regulations on the maximum allowable amount of metal contaminants, for example, for pharmaceutical compounds (< 5 ppm).[3] Palladium catalysts have been immobilized onto a plethora of pre-functionalized solid supports such as mesostructured[4] and amorphous silica,[5] zeolites,[6] organic polymers,[7] ionic liquids,[8] magnetic nanocomposites,[9] carbon nanoforms,[10] halloysite nanotubes,[11] and MOFs[12]. Herein, imidazolium based organic salts have been covalently grafted onto several nanostructured supports

(MWCNTs, CNHs, POSS) in order to be employed as heterogeneous platform for palladium species, namely Pd nanoparticles (NPs) and tetrachloropalladate salts. The overall catalytic performance of the obtained materials has been checked for Suzuki-Miyaura and Heck C−C cross-coupling reactions.

6.2 Imidazolium Salts as Palladium Support

Carbon−carbon bond formation is traditionally associated with homogeneous catalytic processes. In this scenario, soluble palladium complexes are highly active. However, these systems deal with downsides of paramount importance: *i)* the separation of the catalyst from the reaction mixture and thus its recyclability, *ii)* the purification of the final product, and *iii)* the overall high costs. On this background, organic chemical industry is drawing the attention toward the design of cheaper heterogeneous catalysts able to be used in continuous flow reactors. In general terms, it is well known that the catalytic performance of heterogeneous systems is strictly related to an efficient dispersion of the catalyst itself.

In the field of palladium catalyzed coupling reactions, imidazolium salts emerged as suitable dispersion media and palladium supports for the design of functional hybrid materials. In particular, palladium active species can be immobilized onto imidazolium based organic salts as metal nanoparticles (MNPs) or organometallic complexes.

Transition MNPs display unique properties resulting from their large surface to volume ratio. Owing to their low thermodynamic stability, soluble MNPs tend to evolve toward larger aggregates in the absence of stabilizing agents. To avoid their agglomeration and hence the catalytic deactivation, palladium NPs require the use of specific agents able to stabilize them through electronic and/or steric effects.

Ranging from the synthesis to the application, the stabilizing agents play a pivotal role in the control of the MNPs diameter, shape and size distribution, surface properties and thus the catalytic performance. Imidazolium salts are able to provide electrostatic and steric stabilization of transition MNPs.[13] On the ground of this finding, supported imidazolium salts can be used as heterogeneous platform for Pd

NPs in the field of catalysis.[14] The nature of the interaction between imidazolium salts and MNPs is still disputed. In this respect, Serpell *et al.* reported some dissertations on MNPs coated by imidazolium ionic liquids, as showed in Figure 1.[15] In particular, the stabilization of MNPs has been explained through Coulomb repulsions. Such hypothesis arises from: *i)* the interaction between the positively charged MNPs outer surface and the ILs anions; *ii)* the resulting negatively charged layer covered by the cationic species of the organic salts (Figure 1a).[16] Another possible interaction between MNPs and imidazolium moieties was proposed by Finke *et al.* as *N*−heterocyclic carbene (NHC) stabilization of iridium NPs (Figure 1b).[17] Furthermore, based on surface-enhanced Raman spectroscopy (SERS) studies, Dupont *et al.* ascribed the surface stabilization of gold NPs to parallel coordination of imidazolium units (Figure 1c).[18] However, it is worth to mention that the effective stabilization mode of MNPs by imidazolium salts depends on the specific system.

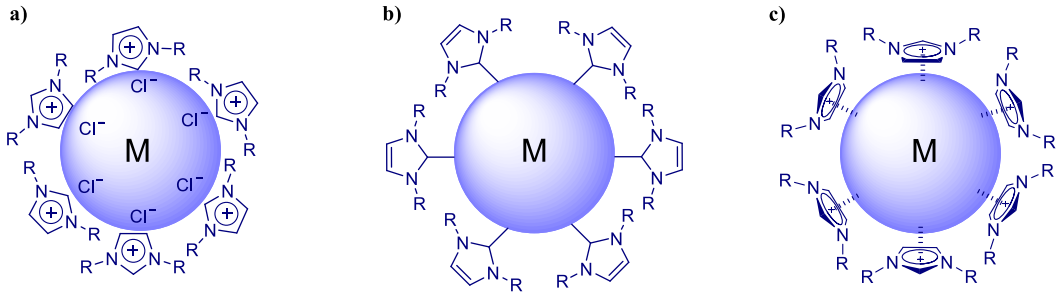

Figure 1. Stabilization of metal nanoparticles in ionic liquids media.[15]

The synthesis of Pd NPs can be performed by following several strategies such as chemical reduction, vapor phase deposition, electrochemical methods, laser ablation, sonochemical reduction, seed-mediated approaches, and microwave reduction.[19] In this PhD dissertation (Chapter VII), imidazolium based cross-linked networks, grafted on both MWNTs and CNHs, have been used as solid supports for Pd NPs. The synthesis of Pd NPs was carried out by the chemical reduction approach. This strategy involves the use of Na_2PdCl_4 as metal precursor and $NaBH_4$ as reducing agent. The reduction process starts with the formation of several nucleation sites which evolves in growing nanoparticles that can increase in size up to the precipitation as bulk metal in the absence of stabilizing agents. Herein,

imidazolium networks have been employed to prevents the undesired agglomeration of the resulting Pd NPs.

Otherwise, Pd^{II} species have been dispersed into imidazolium frameworks in order to be tested as pre-catalysts avoiding the use of a reducing agents. POSS nanostructures have been modified with imidazolium functionalities to be used as support for Pd^{II}.[20] Such hybrids were employed as pre-catalysts for Suzuki-Miyaura and Heck couplings.

In Chapter VIII, a novel hybrid material based on supported tetrachloropalladate species will be presented. In particular, imidazolium modified POSS hybrids grafted into mesostructured SBA-15 have been used as solid supports for the immobilization of Pd^{II} species. Inspired by the promising catalytic performance of POSS imidazolium tetrachloropalladate salts,[20a] our hybrid was prepared by following a modular synthesis in which POSS units were previously grafted into the solid support in order to be modified with imidazolium chloride moieties. The solid was treated with Na_2PdCl_4 to give the final hybrid by ionic exchange. Next, the obtained material was tested as pre-catalyst in Suzuki-Miyaura and Heck reactions.

6.3 References

[1] a) C. C. C. J. Seechurn, M. O. Kitching, T. J. Colacot, V. Snieckus, *Angewandte Chemie International Edition* **2012**, *51*, 5062-5085; b) D. Roy, Y. Uozumi, *Advanced Synthesis & Catalysis* **2018**, *360*, 602-625; c) Á. Molnár, *Chemical Reviews* **2011**, *111*, 2251-2320; d) A. Suzuki, *Angewandte Chemie International Edition* **2011**, *50*, 6722-6737; e) E. i. Negishi, *Angewandte Chemie International Edition* **2011**, *50*, 6738-6764.

[2] a) Yin, J. Liebscher, *Chemical Reviews* **2007**, *107*, 133-173; b) M. Lamblin, L. Nassar-Hardy, J. C. Hierso, E. Fouquet, F. François-Xavier, *Advanced Synthesis & Catalysis* **2010**, *352*, 33-79; c) O. Nicolas, F. François-Xavier, *ChemCatChem* **2016**, *8*, 1998-2009.

[3] G. C. E., P. Kapa, *Advanced Synthesis & Catalysis* **2004**, *346*, 889-900.

[4] S. M. Sarkar, M. L. Rahman, M. M. Yusoff, *New Journal of Chemistry* **2015**, *39*, 3564-3570.

[5] a) M. Opanasenko, P. Stepnicka, J. Cejka, *RSC Advances* **2014**, *4*, 65137-65162; b) C. Pavia, E. Ballerini, L. A. Bivona, F. Giacalone, C. Aprile, L. Vaccaro, M. Gruttadauria, *Advanced Synthesis & Catalysis* **2013**, *355*, 2007-2018.

[6] A. Kumbhar, *Topics in Current Chemistry* **2016**, *375*, 2.

[7] a) C. A. Wang, Y. W. Li, X. M. Hou, Y. F. Han, K. Nie, J. P. Zhang, *ChemistrySelect* **2016**, *1*, 1371-1376; b) X. Wang, S. Min, S. K. Das, W. Fan, K.-W. Huang, Z. Lai, *Journal of Catalysis* **2017**, *355*, 101-109.

[8] S. Navalón, M. Álvaro, H. García, *ChemCatChem* **2013**, *5*, 3460-3480.

[9] a) R. Ma, P. Yang, F. Bian, *New Journal of Chemistry* **2018**, *42*, 4748-4756; b) K. Manjunatha, T. S. Koley, V. Kandathil, R. B. Dateer, G. Balakrishna, B. S. Sasidhar, S. A. Patil, S. A. Patil, *Applied Organometallic Chemistry* **2018**, *32*, e4266.

[10] a) M. Adib, R. Karimi-Nami, H. Veisi, *New Journal of Chemistry* **2016**, *40*, 4945-4951; b) F. Giacalone, V. Campisciano, C. Calabrese, V. La Parola, Z. Syrgiannis, M. Prato, M. Gruttadauria, *ACS Nano* **2016**, *10*, 4627-4636; c) M. Barahman, P. F. S., N. Mozhgan, *Applied Organometallic Chemistry* **2015**, *29*, 40-44; d) M. Navidi, N. Rezaei, B. Movassagh, *Journal of Organometallic Chemistry* **2013**, *743*, 63-69; e) V. Campisciano, V. L. Parola, L. F.Liotta, F. Giacalone, M. Gruttadauria, *Chemistry – A European Journal* **2015**, *21*, 3327-3334.

[11] a) M. Massaro, S. Riela, G. Lazzara, M. Gruttadauria, S. Milioto, R. Noto, *Applied Organometallic Chemistry* **2014**, *28*, 234-238; b) M. Massaro, V. Schembri, V. Campisciano, G. Cavallaro, G. Lazzara, S. Milioto, R. Noto, F. Parisi, S. Riela, *RSC Advances* **2016**, *6*, 55312-55318.

[12] a) S. Rong, L. Bing, L. Bo-Geng, J. Suyun, *ChemCatChem* **2016**, *8*, 3261-3271; b) X. Li, R. Van Zeeland, R. V. Maligal-Ganesh, Y. Pei, G. Power, L. Stanley, W. Huang, *ACS Catalysis* **2016**, *6*, 6324-6328; c) G. Xiong, X.-L. Chen, L.-X. You, B.-Y. Ren, F. Ding, I. Dragutan, V. Dragutan, Y.-G. Sun, *Journal of Catalysis* **2018**, *361*, 116-125.

[13] a) M.-A. Neouze, *Journal of Materials Chemistry* **2010**, *20*, 9593-9607; b) P. Migowski, J. Dupont, *Chemistry – A European Journal* **2006**, *13*, 32-39; c) J. Dupont, J. D. Scholten, *Chemical Society Reviews* **2010**, *39*, 1780-1804.

[14] a) F. Giacalone, M. Gruttadauria, *ChemCatChem* **2016**, *8*, 664-684; b) V. Campisciano, F. Giacalone, M. Gruttadauria, *The Chemical Record* **2017**, *17*, 918-938.

[15] C. J. Serpell, J. Cookson, A. L. Thompson, C. M. Brown, P. D. Beer, *Dalton Transactions* **2013**, *42*, 1385-1393.

[16] S. Özkar, R. G. Finke, *Journal of the American Chemical Society* **2002**, *124*, 5796-5810.

[17] L. S. Ott, M. L. Cline, M. Deetlefs, K. R. Seddon, R. G. Finke, *Journal of the American Chemical Society* **2005**, *127*, 5758-5759.

[18] H. S. Schrekker, M. A. Gelesky, M. P. Stracke, C. M. L. Schrekker, G. Machado, S. R. Teixeira, J. C. Rubim, J. Dupont, *Journal of Colloid and Interface Science* **2007**, *316*, 189-195.

[19] D. B. Pacardo, M. R. Knecht, in *Metal Nanoparticles for Catalysis: Advances and Applications* (Ed.: F. Tao), The Royal Society of Chemistry, **2014**, pp. 112-156.

[20] a) L. A. Bivona, F. Giacalone, E. Carbonell, M. Gruttadauria, C. Aprile, *ChemCatChem* **2016**, *8*, 1685-1691; b) S. Mohapatra, T. Chaiprasert, R. Sodkhomkhum, R. Kunthom, S. Hanprasit, P. Sangtrirutnugul, V. Ervithayasuporn, *ChemistrySelect* **2016**, *1*, 5353-5357; c) V. Somjit, M. W. C. Man, A. Ouali, P. Sangtrirutnugul, V. Ervithayasuporn, *ChemistrySelect* **2018**, *3*, 753-759.

CHAPTER VII

Imidazolium Functionalized Carbon Nanohorns and Carbon Nanotubes as Pd Nanoparticles Support for C–C Cross Coupling

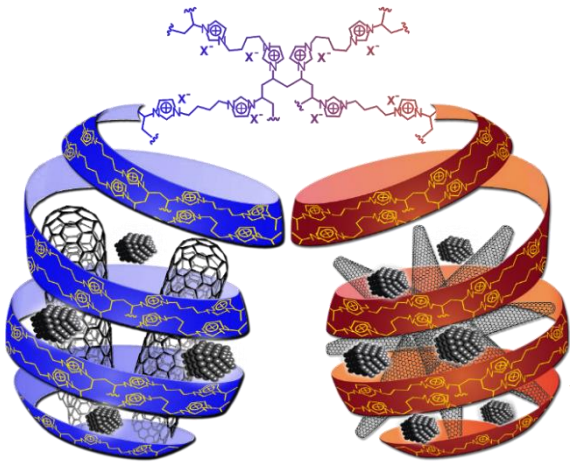

This chapter is based on:

Appl. Organometal. Chem., **2019**, doi: 10.1002/aoc.4848.

CHAPTER VII

Imidazolium Functionalized Carbon Nanohorns and Carbon Nanotubes as Pd Nanoparticles Support for C–C Cross Coupling

7.1 Abstract

Two different carbon nanoforms (CNFs), namely multi-walled carbon nanotubes (MWCNTs) and carbon nanohorns (CNHs), have been chosen as support for the direct polymerization of a bis-vinylimidazolium salt. TEM analyses revealed a templating effect of the CNFs on the growth of the polymeric network, which perfectly covers their whole surfaces creating a cylindrical or a spherical coating for MWCNTs and CNHs, respectively. The CNFs-polyimidazolium have been used as stabilizers for Pd nanoparticles (Pd NPs). The obtained materials have been characterized by means of analytical and spectroscopic techniques, and then employed as easily recoverable and recyclable catalysts for Suzuki and Heck reactions. Quantitative conversions have been reached in almost all the explored reactions, even employing low catalytic loading (down to 0.007 mol%). Suzuki reactions were carried out in pure water under aerobic conditions. Both materials showed excellent activity and recyclability for the investigated C–C coupling reactions with the CNHs-based material resulting slightly more active than the MWCNTs-based one due to a higher superficial exposure of Pd NPs.

7.2 Results and Discussion

Carbon nanotubes and carbon nanohorns were selected as highly attractive materials for the immobilization of imidazolium networks acting as stabilizing agents for palladium nanoparticles. As a result, similar to imidazolium functionalized CNHs reported in Chapter III, two carbon nanostructures were modified with imidazolium based cross-linked networks *via* direct polymerization of a bis-vinylimidazolium salt. The novel hybrid materials were easily prepared through the straightforward synthetic strategy depicted in Scheme 1. Radical polymerization of bis-vinylimidazolium salt **1** onto the MWCNTs and CNHs surface was started by thermal decomposition of radical initiator 2,2'-azobis(2-methylpropionitrile) (AIBN) in ethanol, at reflux.[1] The obtained poly-imidazolium salt coated materials MWCNT-Imi **2** and CNH-Imi **4** were dispersed in water in the presence of Na_2PdCl_4 to proceed with ion-exchange of bromides with tetrachloropalladate ions, followed by reduction with $NaBH_4$ in ethanol leading to the final materials MWCNT-Imi-Pd **3** and CNH-Imi-Pd **5**, respectively.

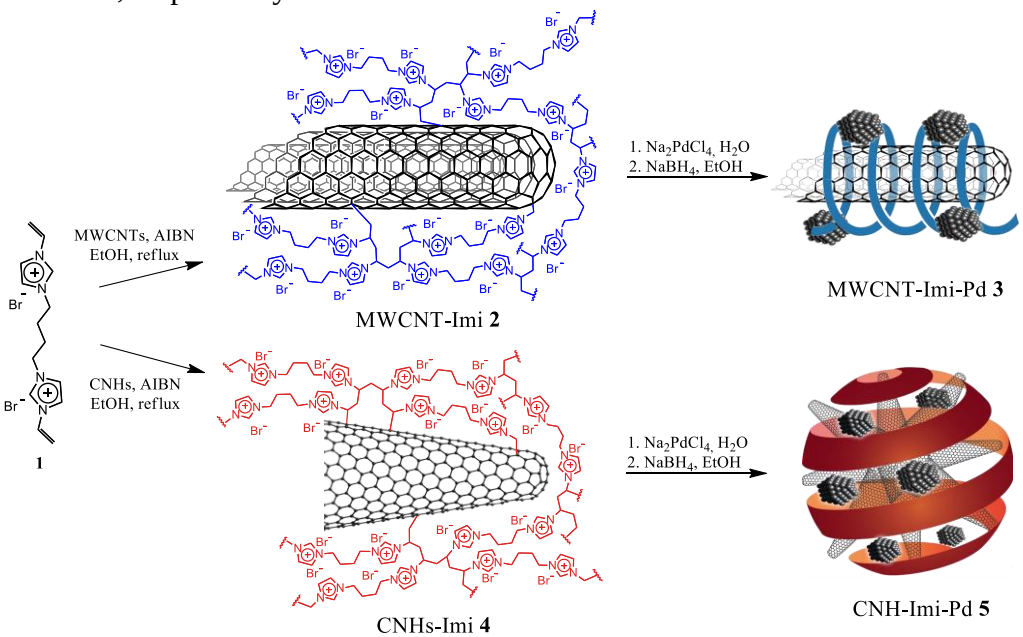

Scheme 1. Synthetic procedure for the preparation of materials MWCNT-Imi-Pd **3** and CNH-Imi-Pd **5**.

It is worth noting that the above approach represents a versatile strategy to accede to a number of heterogeneous catalysts, given that different metal

nanoparticle precursors can be adopted and stabilized or even polyoxometalate species can be immobilized through ionic-exchange. The poly-imidazolium salt loadings of materials MWCNT-Imi **2** and CNH-Imi **4** were estimated from thermogravimetric analysis (TGA) under N_2 by considering the weight losses at 700°C corresponding to 92.5 and 88.6 wt%, respectively (Figure 1).

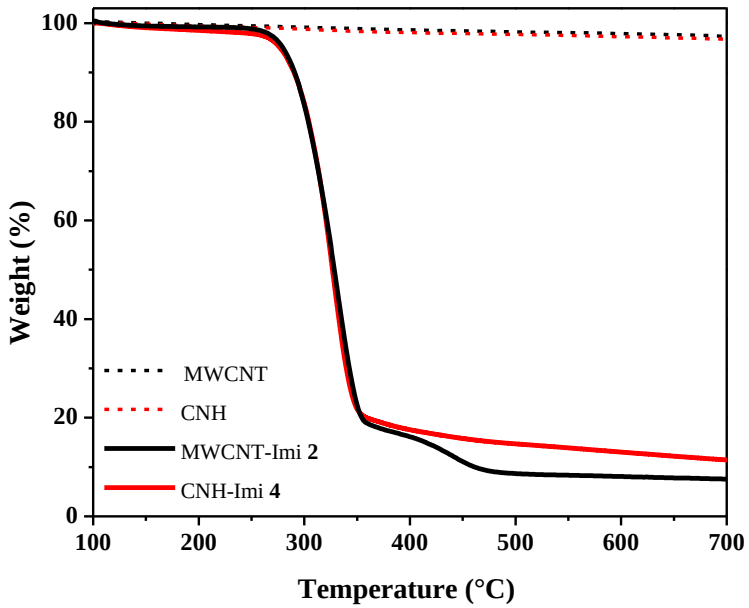

Figure 1. TGA profiles under N_2 of pristine (dashed lines) and functionalized (solid lines) MWCNTs and CNHs.

TGA profiles of pristine MWCNTs and CNHs showed very low weight losses at the same temperature (2.8 and 3.3 wt%, respectively). Therefore, the calculated poly-imidazolium salt loading of materials MWCNT-Imi **2** and CNH-Imi **4** was found to be 2.28 and 2.13 mmol/g, respectively.

Imidazolium functionalized hybrids **2**–**5** were characterized by solid state ^{13}C cross-polarization magic angle spinning NMR (CP-MAS) spectroscopy (Figure 2). The collected spectra of materials **2** and **4** confirmed the good outcoming of the polymerization step, as evidenced by the absence of vinyl signals at around 110 ppm. Carbon atom signals of the imidazolium ring were clearly observed at δ = 120–140 ppm, whereas the aliphatic ones were detected in the 20–60 ppm region. Furthermore, the comparison between Pd supported hybrids and their precursors (**2** and **4**) showed no relevant differences.

The morphology of both pristine and functionalized carbon nanoforms was investigated by high-resolution transmission electron microscopy (HR-TEM,

Figure 3). As evidenced in Figure 3a, pristine MWCNTs were aggregated in ropes and bundles.

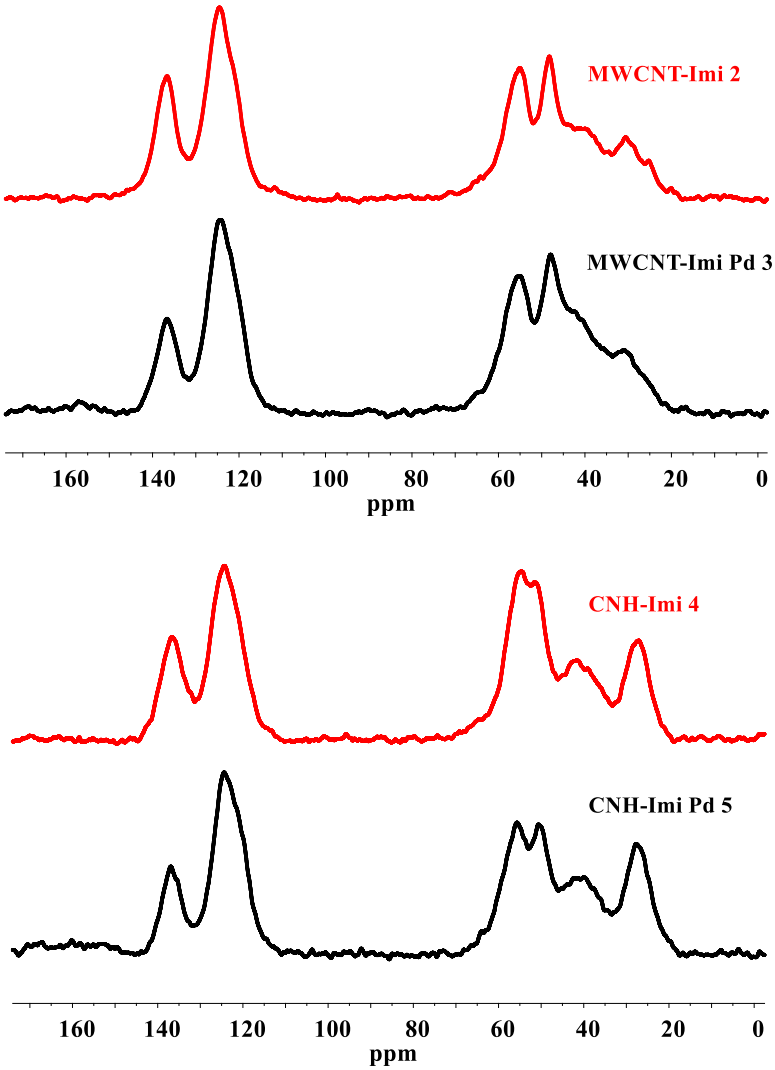

Figure 2. ^{13}C CP-MAS NMR spectra of materials MWCNT-Imi **2**, MWCNT-Imi-Pd **3**, CNH-Imi **4** and CNH-Imi-Pd **5**.

Then, the polymerization of bis-vinylimidazolium salt **1** led to a better dispersion of the CNTs, almost all uniformly wrapped by poly-imidazolium network (Poly-Imi) that creates a perfect cylindrical coating with a mean outer diameter of ~100 nm (Figure 3b). Similar results were obtained by Li, Chen *et al.* which functionalized MWCNTs with a methylimidazolium salt derivative by free-radical polymerization.[2] It is noteworthy to point out that polymerization of bis-vinylmidazolium salts onto different supports, such as silica, could result in a physical mixture composed of supported Poly-Imi and homopolymerized

imidazolium salt, as previously reported.[3] Herein, no traces of isolated domains of homopolymer were found. This finding could be explained considering that CNTs can act as a sort of templating agent that leads the polymerization of the bis-vinylmidazolium salt monomer to take place around the nanotube skeleton. TEM images of imidazolium functionalized CNH-Imi **4** (Figure 3f) showed the presence of a spherical-like coating of Poly-Imi uniformly distributed onto the surface of CNHs. In the case of Pd supported MWCNTs hybrid, only at high magnifications it was possible to detect very small Pd NPs uniformly distributed onto the 3D Poly-Imi network of MWCNT-Imi-Pd **3**. However, it was not possible to estimate the size of such nanoparticles (Figure 3d). Conversely, in CNHs based materials **5**, palladium NPs were clearly observed (Figure 3g–h), showing a bimodal distribution with a mean particle size of 28.8 ± 12.0 nm (n = 66) and 2.6 ± 0.6 nm (n = 282), for the big and the small NPs, respectively. It is interesting to note that, in this case, NPs are mainly located on the outer part of the hybrid material being thus more available for the catalysis.

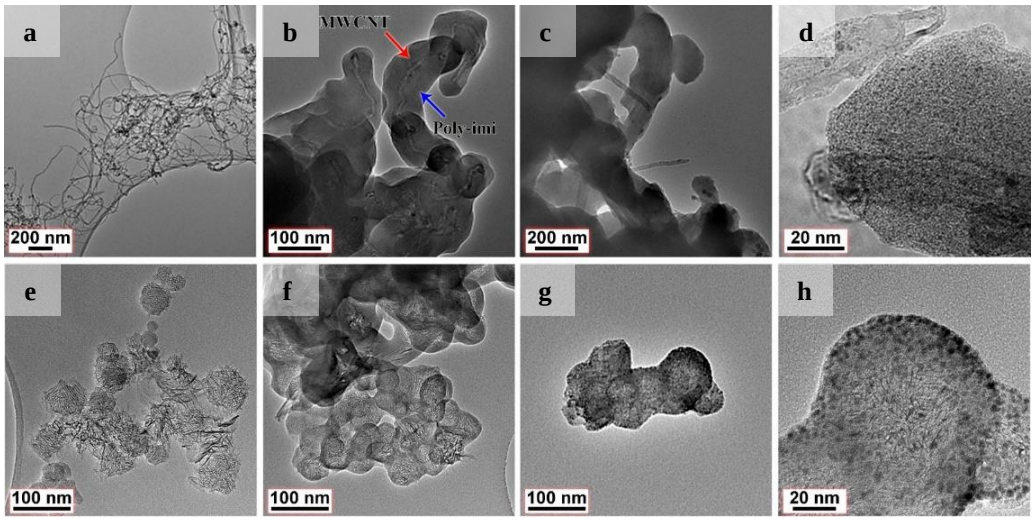

Figure 3. Representative HR-TEM images of a) pristine MWCNT, b) MWCNT-Imi **2**, c-d) MWCNT-Imi-Pd **3**, e) pristine CNHs, f) CNH-Imi **4**, g-h) CNH-Imi-Pd **5**.

Palladium loading of materials MWCNT-Imi-Pd **3** and CNH-Imi-Pd **5** was quantified by microwave plasma-atomic emission spectrometry (MP-AES) to be 7.6 and 7.1 wt%, respectively.

Furthermore, materials MWCNT-Imi-Pd **3** and CNH-Imi-Pd **5** were subjected to X-ray photoelectron spectroscopy (XPS) analysis (Figure 4) to estimate the

degree of reduction of palladium after the treatment with $NaBH_4$. The results, summarized in Table 1, showed how the degree of reduction was quite similar for both materials being the content of Pd(0) equal to 61 and 63% for MWCNT-Imi-Pd **3** and CNH-Imi-Pd **5**, respectively. Moreover, it is worth to note that, although the palladium loading of material **3** is slightly higher than that of **5** (7.6 vs 7.1 wt%), the Pd/C atomic ratio determined by XPS is the same revealing a higher surface exposure of Pd NPs in the latter hybrid (Table 1). This finding is in agreement with HR-TEM analysis.

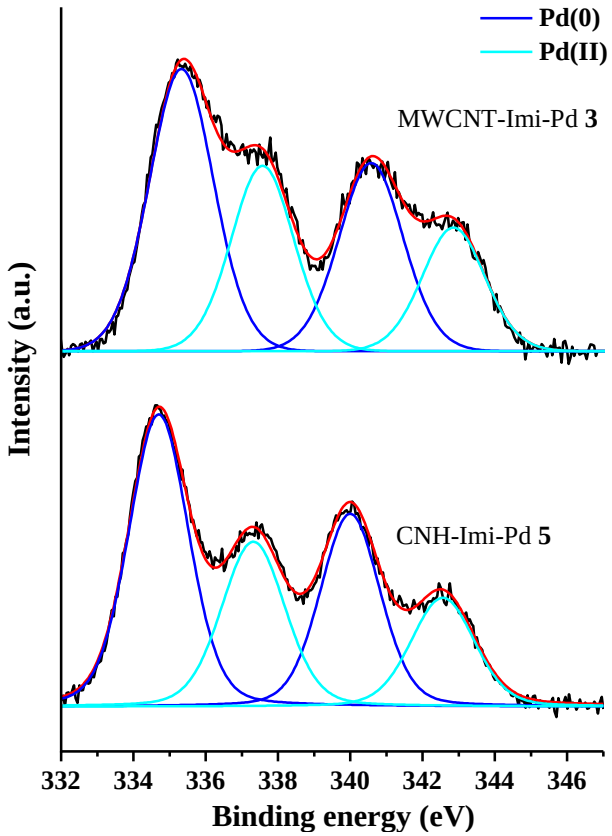

Figure 4. High-resolution XPS of the Pd3d region of materials MWCNT-Imi-Pd **3** and CNH-Imi-Pd **5**.

Table 1. $Pd3d_{5/2}$ binding energies (eV), relative percentages (%) and Pd/C atomic ratios of MWCNT-Imi-Pd **3** and CNH-Imi-Pd **5**.

	MWCNT-Imi-Pd **3**	CNH-Imi-Pd **5**
Pd(0)	335.3 (61)	334.7 (63)
Pd(II)	337.6 (39)	337.3 (37)
Pd/C	0.016	0.016

Once the materials were fully characterized, MWCNT-Imi-Pd **3**, and CNH-Imi-Pd **5** were tested as heterogeneous catalysts in the Suzuki reaction.

The catalytic runs were performed in pure water at 100 °C. Firstly, the coupling of 4-bromobenzaldehyde with phenylboronic acid was selected as probe reaction to investigate the effect of three different bases, namely K_2CO_3, K_3PO_4, and diisopropylamine (DIPA). For doing so, catalyst **3** was employed at 0.1 mol%. When K_2CO_3 and K_3PO_4 were used as base, the conversion into biphenyl-4-carboxaldheyde was found to be 70% and 75%, respectively after 6 h (Table 1, entries 1–2). However, the same coupling, carried out in the presence of DIPA, gave rise to a quantitative conversion in just 2 h (entry 3). Such reaction was also catalyzed by CNH-Imi-Pd **5** at 0.07 mol% affording a quantitative conversion after 2 h. On the grounds of this finding, DIPA was chosen as the best base for additional investigations. Both the solids **3** and **5** were tested at 0.1 mol% of Pd in the reaction between phenylboronic acid and the less reactive 4-bromoanisole. Data reported in Table 2 (entries 5–7) showed a higher catalytic activity of CNH-Imi-Pd **5** by comparison with MWCNT-Imi-Pd **3**.

Table 2. Screening of reaction conditions for the Suzuki–Miyaura reaction.[a]

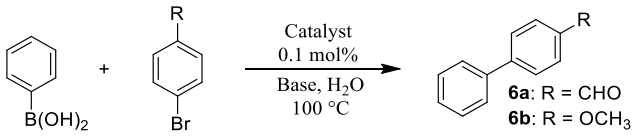

Entry	Catalyst	R	Base	Time [h]	Conv. [%][b]
1	**3**	CHO	K_2CO_3	6	70
2	**3**	CHO	K_3PO_4	6	75
3	**3**	CHO	DIPA	2	>99
4[c]	**5**	CHO	DIPA	2	99
5	**3**	OCH_3	DIPA	1	87
6	**5**	OCH_3	DIPA	1	99
7[c]	**5**	OCH_3	DIPA	1	93

[a] Reaction conditions: aryl bromide (0.5 mmol), phenylboronic acid (0.55 mmol), base (2 equiv.), catalyst (0.1 mol%), solvent (1.2 mL). [b] Conversion determined by ^{1}H NMR. [c] CNH-Imi-Pd **5** used at 0.07 mol%.

The catalytic versatility of MWCNT-Imi-Pd **3** and CNH-Imi-Pd **5** was checked in the Suzuki couplings between a broad spectrum of substrates including several aryl bromides, boronic acids and one pinacol ester (Table 3). In this context, materials **3** and **5** were tested using a Pd loading of 0.1 and 0.07 mol%, respectively.

Table 3. Suzuki–Miyaura reactions catalyzed by materials MWCNT-Imi-Pd **3** and CNH-Imi-Pd **5**.[a]

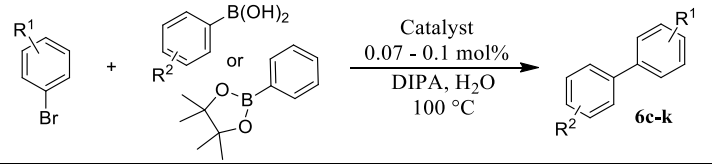

Entry	R^1	R^2	Product	Time [h]	MWCNT-Imi-Pd **3** Conv. [b] [%]	CNH-Imi-Pd **5** Conv. [b] [%]
1	4-$COCH_3$	H	**6c**	3	99	99
2	3-$COCH_3$	H	**6d**	3	99	99
3	4-CN	H	**6e**	5	99	99
4	4-NO_2	H	**6f**	4	95	99
5	3-CH_3	H	**6g**	3	78	93
6	4-OCH_3	2-CH_3	**6h**	5	69	84
7	4-CHO	4-OCH_3	**6i**	3	99	99
8	4-$COCH_3$	-[c]	**6c**	6	81	80
9	4-OCH_3	4-CHO	**6j**	5	47	36
10	4-CHO	4-CHO	**6k**	24	99	99
11[d]	4-$COCH_3$	H	**6c**	16	95	99

[a] Reaction conditions: aryl bromide (0.5 mmol), phenylboronic acid (0.55 mmol), DIPA (1 mmol), catalyst (0.07–0.1 mol%), H_2O (1.2 mL). [b] Conversion determined by ^1H NMR. [c] Phenylboronic acid pinacol ester was used. [d] Reaction conditions: 4-bromoacetophenone (3 mmol), phenylboronic acid (3.3 mmol), DIPA (6 mmol), catalyst (MWCNT-Imi-Pd **3** 0.01 mol% or CNH-Imi-Pd **5** 0.007 mol%), H_2O (3.6 mL).

Conversions in the corresponding biphenyls were from good to excellent in almost all the cases being CNH-Imi-Pd **5** more active than MWCNT-Imi-Pd **3**. This difference in activity is more pronounced when 3-bromotoluene was reacted with phenylboronic acid or the electron rich 4-bromoanisole was coupled with *o*-tolylboronic acid (Table 3, entries 5 and 6). It is noteworthy that the catalytic performances of both materials were quite similar in the reaction between phenylboronic acid pinacol ester and 4-bromoacetophenone, or in the coupling of 4-formylphenylboronic acid with 4-bromoanisole (Table 3, entries 8 and 9). However, CNH-Imi-Pd **5** still showed a slightly higher activity, in terms of turnover number (TON), owing to its lower Pd loading compared to MWCNT-Imi-Pd **3**. As an aside, TON values were defined as moles of aryl halide converted/moles of palladium. Indeed, even if CNH-Imi-Pd **5** gave rise to a lower conversion (36% *vs* 47%, entry 9) in the reaction between 4-formylphenylboronic acid and 4-bromoanisole, it is also true that, catalyst **5** displayed a higher TON value than that reached by MWCNTs based Pd hybrid (TON: 514 *vs* 470). The somewhat different catalytic activity may be ascribed to a better NPs accessibility in CNHs based material **5**. Although MWCNT-Imi-Pd **3** has both a higher Pd content and lower Pd NPs size, palladium is probably more dispersed in the inner layers of the polymeric network, being less available to the catalysis. On the contrary, CNH-Imi-Pd **5** exhibit lower Pd content and higher NPs size. However, as evidenced by TEM analysis, in the solid **5** Pd NPs seem to be mostly exposed on the external surface of the hybrid resulting more accessible to the reactants during the catalysis.

A further experiment was performed with a reduced catalytic loading. The reaction between 4-bromoacetophenone and phenylboronic acid was chosen for this purpose. In particular, catalyst **3** was tested at 0.01 mol%, whereas CNH-Imi-Pd **5** was employed with a palladium loading of 0.007 mol% (Table 3, entry 11). This reaction confirmed the different activity of the two catalysts. After 16 h, MWCNT-Imi-Pd **3** was able to reach 95% of conversion, whereas, in the same time, CNH-Imi-Pd **5** allowed a full conversion into the corresponding product. Taking into account the different catalytic loading, it is worth to mention the reached TON values which highlight the different activity of the two catalysts: 9500 for the solid **3** and 14286 for material **5**.

Data reported in Table 4 show a comparison between the more active CNH-Imi-Pd **5** and other catalytic systems for the Suzuki reaction between 4-bromoanisole and phenylboronic acid reported in literature. Such comparison is not strictly direct because the majority of reactions were not carried out in pure water as in our case.

Table 4. Comparison between CNH-Imi-Pd **5** and other reported catalytic systems in the Suzuki–Miyaura coupling of 4-bromoanisole with phenylboronic acid.

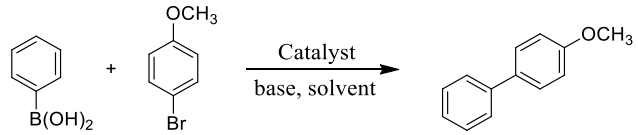

Entry	Catalyst	Pd [mol%]	Conditions	Time	Yield (%)	Ref.
1	SWCNT-DETA/Pd^{II}	1	K_2CO_3, H_2O/EtOH (1:1), 60 °C	1.3 h	96	[4]
2	SWCNT-Metformine/Pd^{II}	1	K_2CO_3, H_2O/EtOH (1:1), 50 °C	1 h	90	[5]
3	MWCNT-Schiff base/Pd^{II}	0.1	K_2CO_3, H_2O/DMF (1:1), 60 °C	3 h	99	[6]
4	MWCNT-(*S*)-methyl histidinate/Pd^{II}	0.09	K_2CO_3, H_2O/EtOH (1:1), r.t.	1 h	80	[7]
5	SWCNT@Fe_3O_4@SiO_2/Pd	1.5	Cs_2CO_3, EtOH, 80 °C	15 h	91	[8]
6	MWCNT/Pd	0.1	K_2CO_3, TBAB, H_2O, 120 °C	1 h	96	[9]
7	MWCNT/Pd	0.3	Na_2CO_3, EtOH, 90 °C	8 h	99	[10]
8	MWCNT/Pd/PdO	0.1	DIPA, H_2O, 90 °C	4 h	99	[11]
9	Graphene/MWCNTs/Pd	0.5	K_2CO_3, H_2O/EtOH (1:1), 60 °C	1.5 h	92	[12]
10	MWCNT-Schiff base/Pd	0.2	K_2CO_3, H_2O/EtOH (1:1), r.t.	2.5 h	92	[13]
11	ox-SWCNH/Pd	0.05	Na_2CO_3, NMP/H_2O (2:1), 120 °C	2 h	91	[14]
12	Pd/C	1.5	DIPA, H_2O 100 °C	20 min	93	[15]
13	CNH-Imi-Pd	0.07	DIPA, H_2O, 100 °C	1 h	93	This work

Examples concerning both Pd^{II} complexes and Pd NPs supported onto SWCNTs, MWCNTs, and oxidized CNHs were taken into account. Analysis of data in Table 4 underlines that CNH-Imi-Pd **5** exhibits higher or comparable activity with the other examined catalytic systems. Furthermore, it is possible to compare the catalytic activity of the herein presented CNH-Imi-Pd **5** with commercial Pd/C catalyst tested in the same reaction conditions (water, DIPA, 100 °C). Pd/C catalyst reached in just twenty minutes a 93% yield into the corresponding product by using an over twenty-fold higher Pd loading than in the case of CNH-Imi-Pd **5** (compare entries 12 and 13).

The recyclability of the solids **3** and **5** was investigated in the Suzuki reaction between 4-bromoacetophenone and phenylboronic acid (Figure 5). Both catalysts retained their activity over five cycles affording the desired product in quantitative yield.

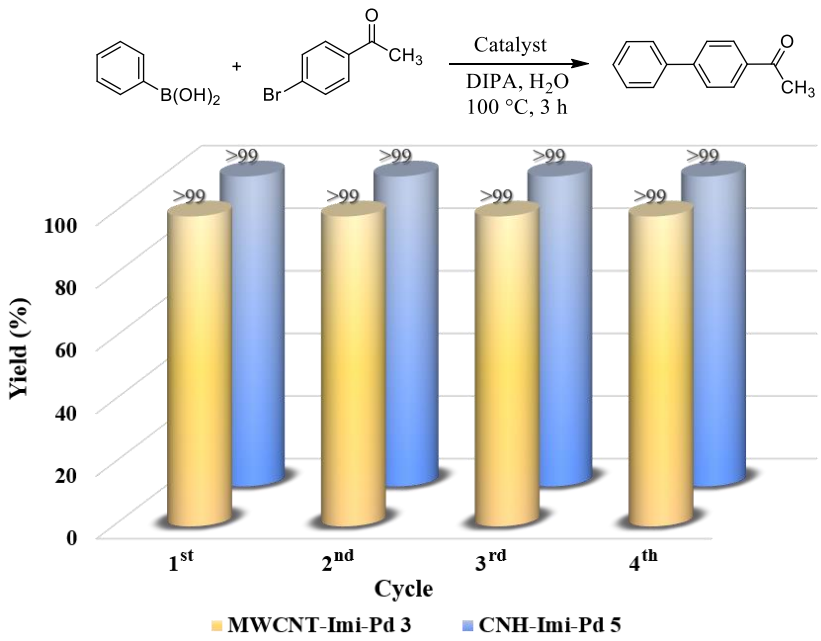

Figure 5. Recycling experiments of MWCNT-Imi-Pd **3** (0.1 mol%) and CNH-Imi-Pd **5** (0.07 mol%) in the Suzuki reaction.

Furthermore, MWCNT-Imi-Pd **3** and CNH-Imi-Pd **5** were tested in the catalysis of the Heck reaction with the same palladium loading used for the Suzuki coupling, (0.1 and 0.07 mol%, respectively). Both electron-rich and electron-poor aryl iodides were reacted with different alkenes, such as styrene, 4-chlorostyrene and methyl acrylate using dimethylformamide as solvent and triethylamine as base at 120 °C.

The conversions into the corresponding products were from good to excellent (Table 5-6).

Table 5. Mizoroki–Heck reactions catalyzed by materials MWCNT-Imi-Pd **3** and CNH-Imi-Pd **5**.[a]

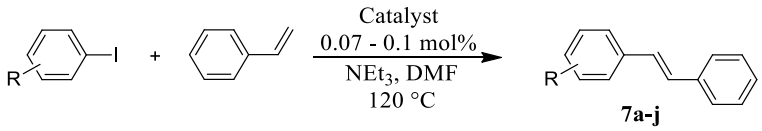

Entry	R	Product	Time [h]	Conv. [%] / [Selectivity][b]	
				3	**5**
1	H	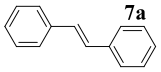 **7a**	5	99 [91]	99 [93]
2	4-CH_3	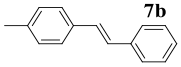 **7b**	5	86 [86]	79 [85]
3	4-OCH_3	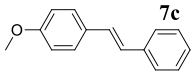 **7c**	5	87 [85]	87 [85]
4	3-OCH_3	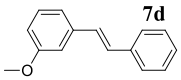 **7d**	5	90 [87]	92 [86]
5	4-$COCH_3$	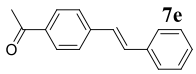 **7e**	5	91 [92]	99 [93]
6	4-NO_2	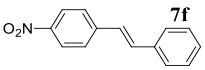 **7f**	24	63 [93]	70 [93]
7	3-Br	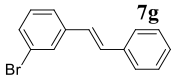 **7g**	5	86 [92]	82 [91]
8	2-C_4H_3S	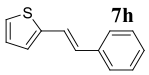 **7h**	5	81 [91]	89 [89]
9	4-$COCH_3$	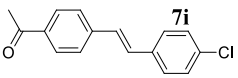 **7i**	5	99 [98]	99 [96]
10[c]	4-CHO	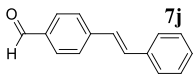 **7j**	17	81 [96]	93 [96]

[a] Reaction conditions: aryl iodide (0.5 mmol), alkene (0.75 mmol), NEt_3 (1 mmol), catalyst (0.07–0.1 mol%), DMF (1 mL). [b] Conversion and selectivity toward *trans* alkene determined by ^1H NMR. [c] 4-Bromobenzaldehyde was used.

Table 6. Mizoroki–Heck reactions catalyzed by materials MWCNT-Imi-Pd **3** and CNH-Imi-Pd **5**.[a]

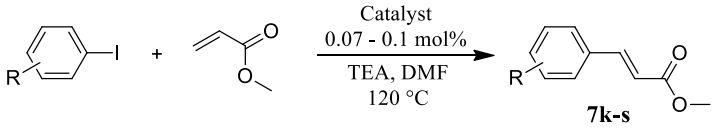

Entry	R	Product	Time [h]	Conv. [%][b]	
				3	5
1	H	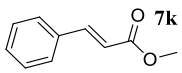 **7k**	3	99	99
1	4-CH_3	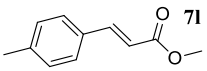 **7l**	3	99	99
3	4-OCH_3	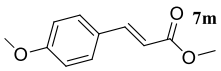 **7m**	3	99	99
4	3-OCH_3	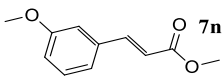 **7n**	3	99	99
5	4-$COCH_3$	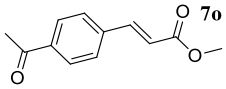 **7o**	3	99	99
6	4-NO_2	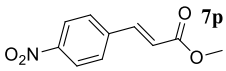 **7p**	3	99	99
7	3-Br	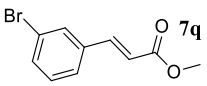 **7q**	3	94	94
8	2-C_4H_3S	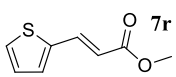 **7r**	3	99	99
9	4-CHO	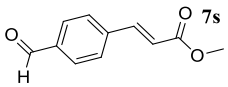 **7s**	3	99	99
10[c]	4-OCH_3	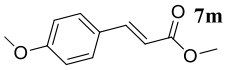 **7m**	5	99	99

[a] Reaction conditions: aryl iodide (0.5 mmol), alkene (0.75 mmol), NEt_3 (1 mmol), catalyst (0.07–0.1 mol%), DMF (1 mL). [b] Conversion and selectivity toward *trans* alkene determined by ^1H NMR. [c] Reaction conditions: 4-iodoanisole (3 mmol), methyl acrylate (4.5 mmol), NEt_3 (6 mmol), catalyst (MWCNT-Imi-Pd **3** 0.01 mol% or CNH-Imi-Pd **5** 0.007 mol%), DMF (3 mL).

Once again, taking into account its lower catalytic loading, CNH-Imi-Pd **5** showed a higher activity than MWCNT-Imi-Pd **3**, especially when styrene and 4-

chlorostyrene were used (Table 5). Moreover, 4-bromobenzaldehyde was coupled with styrene affording good results after 17 h of reaction (Table 5, entry 10). Regioselectivity towards *trans* alkene isomer in the Heck reaction between methyl acrylate and several aryl iodides was excellent and no traces of by-products were detected (Table 6). However, when styrene and 4-chlorostyrene were employed, the regioselectivity was lower with the formation of the corresponding *gem*-alkenes in variable amounts between 2 and 15 mol% (Table 5). A further experiment with a tenfold lower catalytic loading was carried out using MWCNT-Imi-Pd **3** and CNH-Imi-Pd **5** in the reaction between 4-iodoanisole and methyl acrylate (Table 6, entry 10). In the adopted conditions, the low catalytic loadings allowed a quantitative conversion into the desired product after 5 h. Then, the same reaction between 4-iodoanisole and methyl acrylate was chosen to assess the recyclability of MWCNT-Imi-Pd **3** and CNH-Imi-Pd **5** with a palladium loading of 0.1 and 0.07 mol%, respectively. Both catalysts gave rise to a complete conversion into the corresponding product over the six cycles investigated. At the end of each catalytic run, the solids were simply recovered by centrifugation and successfully reused retaining their catalytic activity (Figure 6).

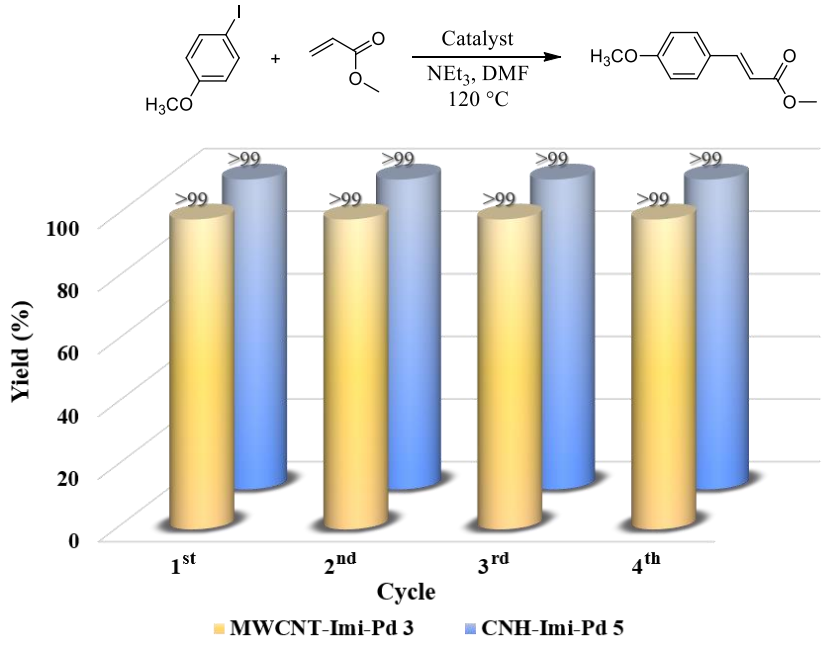

Figure 6. Recycling experiments of MWCNT-Imi-Pd **3** (0.1 mol%) and CNH-Imi-Pd **5** (0.07 mol%) in the Heck reaction between 4-iodoanisole and methyl acrylate.

7.3 Conclusions

A straightforward synthetic procedure has been applied for the design of imidazolium functionalized carbon nanostructures. The direct radical polymerization of a bis-vinylimidazolium dibromide salt was performed in the presence of different pristine carbon nanoforms, namely multi-walled carbon nanotubes and carbon nanohorns, allowing to obtain two CNFs-polyimidazolium hybrids. Interestingly, both carbon nanostructures acted as templates for the growth of the highly cross-linked imidazolium network despite the random nature of the polymerization process. The hybrids were hence employed as novel supports and stabilizers for palladium nanoparticles. The obtained materials were characterized by means of TGA, ^{13}C CP-MAS NMR, MP-AES, XPS and HR-TEM. This latter technique revealed two different situations regarding both the dimensions and the distribution of Pd NPs on the materials MWCNT-Imi-Pd **3** and CNH-Imi-Pd **5**. If on the one hand, only at high magnifications, it was possible to observe the presence of very small Pd NPs uniformly distributed onto material **3**, on the other hand, material **5** is characterized by the presence of bigger Pd NPs mainly located on the outer part of the hybrid material. Because of the small size of Pd NPs dispersed onto material **3**, it was not possible to estimate their mean dimensions. On the contrary, material **5** showed a bimodal distribution with a mean particle size of 28.8 ± 12.0 nm and 2.6 ± 0.6 nm. The two catalysts, MWCNT-Imi-Pd **3** and CNH-Imi-Pd **5**, were extensively used with a large set of substrates in both Suzuki and Heck reactions, giving C–C coupled products in high conversions. In the case of Suzuki reactions in pure water, results were comparable or even better than those obtained with commercial Pd/C[15] or other supported Pd-based catalysts.[4-14, 16] Both catalysts were recovered after centrifugation and reused up to five cycles without loss in catalytic activity. Moreover, the catalytic loading was scaled down to 0.01 and 0.007 mol% for MWCNT-Imi-Pd **3** and CNH-Imi-Pd **5** respectively, still giving high TON values. Carbon nanohorns-based material proved to be a slightly more active catalyst for the investigated C–C coupling reactions. This behaviour could be ascribed to a higher NPs accessibility to the reactants. The simple preparation and the high catalytic activity even in consecutive cycles make such catalysts

interesting for application in large scale and for continuous flow conditions. Several heterogeneous catalysts, based on different metal NPs or even negatively charged species such as polyoxometalate, can be prepared by following the herein presented synthetic approach.

7.4 Experimental Section

Spectroscopic and analytical methods

Chemicals and solvents were purchased from commercial suppliers and used without further purification. For thin-layer chromatography (TLC), silica gel plates (Merck 60 F254) were used and compounds were visualized by irradiation with UV light and/or by treatment with a $KMnO_4$ solution. ^{1}H spectra were recorded with a Bruker 300 MHz spectrometer. The ^{13}C CPMAS NMR spectra were acquired by means of a spectrometer Bruker Avance II 400 operating at 400.15 and 100.63 MHz for ^{1}H and ^{13}C nuclides respectively and equipped with a 4 mm (H-X) double channel CPMAS probe. All spectra were acquired with a MAS speed of 8kHz, 1024 scans, a contact time of 2 ms, a delay time of 3 sec and an excitation pulse of 4.7 microseconds on the ^{1}H nucleus. The optimization of the Hartmann-Hahn condition has been obtained using an adamantane standard sample. This compound was also used as the external chemical shift reference. All samples were placed in 4 mm zirconia rotors filled with Kel-F caps. Thermogravimetric analysis (TGA) was performed under nitrogen flow from 100 to 1000 °C with a heating rate of 10 °C min^{-1} in a Mettler Toledo TGA/DSC STAR System. TEM micrographs were recorded on a high-resolution transmission electron microscope (HRTEM) JEOL JEM-2100 operating at 200 kV accelerating voltage. Samples were dispersed in toluene and drop cast onto carbon coated copper TEM grids for HR-TEM analysis. The imaging conditions were carefully tuned by lowering the accelerating voltage of the microscope and reducing the beam current density to a minimum in order to minimize the electron beam induced damage of the sample. Microwave Plasma-Atomic Emission Spectroscopy (MP-AES) analyses were carried out with a 4200 MP-AES, Agilent. Analyses were conducted using a calibration curve, obtained by dilution. X-ray photoelectron spectroscopy (XPS) analyses were performed with a VGMicrotech ESCA 3000Multilab, equipped with a dual Mg/Al anode. The spectra were excited with the unmonochromatized Al Kα source (1486.6 eV) run at 14 kV and 15 mA. The analyzer was operated in the constant analyser energy (CAE) mode. For the individual peak energy regions, a pass energy of 20 eV set across the hemispheres was used. Survey spectra were measured at 50 eV pass energy. The

sample powders were mounted on a double-sided adhesive tape. The pressure in the analysis chamber was in the range of 10^{-8} Torr during data collection. The constant charging of the samples was removed by referencing all the energies to the C1s set at 284.6 eV. The invariance of the peak shapes and widths at the beginning and at the end of the analyses ensured absence of differential charging. Analyses of the peaks were carried out with the software provided by VG, based on the non-linear least squares fitting program using a weighted sum of Lorentzian and Gaussian component curves after background subtraction according to Shirley and Sherwood.[17] Atomic concentrations were calculated from peak intensity using the sensitivity factors provided with the software. The binding energy values are quoted with a precision of ±0.15 eV and the atomic percentage with a precision of ±10%.

Synthesis of bis-vinylimidazolium salt 1

Bis-vinylimidazolium salt **1** was prepared following a reported procedure with minor changes.[1] A solution of 1,4-dibromobutane (1.50 mL, 12.43 mmol) and 1-vinylimidazole (2.45 mL, 26.53 mmol) in toluene (11 mL) was stirred at 90 °C. After 21 h a white precipitate was formed and toluene was removed by simple decantation. Afterwards, methanol was added and gently warmed to solubilize the solid. The volume was reduced by rotary evaporator obtaining a yellowish viscous oil that after addition of diethyl ether and sonication gave rise to a white precipitate. Diethyl ether was then removed and the white solid was further washed two times with diethyl ether and dried under vacuum at 40 °C. Bis-vinylimidazolium salt **1** was obtained as a white solid (4.516 g; 90%).

Synthesis of MWCNT-Imi 2 and CNH-Imi 4

In a two-neck round-bottom flask, a suspension of MWCNTs or CNHs (40 mg) and bis-vinylimidazolium salt **1** (674 mg, 1.67 mmol) in absolute ethanol (15 mL) was sonicated for 20 minutes. Afterwards, AIBN (28 mg, 0.17 mmol) was added and the mixture was degassed by bubbling argon for 20 minutes. The mixture was heated at 78 °C while stirring under argon. After 20 h, the mixture was filtered and the solid washed with methanol and diethyl ether. After drying

under vacuum at 40 °C, MWCNT-Imi **2** was obtained as a black/grey solid (617 mg) and CNH-Imi **4** as a black solid (546 mg).

Synthesis of MWCNT-Imi-Pd 3 and CNH-Imi-Pd 5

$PdCl_2$ (37.57 mg, 0.21 mmol) and NaCl (246.68 mg, 4.20 mmol) were transferred in a round-bottom flask and water (15 mL) was added. The mixture was heated at 80 °C for 30 minutes until the formation of a brown solution. The obtained solution was allowed to reach the room temperature and was added dropwise to a stirring suspension of MWCNT-Imi **2** or CNH-Imi **4** (200 mg) in water (12.5 mL). The resulting mixture was stirred at room temperature for 22 h. The suspension was then filtered and the solid was washed with water, methanol and diethyl ether. Once dried, the resulting solid was suspended in absolute ethanol (15 mL) and sonicated for 15 minutes. After the sonication, the suspension was stirred and a freshly prepared suspension of $NaBH_4$ (56.74 mg, 1.47 mmol) in absolute ethanol (10 mL) was added dropwise under stirring to previous suspension. The resulting mixture was stirred at room temperature for 6 h. The suspension was then filtered and the resulting solid was washed with water, methanol and acetone. After drying under vacuum at 40 °C, MWCNT-Imi-Pd **3** and CNH-Imi-Pd **5** were obtained as black solids (183 and 184 mg, respectively).

General procedure for the Suzuki reaction

Aryl bromide (0.5 mmol), boronic acid or phenylboronic acid pinacol ester (0.55 mmol), diisopropylamine (1 mmol), catalyst **3** (0.70 mg – 0.1 mol%) or **5** (0.52 mg – 0.07 mol%) and water (1.2 mL) were transferred in a glass vial with a screw cap and heated at 100 °C under stirring for the required time. Then, the reaction mixture was allowed to cool down to room temperature, diluted with water and extracted three times with dichloromethane. The combined organic layers were dried with anhydrous Na_2SO_4 and the solvent was evaporated under vacuum. The residue was filtered by a short pad of silica using a mixture of hexane and ethyl acetate as eluent. The conversions were estimated by ^1H NMR spectroscopy.

General recycling procedure in the Suzuki reaction

4-bromoacetophenone (1 mmol), phenylboronic acid (1.1 mmol), diisopropylamine (2 mmol), catalyst **3** (1.40 mg – 0.1 mol%) or **5** (1.05 mg – 0.07 mol%) and water (2.4 mL) were transferred in a glass vial with a screw cap and heated at 100 °C under stirring. After 3h the reaction mixture was allowed to cool down to room temperature, diluted with ethyl acetate and centrifuged. Organic layer was recovered and catalyst was further washed two times with ethyl acetate, then with a mixture of methanol/ethyl acetate 2:1 and finally with diethyl ether. Once dry, the catalyst was used in the next cycle. The recovered organic layers were combined and evaporated under reduced pressure, diluted with water and extracted three times with dichloromethane. The combined organic layers were then dried with anhydrous Na_2SO_4 and the solvent was evaporated under vacuum. The residue was purified by column chromatography using a mixture of hexane and ethyl acetate as eluent.

General procedure for the Heck reaction

Aryl iodide (0.5 mmol), alkene (0.75 mmol), triethylamine (1 mmol), catalyst **3** (0.70 mg – 0.1 mol%) or **5** (0.52 mg – 0.07 mol%) and DMF (1 mL) were transferred in a glass vial with a screw cap and heated at 120 °C under stirring for the required time. Then, the reaction mixture was allowed to cool down to room temperature, diluted with water and extracted three times with diethyl ether. The combined organic layers were dried with anhydrous Na_2SO_4 and the solvent was evaporated under vacuum. The residue was filtered by a short pad of silica using a mixture of hexane and ethyl acetate as eluent. The conversions were estimated by ^{1}H NMR spectroscopy.

General recycling procedure in the Heck reaction

4-iodoanisole (1 mmol), methyl acrylate (1.5 mmol), triethylamine (2 mmol), catalyst **3** (1.40 mg – 0.1 mol%) or **5** (1.04 mg – 0.07 mol%) and DMF (2 mL) were transferred in a glass vial with a screw cap and heated at 120 °C under stirring. After 3 h the reaction mixture was allowed to cool down to room temperature, diluted with diethyl ether and centrifuged. Organic layer was

recovered and catalyst was further washed with diethyl ether, and then four times with methanol, water, methanol again and finally with diethyl ether. Once dry, the catalyst was used in the next cycle. The recovered organic layers were combined and evaporated under reduced pressure, diluted with water and extracted three times with diethyl ether. Then, the combined organic layers were dried with anhydrous Na_2SO_4 and the solvent was evaporated under vacuum. The residue was purified by column chromatography using a mixture of hexane and ethyl acetate as eluent.

7.5 References

[1] P. Agrigento, S. M. Al-Amsyar, B. Sorée, M. Taherimehr, M. Gruttadauria, C. Aprile, P. P. Pescarmona, *Catalysis Science & Technology* **2014**, *4*, 1598-1607.

[2] Y. Ren, Z. Zhou, G. Yin, G. X. Chen, Q. Li, *Materials Letters* **2016**, *166*, 133-136.

[3] H. A. Beejapur, F. Giacalone, R. Noto, P. Franchi, M. Lucarini, M. Gruttadauria, *ChemCatChem* **2013**, *5*, 2991-2999.

[4] R. Ghorbani-Vaghei, S. Hemmati, M. Hashemi, H. Veisi, *Comptes Rendus Chimie* **2015**, *18*, 636-643.

[5] H. Veisi, A. Khazaei, M. Safaei, D. Kordestani, *Journal of Molecular Catalysis A: Chemical* **2014**, *382*, 106-113.

[6] M. Navidi, N. Rezaei, B. Movassagh, *Journal of Organometallic Chemistry* **2013**, *743*, 63-69.

[7] A. R. Hajipour, Z. Khorsandi, *Applied Organometallic Chemistry* **2016**, *30*, 256-261.

[8] D. Khalili, A. R. Banazadeh, E. Etemadi-Davan, *Catalysis Letters* **2017**, *147*, 2674-2687.

[9] A. Ohtaka, J. M. Sansano, C. Nájera, I. Miguel-García, Á. Berenguer-Murcia, D. Cazorla-Amorós, *ChemCatChem* **2015**, *7*, 1841-1847.

[10] P.-P. Zhang, X.-X. Zhang, H.-X. Sun, R.-H. Liu, B. Wang, Y.-H. Lin, *Tetrahedron Letters* **2009**, *50*, 4455-4458.

[11] F. Yang, C. Chi, S. Dong, C. Wang, X. Jia, L. Ren, Y. Zhang, L. Zhang, Y. Li, *Catalysis Today* **2015**, *256*, 186-192.

[12] H.-q. Song, Q. Zhu, X.-j. Zheng, X.-g. Chen, *Journal of Materials Chemistry A* **2015**, *3*, 10368-10377.

[13] H. Veisi, R. Azadbakht, F. Saeidifar, M. R. Abdi, *Catalysis Letters* **2017**, *147*, 976-986.

[14] T. Itoh, H. Danjo, W. Sasaki, K. Urita, E. Bekyarova, M. Arai, T. Imamoto, M. Yudasaka, S. Iijima, H. Kanoh, K. Kaneko, *Carbon* **2008**, *46*, 172-175.

[15] X. Rao, C. Liu, Y. Zhang, Z. Gao, Z. Jin, *Chinese Journal of Catalysis* **2014**, *35*, 357-361.

[16] a) G. Park, S. Lee, S. J. Son, S. Shin, *Green Chemistry* **2013**, *15*, 3468-3473; b) A. Chatterjee, T. R. Ward, *Catalysis Letters* **2016**, *146*, 820-840; c) D. Zhang, C. Zhou, R. Wang, *Catalysis Communications* **2012**, *22*, 83-88; d) M. Lamblin, L. Nassar-Hardy, J.-C. Hierso, E. Fouquet, F.-X. Felpin, *Advanced Synthesis & Catalyis* **2010**, *352*, 33-79.

[17] D. A. Shirley, *Physical Review B* **1972**, *5*, 4709-4714.

CHAPTER VIII

Supported Imidazolium Modified POSS Hybrids as Palladium Platform for C–C Cross Couplings

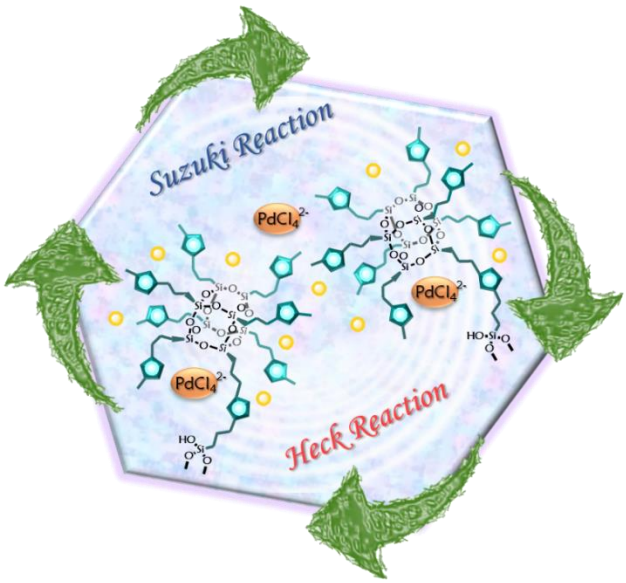

This chapter is based on a *manuscript in preparation*

CHAPTER VIII

Supported Imidazolium Modified POSS Hybrids as Palladium Platform for C–C Cross-Couplings

8.1 Abstract

Supported imidazolium modified polyhedral oligomeric silsesquioxanes (POSS) have been used as platform for Pd^{II} species. Such material was successfully tested as pre-catalyst in C−C cross couplings, namely Suzuki-Miyaura and Heck reactions. In both cases, the solid proved to be highly efficient and easily recoverable from the reaction mixture. The recyclability was verified for up to seven cycles without showing any activity decrease. Interestingly only Pd^{II} was detected in the reused catalyst in the Heck reaction. Therefore, the versatility of our material was extensively investigated by using various aryl halides endowed with electron-donating or electron-withdrawing groups. Our palladium nanocomposite was able to promote both Suzuki and Heck reactions down to 0.0007 mol% showing outstanding turnover frequency (TOF) values of 114,286 and 32,381 h^{-1}, respectively.

8.2 Results and Discussion

According to the synthetic procedure reported in Chapter IV,[1] octakis(3-chloropropyl)-octasilsesquioxane (compound **1**) was reacted with triethoxy-3-(2-imidazolin-1yl)propylsilane to give compound **2** that was directly grafted onto mesostructured SBA-15 to afford the solid **3**. The functionalization of supported POSS nanostructures with imidazolium chloride peripheries (material **4**) was obtained from the reaction between material **3** and 1-methylimidazole. The imidazolium loading of solid **4** was estimated by means of combustion chemical analysis (C, H, N) and was found to be 0.81 mmol/g. This synthetic strategy allowed to obtain a promising catalytic support endowed with a specific surface area of 272 m^2/g, total pore volume of 0.87 cm^3/g, and pore size distribution around 14 nm. The interesting textural properties of the solid make this material suitable for high flow catalytic applications. Considering its high value of pore size distribution, enabling internal diffusion paths, the hybrid **4** was designed as a sort of nanoreactor based on imidazolium modified POSS units as solid support for Pd species (Scheme 1).

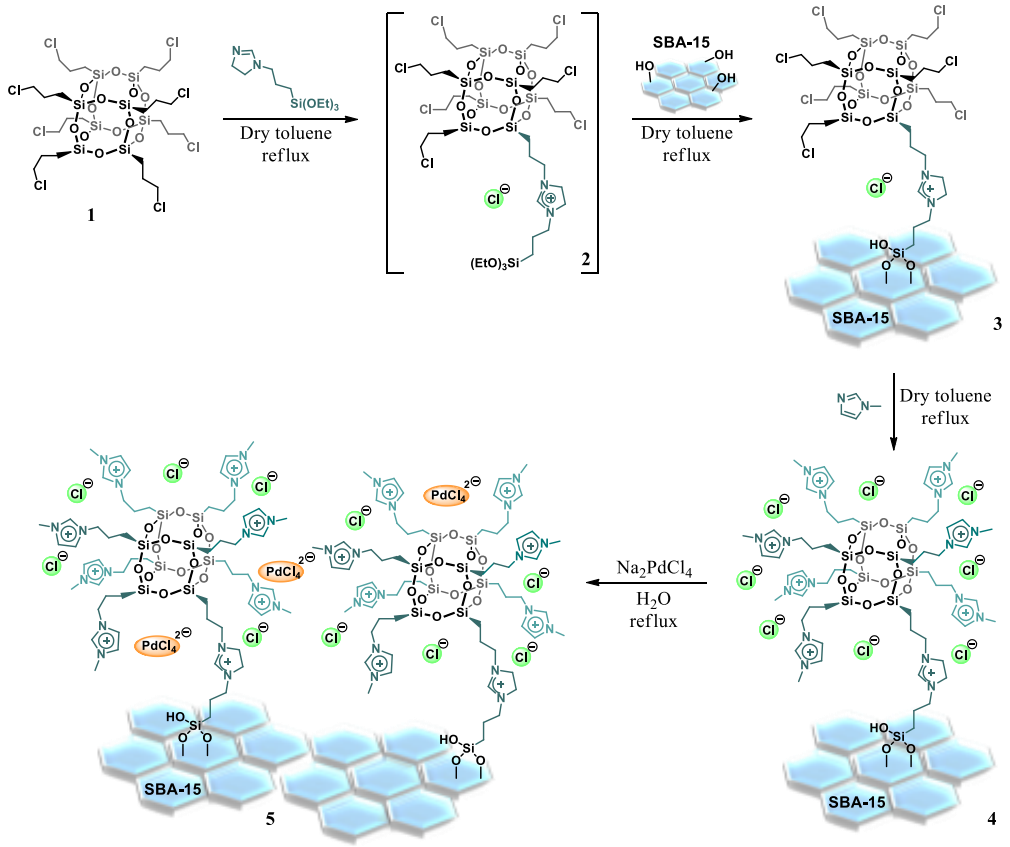

Scheme 1. Synthesis of Pd^{II} imidazolium functionalized POSS hybrid.

For doing so, the solid **4** was treated with a solution of Na_2PdCl_4 to give the final material **5** by anionic metathesis reaction.

The thermal behavior of the final hybrid **5** and its precursor **3** and **4** was investigated by means of thermogravimetric analysis (TGA, Figure 1). The decomposition of organic functionalities started in the range 240–250 °C, being the solid **5** slightly more stable than its precursor **3** and **4**. The good thermal robustness of the final hybrid **5** is promising for its repeated use under heating regimes.

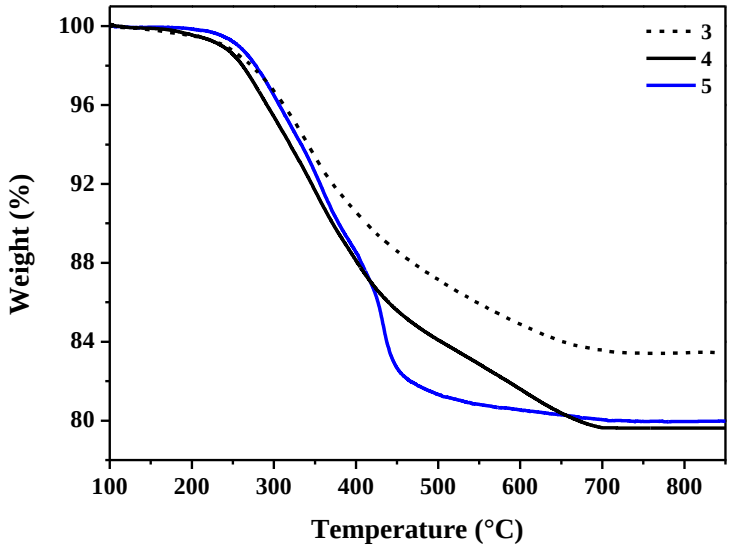

Figure 1. TGA profiles of imidazolium functionalized POSS hybrids.

Then, palladium loading of **5** was quantified by using inductively coupled plasma optical emission spectroscopy (ICP-OES) to be 1.5 wt%. X-ray photoelectron spectroscopy (XPS) analysis was performed to evaluate the oxidation state of supported palladium species onto the surface of the solid **5** (Figure 2). Small angle X-ray scattering (SAXS) measurements were carried out on both pristine and functionalized SBA-15 (Figure 3). SAXS analysis revealed the ordered mesostructure of SBA-15 showing a scattering pattern composed of a peak centered at 0.43° 2θ and two peaks, not clearly resolved, at 0.71° 2θ and 0.73° 2θ. The diffraction patterns are in line with the typical profile for hexagonal (*p6mm*)[2] mesoporous silica SBA-15. The most intense peak was indexed as (100) reflection, the other two features, almost merging in a broad

one, were ascribed to (110) and (200) secondary peaks. According to the Bragg's law, the plane distance d (100) was computed as d = 20.55 nm and the unit cell parameter as α_0 = 23.76 nm. Moreover, the patterns of POSS modified SBA-15 **3** and **4** proved that the ordered structure of pristine SBA-15 is preserved. Indeed, the pore-to-pore distance α_0 is the same for all the solids. By comparison with pristine SBA-15, in the case of functionalized material it is possible to observe a decrease in intensity of the signals due to the presence of POSS nanostructures. However, the structural order of the pores of the pristine solid support was not affected, being constant the ratio between the relative reflections of SBA-15, samples **3** and **4**.

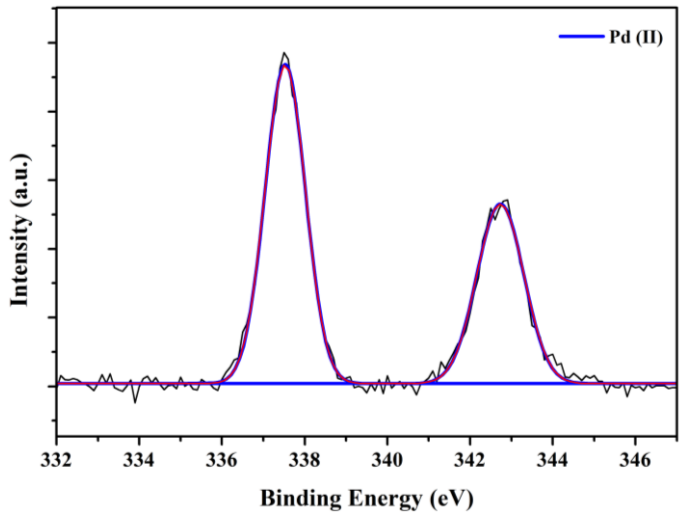

Figure 2. Pd 3d core level XPS analysis of **5**.

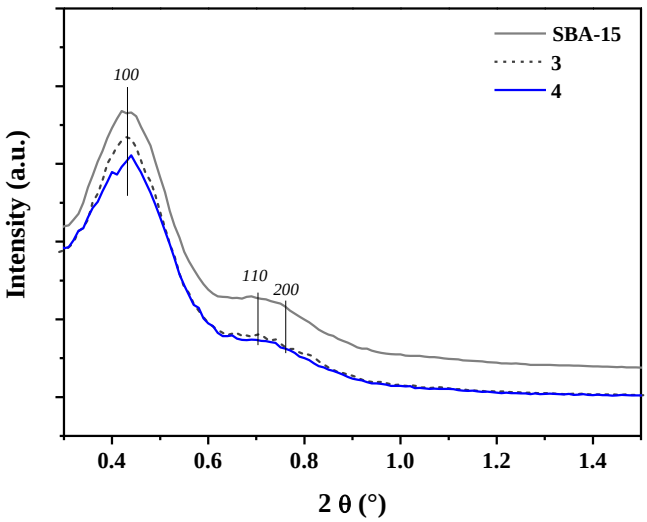

Figure 3. SAXS patterns of SBA-15, **3**, **4**.

^{13}C and ^{29}Si solid state cross polarization-magic angle spinning (CP-MAS) NMR measurements were performed on both the final material **5** and its precursor **4**. All the solid state ^{13}C CP-MAS NMR experiments were recorded using the TOSS (total suppression side band) pulse sequence to displace the spinning side bands while leaving the isotropic signals. By comparison of **4** and **5** NMR spectra, it is interesting to note an excellent overlapping of the signals proving that the subsequent immobilization of palladium species had no remarkable effect on the chemical shift (Figure 4). In CP-MAS ^{13}C NMR spectra the peculiar signals of the carbon atoms of imidazolium ring were detected in the range δ = 122–137 ppm, whereas the aliphatic ones resonated in the range δ = 10–52 ppm. The weak signal located at δ = ~158 ppm can be ascribed to the C2 imidazolidinium carbon atom.

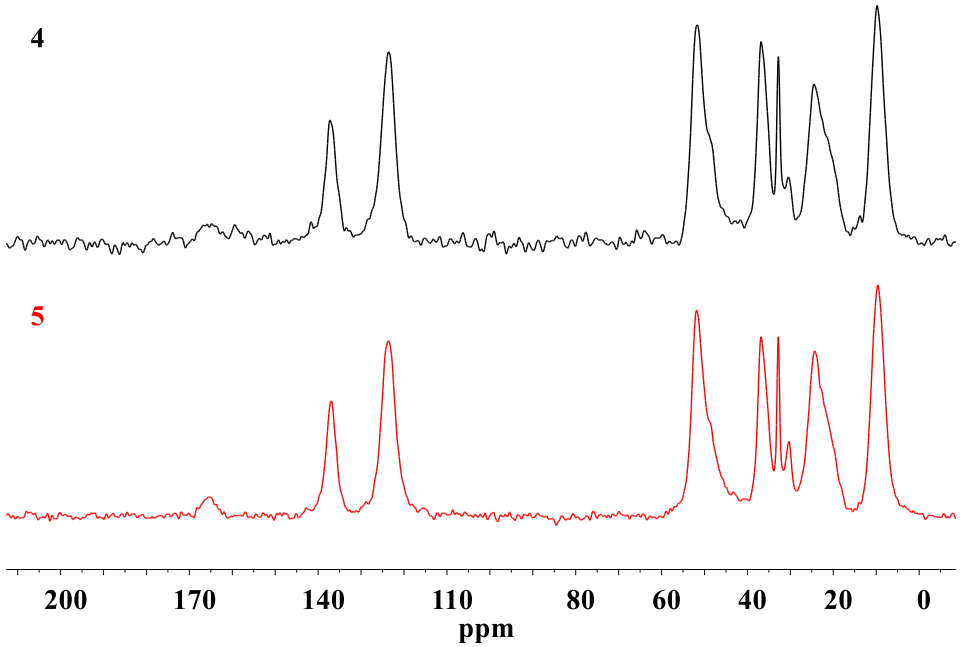

Figure 4. ^{13}C CP-MASS TOSS NMR spectra of **4** (black line) and **5** (red line).

In CP-MAS ^{29}Si NMR spectra the presence of $Q^4[(SiO)_4Si]$ (δ = -118 ppm) and $Q^3[(SiO)_3SiOH]$ (δ = -110 ppm) units was observed. The signal at δ = -75 ppm was assigned to the completely condensed T^3 silicon units $[R\text{-}Si(OSi)_3]$ of both POSS nanocage and the organosilane silicon acting as linker between the solid support and the POSS itself, whereas the signal at δ = -67 ppm was attributed to T^2 $[R\text{-}Si(OSi)_2OR]$ silicon atoms bridging bulky SBA-15 to POSS units (Figure 5).

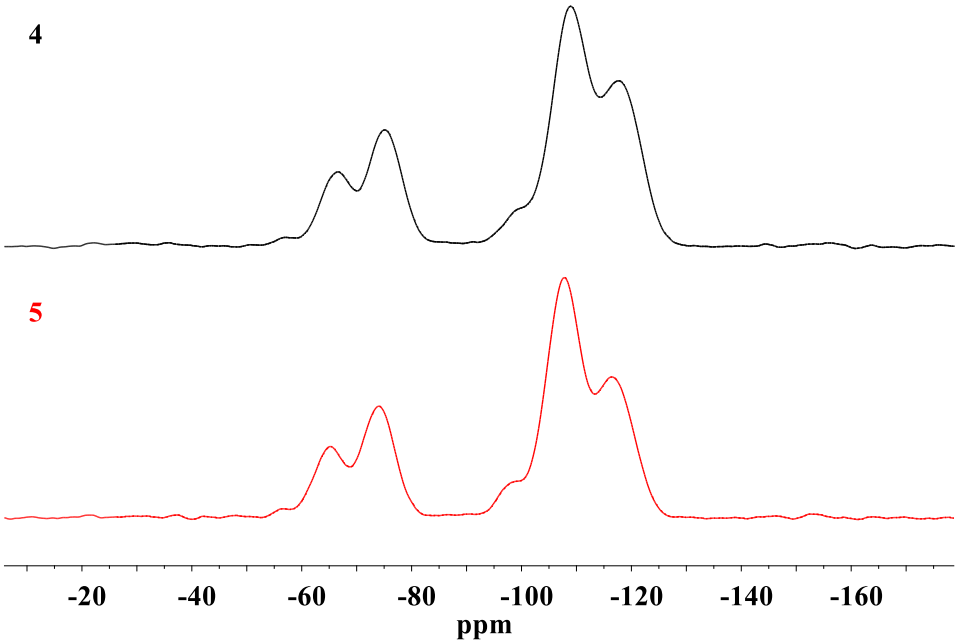

Figure 5. ^{29}Si CP-MASS NMR spectra of **4** (black line) and **5** (red line).

Then, material **5** was tested as heterogeneous pre-catalyst at 0.07 mol% Pd loading in Heck and Suzuki-Miyaura reactions. In both cases, the catalytic performances were extensively evaluated in terms of selectivity, turnover number (TON, calculated as moles of aryl halide converted/moles of Pd), turnover frequency (TOF = TON h^{-1}), and recyclability. The conversion of starting aryl halides was estimated by ^{1}H NMR analysis of the reaction mixture. Heck reactions were performed by coupling several aryl iodides with methyl acrylate or styrene using DMF as solvent and triethylamine as base, at 120 °C. The reactions between aryl iodides and methyl acrylate afforded from high to quantitative conversion in 3 h (Table 1). Excellent results were also obtained in terms of regioselectivity by giving *trans* isomer as the only reaction product.

However, lower levels of regioselectivity were observed in the Heck reactions between aryl iodides and styrene (Table 2). Such couplings were carried out for 20 h leading to both *trans* isomer and *gem*-alkene (5–14%). This finding, already reported in literature,[3] was ascribed to the α-migration step of the aryl group during the catalytic cycle when electron rich olefins are used. Further experiments were performed with a decreased palladium loading in the coupling between 4-iodoanisole and methyl acrylate (Table 3). Improved TOF values were achieved ranging from 0.07 to 0.0007 mol% of Pd.

Table 1. Heck reactions catalyzed by **5**[a].

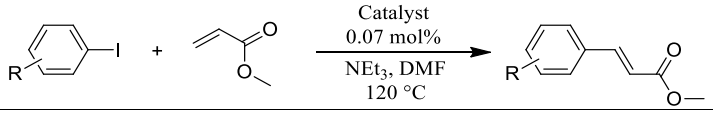

Entry	R	Product	Conv. [%]	TOF [h^{-1}]
1	H	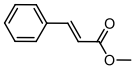	>99	476
2	4-CH_3	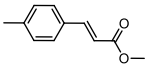	>99	476
3	4-$COCH_3$	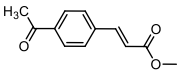	99	471
4	4-OCH_3	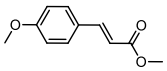	99	471
5	3-OCH_3	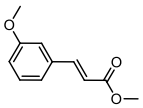	99	471
6	4-NO_2	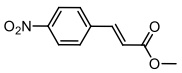	>99	476
7	2-C_4H_3S	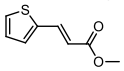	91	433

[a] Reaction conditions: aryl halide (0.5 mmol), methyl acrylate (0.75 mmol), triethylamine (1 mmol), DMF (1 mL), catalyst (2.5 mg), 120 °C, 3 h.

Table 2. Heck reactions catalyzed by **5**[a].

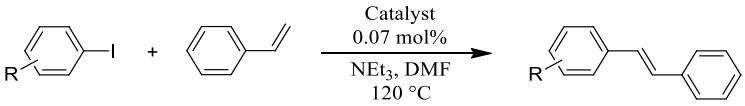

Entry	R	Product	S [%]	Conv. [%]	TOF [h^{-1}]
1	H	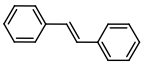	91	99	71
2	4-CH_3	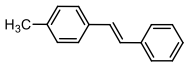	89	98	70
3	4-$COCH_3$	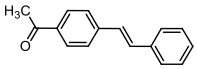	92	99	71
4	4-OCH_3	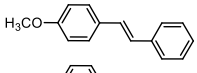	86	98	70
5	3-OCH_3	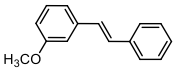	87	89	64
6	4-NO_2	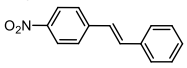	94	>99	71
7	2-C_4H_3S	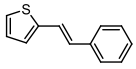	95	>99	71

[a] Reaction conditions: aryl iodide (0.5 mmol), styrene (0.75 mmol), triethylamine (1 mmol), DMF (1 mL), catalyst (2.5 mg), 120 °C, 20 h.

Table 3. Screening of catalyst loading in the reactions be-tween 4-iodoanisole and methyl acrylate.

Entry	Catalyst [mol%]	Conv. [%]	TOF [h^{-1}]
1[a]	0.07	>99	476
2[b]	0.007	99	4,714
3[c]	0.0007	68	32,381

[a] Reaction conditions: 4-iodoanisole (0.5 mmol), methyl acrylate (0.75 mmol), triethylamine (1 mmol), DMF (1 mL), catalyst (2.5 mg), 120 °C, 3 h; [b] Reaction conditions: 4-iodoanisole (2 mmol), methyl acrylate (3 mmol), triethylamine (4 mmol), DMF (2 mL), catalyst (1 mg), 120 °C, 3 h; [c] Reaction conditions: 4-iodoanisole (4 mmol), methyl acrylate (6 mmol), triethylamine (8 mmol), DMF (4 mL), catalyst (0.2 mg), 120 °C, 3 h.

In order to investigate the recyclability of the material, the above mentioned coupling reaction was selected as benchmark process (Figure 6). In doing so, the solid was tested up to six cycles at 0.07 mol% without showing any decrease in the catalytic activity. Then, the catalyst recovered from the sixth cycle was successfully employed at 0.007 mol% for a seventh cycle. Interestingly, in the 7th cycle conversion was very close to that observed in the first cycle with the same catalytic loading (99%, Table 3, entry 2). This result confirms the excellent activity and recyclability of material **5**.

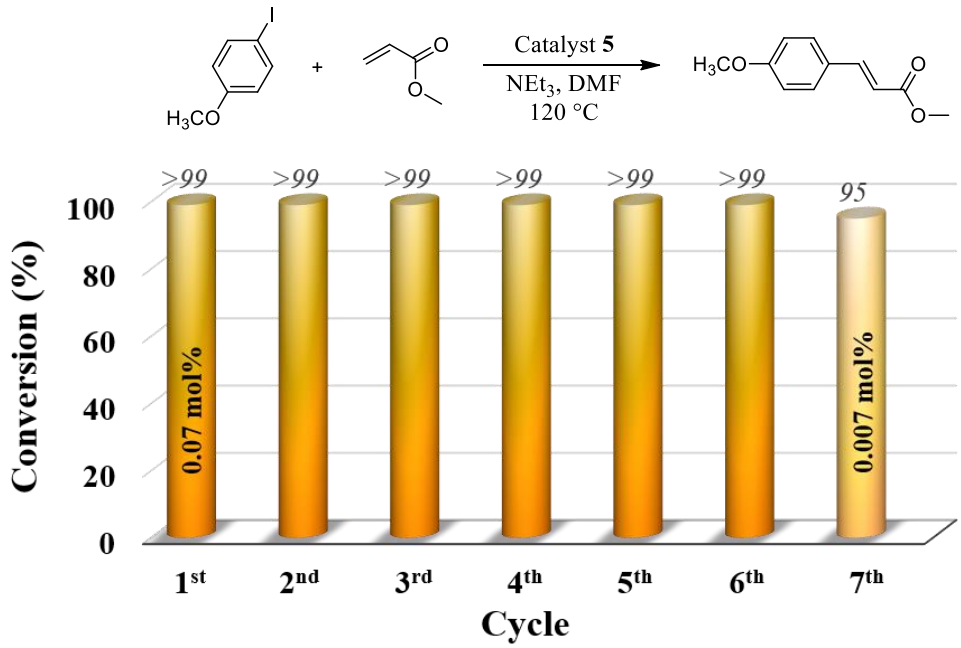

Figure 6. Recycling tests of **5** in the Heck reaction between 4-iodoanisole and methyl acrylate.

Transmission electron microscopy (TEM) measurements were carried out on both fresh and reused material (Figure 7). TEM analysis of the as-synthesized and the reused material revealed the morphology of the bidimensional mesostructured functionalized SBA-15 without showing the presence of reduced Pd nanoparticles (Figure 5).

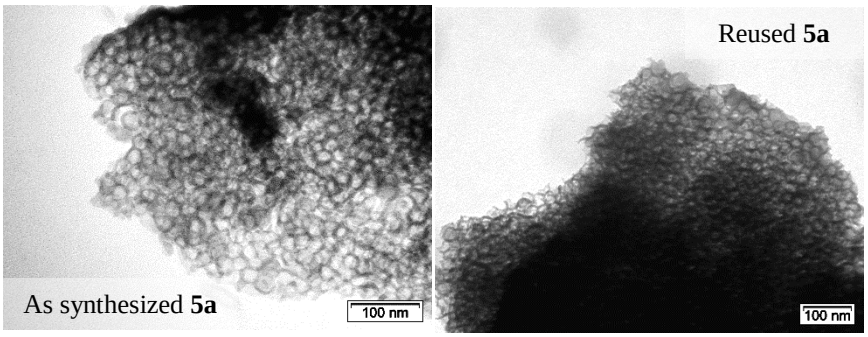

Figure 7. TEM pictures of the as-synthesized (left) and the reused (right) catalyst **5** in the Heck reaction.

The reused catalyst **5** in the Heck reaction was further characterized by using XPS analyses. As evidenced by Figure 8, the XPS spectrum of the Pd 3d region clearly showed the absence of reduced Pd. Only the presence of Pd^{II} was detected.

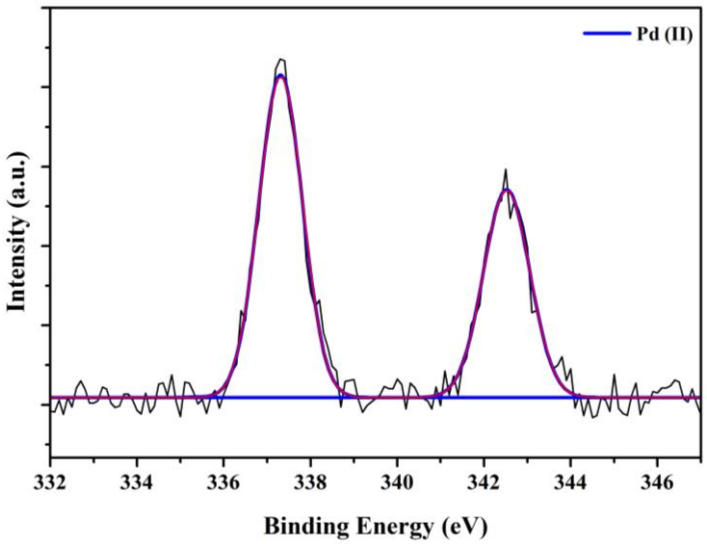

Figure 8. Pd 3d core level XPS spectrum of **5** after recycling tests in the Heck reaction.

Although the literature is plenty of supported palladium-catalyzed Heck reactions, only a few examples concern with the use of Pd^{II}-based catalysts and

their study by XPS after reuse. On unmodified SiO_2, most of Pd^{II}, from $Pd(acac)_2$, was reduced to Pd^0 during the Heck reaction.[4] On the other hand, bis-carbene-pincer complexes of Pd^{II} on montmorillonite K-10 or a polystyrene-supported palladacycle did not show Pd^0 after reuse in the XPS analysis.[5]

Next, the catalytic activity of **5** was investigated in Suzuki reaction between phenylboronic acid and a set of aryl bromides bearing either electron-donating or electron-withdrawing groups. The catalytic tests were run at 50 °C in a mixture ethanol/water (1:1) using K_2CO_3 as base (Table 4).

Table 4. Suzuki-Miyaura reactions catalyzed by **5**[a].

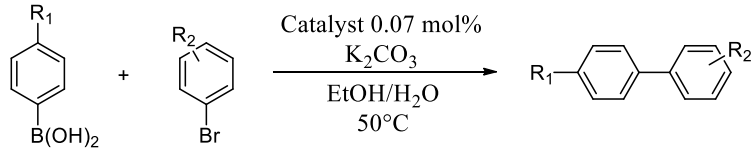

Entry	R^1	R^2	Product	Conv.[b] [%]	TOF [h^{-1}]
1	H	4-CHO	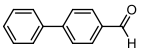	>99	1429
2	H	4-CH_3	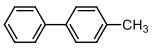	93	1329
3	H	3-CH_3	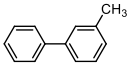	99	1414
4	H	4-CN	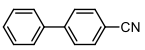	>99	1429
5	H	4-$COCH_3$	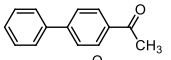	>99	1429
6	H	3-$COCH_3$	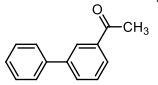	>99	1429
7	H	4-NO_2	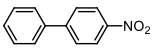	>99	1429
8	H	4-OCH_3	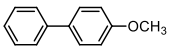	95	1357
9	H	3-OCH_3	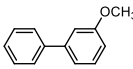	75	1071
10[c]	4-CHO	4-OCH_3	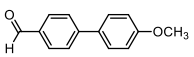	64	305
11[c]	2-CH_3	4-OCH_3	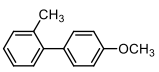	88	419

[a] Reaction conditions: aryl halide (0.5 mmol), phenylboronic acid (0.55 mmol), K_2CO_3 (0.6 mmol), $EtOH/H_2O$ (1:1, 1.2 mL), catalyst (0.07 mol%), 50 °C, 1h. [b] Conversion estimated by ^{1}H NMR analysis. [c] Reaction performed in 3 h.

As showed in Table 4, aryl bromides with electron withdrawing substituents such as 4-CHO, 4-CN, 3-$COCH_3$, 4-$COCH_3$, and 4-NO_2 reacted with phenylboronic acid providing the corresponding cross-coupling products in quantitative conversions in 1 h. On the other hand, aryl bromides with electron-donating groups such as 3-CH_3, 4-CH_3, 3-OCH_3, 4-OCH_3, gave slightly lower conversions. Moreover, 4-bromo anisole was employed for further catalytic tests with two additional phenyl boronic acids (entries 10–11). Such reactions were performed in 3 h. The coupling between the electron-donating 4-iodoanisole and the less reactive 4-formylphenylboronic acid gave rise to 64% conversion whereas the reaction with the *o*-tolylboronic acid led to an 88% conversion. On the ground of this finding, a screening of palladium loading was carried out in the reaction between 4-bromobenzaldehyde and phenylboronic acid (Table 5). In particular, the catalyst amount was decreased down to 0.007 and 0.0007 mol% affording turnover frequency of 14,143 and 114,286 h^{-1}, respectively. Moreover, a further catalytic test was run at higher temperature, namely 120 °C in 5 minutes with a palladium loading of 0.0007 mol%. In this case, the aryl bromide conversion was complete and led to the remarkable TOF value of 1,721,170 h^{-1}.

Table 5. Screening of catalyst loading in the reactions be-tween phenylboronic acid and 4-bromobenzaldehyde.

Entry	Catalyst [mol%]	Conv. [%]	TOF [h^{-1}]
1[a]	0.07	>99	1,429
2[b]	0.007	99	14,143
3[c]	0.0007	80	114,286
4[d]	0.0007	>99	1,721,170

[a] Reaction conditions: aryl bromide (0.5 mmol), phenylboronic acid (0.55 mmol), K_2CO_3 (0.6 mmol), EtOH/H_2O (1:1, 1.2 mL), catalyst (2.5 mg), 50 °C, 1 h; [b] Reaction conditions: aryl bromide (2 mmol), phenylboronic acid (2.2 mmol), K_2CO_3 (2.4 mmol), EtOH/H_2O (1:1, 2.4 mL), catalyst (1 mg), 50 °C, 1 h; [c] Reaction conditions: aryl bromide (4 mmol), phenylboronic acid (4.4 mmol), K_2CO_3 (4.8 mmol), EtOH/H_2O (1:1, 4.8 mL), catalyst (0.2 mg), 50 °C, 1 h. [d] Reaction conditions: 4-bromoacetophenone (2 mmol), phenyl-boronic acid (2.2 mmol), K_2CO_3 (2.4 mmol), EtOH/H_2O (1:1, 2.4 mL), catalyst (0.1 mg), 5 min, 120 °C.

Finally, the recyclability of **5** in the Suzuki reaction was verified with the coupling between 4-bromobenzaldheyde and phenylboronic acid (Figure 9).

It is worth to observe that 0.07 mol% of catalyst allowed to obtain a quantitative yield and conversion of the selected aryl bromide within 1 h in six consecutive runs. Next, the spent catalyst recovered from the 6th cycle was employed for two additional recycling tests with two decreased amounts of catalyst, namely 0.007 and 0.0007 mol%. By comparison with the results obtained with the as-synthesized solid **5** (Table 5, entries 2,3), it was possible to assess that the reused catalyst showed full recyclability up to seven cycles even with a decreased palladium loading.

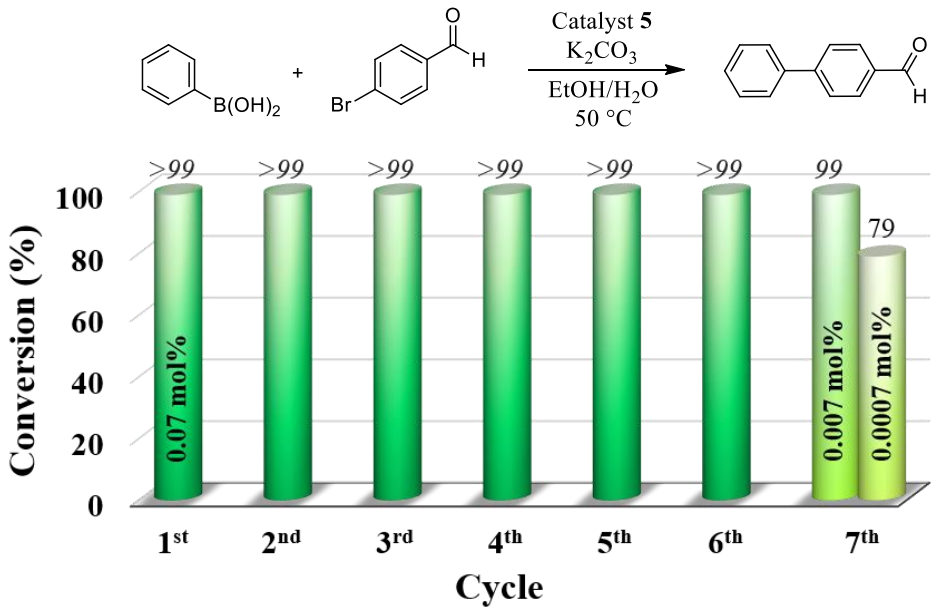

Figure 9. Recycling tests of **5** in the Suzuki reaction between 4-bromobenzaldehyde and phenylboronic acid.

Moreover, XPS analysis of the Pd 3d core level on the spent catalyst revealed the presence of both Pd^0 and Pd^{II} species (Figure 8). The *in situ* reduction of Pd^{II} into Pd^0 during the catalytic tests was clearly detected by the appearance of the signals centered at 335 ($3d_{5/2}$) and 340.4 ($3d_{3/2}$) eV and resulted in a percentage of metallic Pd of 44% respect to Pd^{II}. TEM measurements were carried out on the reused material in the Suzuki reaction (Figure 9).

TEM analysis of the catalyst recovered from the 6th cycle showed a fine dispersion of palladium nanoparticles. TEM pictures were collected using bright field and dark field diffraction contrast imaging. In both cases the presence of Pd NPs was clearly discernable.

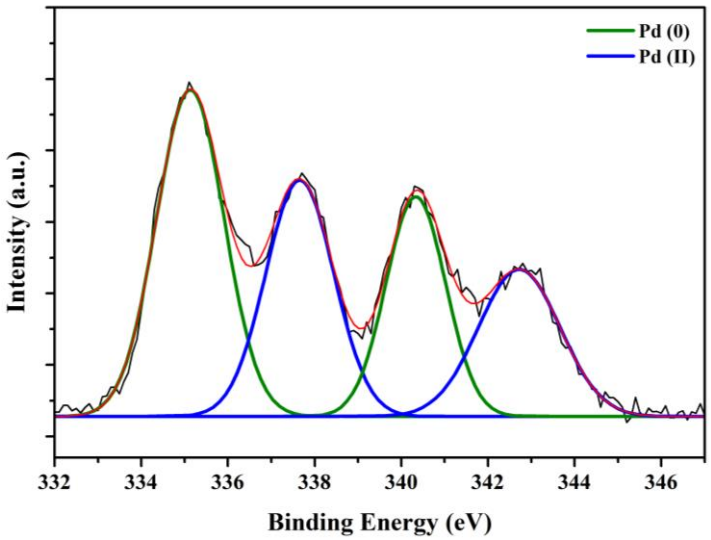

Figure 10. Pd 3d core level XPS spectrum of **5** after recycling tests in the Suzuki reaction.

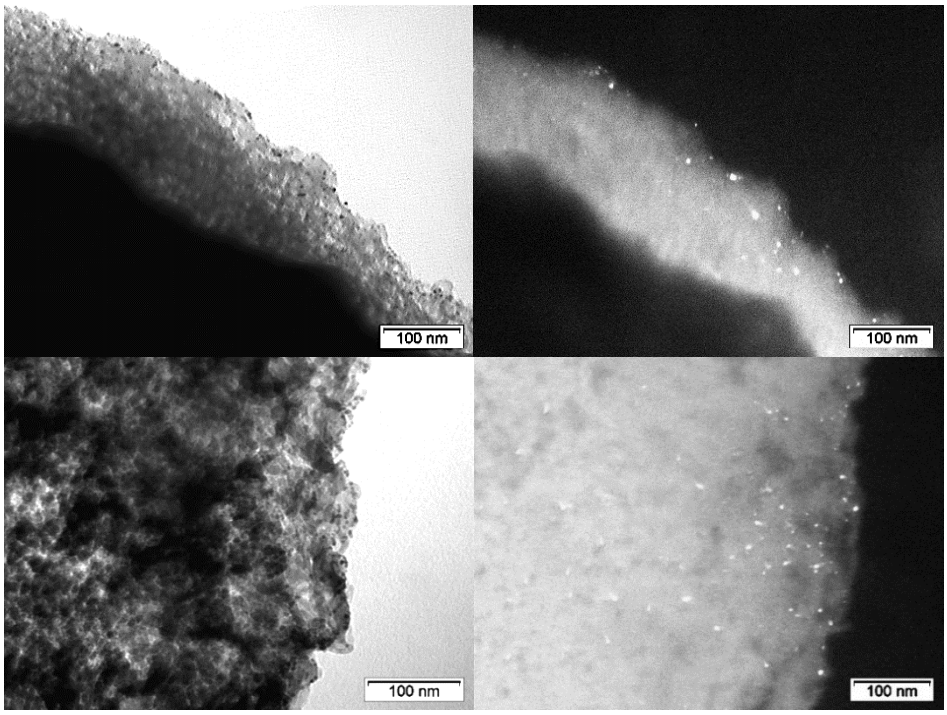

Figure 11. TEM pictures of the reused catalyst **5** in the Suzuki reaction in bright field (left) and in dark field (right).

8.3 Conclusions

Imidazolium functionalized POSS nanostructures were successfully grafted onto mesostructured SBA-15 allowing to obtain a suitable stabilizing support for Pd^{II} pre-catalytic species. Our palladium nanocomposite **5** was easily prepared *via* ionic exchange between chloride and $PdCl_4^{2-}$ anionic species. The final hybrid was characterized by means of several techniques such as TGA, SAXS, ICP-OES, XPS and TEM. Once characterized, the catalytic activity of the material was investigated toward Suzuki and Heck cross-coupling reactions. In both processes, the catalytic performances were evaluated in terms of turnover frequency, versatility and recyclability. The versatility of **5** was investigated with a plethora of aryl halides at 0.07 mol% of Pd providing high conversions into the corresponding products. Additional tests were carried out by using the material with a palladium loading decreased to 0.0007 mol% leading to the outstanding TOF value of 1,721,170 h^{-1} in the Suzuki reaction between 4-bromobenzaldehyde and phenylboronic acid. Moreover, the solid proved to be highly recyclable up to seven cycles without showing any decrease in the catalytic activity. The recyclability of the material was verified at 0.07 mol% of Pd for six consecutive runs. Then, the catalyst recovered from the sixth cycle was employed for further recycling experiments by using a decreased amount of Pd namely 0.007 and 0.0007 mol% for the Suzuki reaction, and 0.007 mol% in the Heck coupling. The direct comparison of these catalytic tests with the analogous ones performed with the as-synthesized catalyst allowed to assess the fully recyclability and robustness of the material. On the ground of these results, the remarkable activity together with the high robustness make the material a promising candidate for C−C couplings under continuous flow conditions.

8.4 Experimental Section

Spectroscopic and analytical methods

Thermogravimetric analysis (TGA) measurements were carried out under oxygen flow from 100 to 1000 °C with a heating rate of 10 °C min^{-1} in a Mettler Toledo TGA STAR. Combustion chemical analysis was performed on a PerkinElmer 2400 Series II Elemental Analyzer System. N_2 adsorption-desorption measurements were carried out at 77 K by using a volumetric adsorption analyzer (Micromeritics Tristar 3000). Before the analysis, the samples were pretreated at 150 °C for 16 h under reduced pressure (0.1 mbar). The BET method was applied in the p/p^0 = 0.05–0.30 range to calculate the specific surface area, whereas the pore size distributions were estimated from the adsorption isotherm using the BJH method. Inductively coupled plasma optical emission spectroscopy (ICP-OES) analysis was carried out with an Optima 8000 ICP-OES Spectrometer. X-ray photoelectron spectroscopy (XPS) analyses were performed with a Thermo Fisher ESCALAB 250Xi instrument equipped with a monochromatic Al Kα X-ray source (1486.6 eV) and a hemispherical deflector analyzer (SDA) working at constant pass energy (CAE) allowing to obtain a constant energy resolution on the whole spectrum. The experiments were performed using a 200 μm diameter X-ray spot. The charge neutralization of the sample was achieved with a flood gun using low energy electrons and argon ions. The pressure in the analysis chamber was in the range of 10^{-8} Torr during data collection. Survey spectra were recorded with a 150 eV pass energy, whereas high-resolution individual spectra were collected with a 25 eV pass energy. Analyses of the peaks were carried out with the software Thermo Avantage, based on the non-linear squares fitting program using a weighted sum of Lorentzian and Gaussian component curves after background subtraction according to Shirley and Sherwood.[6] Full width at half maximum (FWHM) values were fixed for all the signals. Small-angle X-ray scattering (SAXS) experiments were performed on a Bruker Nanostar SAXS System equipped with 2D detector using Cu Kα radiation (λ=1.5418 Å). The SAXS measurements were collected in the range 0.3–1.5° 2θ by using a 0.02° step size

and a counting time of 1.3 s per step. Solid state CP-MAS-TOSS ^{13}C-NMR spectra were recorded at room temperature, on a Bruker Avance 500 Spectrometer operating at 11.7 T, using a contact time of 2 ms, a spinning rate of 5 KHz and a Bruker probe of 4mm. CP-MAS ^{29}Si-NMR spectra were recorded at room temperature, on a Bruker Avance 500 Spectrometer operating at 11.7 T, using a contact time of 2 ms, a spinning rate of 8 KHz and a Bruker probe of 4mm. Transmission electron microscopy (TEM) pictures were recorded on a Philips TECNAI 10 microscope at 80 kV.

Preparation of SBA-15

Mesoporous SBA-15 was prepared starting from tetraethyl orthosilicate (TEOS) as silica source, Pluronic P123 ($EO_{20}PO_{70}EO_{20}$) as template, and mesitylene as swelling agent, according to a published procedure.[7]

Synthesis of material 4

Hybrid **4** was synthesized according to literature procedures.[1]

Synthesis of material 5

In a round bottom flask, supported imidazolium modified POSS **4** (300 mg) was dispersed and sonicated in distilled water (3 mL). In the meanwhile, a sodium tetrachloropalladate solution was prepared by using $PdCl_2$ (0.07 mmol, 12.4 mg), 20 equiv. of NaCl (1.4 mmol, 81.8 mg) in distilled water (4 mL). The above mixture was heated at 80 °C for 20 min. Then, it was allowed to cool down to room temperature. The obtained brown Na_2PdCl_4 solution was added dropwise to the suspension of **4**. The reaction mixture was stirred at room temperature for 16 h. Then, the solid was recovered by centrifugation and washed with water, methanol and diethyl ether. Before each centrifugation, the solid was sonicated for 5 min in the washing solvent. After the last washing, it was dried overnight at 60 °C obtaining catalyst **5** as pale yellow powder (299 mg).

General procedure for the Heck reaction

The catalytic tests were carried out in a 3 mL screw cap glass vial in which pre-catalyst **5** (0.07 mol%), aryl iodide (0.5 mmol), alkene (0.75 mmol), triethylamine (1 mmol) and DMF (1 mL) were placed. The reaction mixture was sonicated for a short time and heated at 120 °C under stirring for a given time. Then, the reaction mixture was allowed to cool down to room temperature, diluted with water in order to be extracted with diethyl ether. The organic layer was dried with Na_2SO_4, filtered and evaporated under vacuum. The conversions of the products were estimated by ^{1}H NMR analysis.

Recycling procedure of 5 in the Heck reaction

Recycling tests were performed in a 10 mL screw cap glass vial in which pre-catalyst **5** (0.07 mol%, 10 mg), 4-iodoanisole (2 mmol), methyl acrylate (3 mmol), triethylamine (4 mmol) and DMF (4 mL) were placed. The reaction mixture was sonicated for a short time and heated at 120 °C under stirring for 3h. Then, it was allowed to cool down to room temperature and centrifuged in order to recover the catalyst. The solid **5** was washed, sonicated and centrifuged with ethyl acetate, methanol and diethyl ether. Once dried, it was used for the next catalytic cycle. The recovered organic layers were evaporated under reduced pressure then treated with water and extracted with diethyl ether. The combined organic layers were dried with Na_2SO_4, filtered and evaporated under vacuum. The conversions of the products were estimated by ^{1}H NMR analysis.

General procedure for the Suzuki reaction

The catalytic tests were carried out in a 3 mL screw cap glass vial in which pre-catalyst **5** (0.07 mol%), aryl bromide (0.5 mmol), phenylboronic acid (0.55 mmol) and K_2CO_3 (0.6 mmol) were placed. Then, distilled water (0.6 mL) and ethanol (0.6 mL) were added. The reaction mixture was sonicated for a short time and heated at 50 °C under stirring for a given time. Then, the reaction mixture was allowed to cool down to room temperature, diluted with water in order to be extracted with dichloromethane. The organic layer was dried with

Na_2SO_4, filtered and evaporated under vacuum. The conversions of the products were estimated by ^1H NMR analysis.

Recycling procedure of 5 in the Suzuki reaction

Recycling tests were performed in a 10 mL screw cap glass vial in which pre-catalyst **5** (0.07 mol%, 10 mg), 4-bromobenzaldehyde (2 mmol), phenylboronic acid (2.2 mmol) and K_2CO_3 (2.4 mmol) were placed. Then, distilled water (2.4 mL) and ethanol (2.4 mL) were added. The reaction mixture was sonicated for a short time and heated at 50 °C under stirring for 1 h. Then, it was allowed to cool down to room temperature and centrifuged in order to recover the catalyst. The solid **5** was washed, sonicated and centrifuged with ethyl acetate, methanol and diethyl ether. Once dried, it was used for the next catalytic cycle. The recovered organic layers were evaporated under reduced pressure then treated with water and extracted with dichloromethane. The combined organic layers were dried with Na_2SO_4, filtered and evaporated under vacuum. The conversions of the products were estimated by ^1H NMR analysis.

8.5 References

[1] C. Calabrese, L. F. Liotta, F. Giacalone, M. Gruttadauria, C. Aprile, *ChemCatChem*.

[2] D. Zhao, J. Feng, Q. Huo, N. Melosh, G. H. Fredrickson, B. F. Chmelka, G. D. Stucky, *Science* **1998**, *279*, 548-552.

[3] a) P. Fristrup, S. Le Quement, D. Tanner, P.-O. Norrby, *Organometallics* **2004**, *23*, 6160-6165; b) J. Ruan, J. Xiao, *Accounts of Chemical Research* **2011**, *44*, 614-626.

[4] L. Huang, Y. Wang, Z. Wang, F. Chen, J. Tan, P. K. Wong, *Physical Chemistry* **2012**, *2*, 27-34.

[5] a) M. Poyatos, F. Márquez, E. Peris, C. Claver, E. Fernandez, *New Journal of Chemistry* **2003**, *27*, 425-431; b) E. Alacid, C. Nájera, *ARKIVOC* **2008**, *8*, 50-67.

[6] D. A. Shirley, *Physical Review B* **1972**, *5*, 4709-4714.

[7] L. Wang, T. Qi, Y. Zhang, J. Chu, *Microporous and Mesoporous Materials* **2006**, *91*, 156-160.

CHAPTER IX

General Conclusions

CHAPTER IX

General Conclusions

This PhD dissertation surveyed the development of novel hybrid materials endowed with imidazolium based organic salts as heterogeneous catalytic systems.

Several imidazolium salts have been covalently grafted onto emerging nanostructures such as carbon nanohorns (CNHs), multi-walled carbon nanotubes (MWCNTs), and polyhedral oligomeric silsesquioxanes (POSS). The design of the catalysts has been previously optimized by changing some reaction parameters.All the solids were fully characterized by several techniques such as thermogravimetric analysis, multinuclear solid state NMR, transmission electron microscopy, N_2 physisorption, combustion chemical analysis, X-ray photoelectron spectroscopy, among others. The obtained materials were employed as organocatalysts for the conversion of carbon dioxide and as stabilizing supports for palladium species in order to be used in C–C cross couplings. In particular, CO_2 conversion was carried out in solvent- and metal-free reaction conditions. The catalytic performances of all the hybrids were extensively evaluated in terms of selectivity, recyclability, productivity, and turnover number/turnover frequency values.

Carbon nanostructures were functionalized *via* a straightforward one-step procedure based on the radical polymerization of various bis-vinylimidazolium salts in the presence of the pristine support leading to a broad series of hybrids. The catalytic activity of imidazolium modified carbon nanohorns was explored in the synthesis of cyclic carbonates from carbon dioxide and epoxides by studying the influence of the organic linker between the imidazolium units, and the effect of the anionic species. In this context, the solids based on an imidazolium network with the *p*-xylyl as organic linker showed an increase of the catalytic activity during the recycling tests. This particular behaviour was ascribed to some modifications of the cross-linked polymeric network depending on the reaction conditions. Then, both carbon nanohorns and multi-walled carbon nanotubes were modified with

imidazolium salts through the same synthetic strategy by using a bis-vinylimidazolium bromide salt bearing the butyl as organic linker. The obtained solids were prepared in order to be employed as stabilizing supports for palladium nanoparticles. The corresponding hybrids were successfully tested as heterogeneous catalysts in C–C couplings being carbon nanohorns based material slightly more active than imidazolium functionalized carbon nanotubes.

Furthermore, a series of catalytic materials based on imidazolium modified POSS nanostructures (POSS-Imi) grafted on amorphous silica (SiO_2) and mesostructured SBA-15 has been prepared by following a modular synthesis which represents a promising approach for the design of a wide library of hybrid functional materials. The catalytic activity was investigated in the conversion of carbon dioxide into cyclic carbonates. The performances of the solids were stepwise improved, by finely tuning POSS-Imi units in terms of nucleophilic active species (Cl^-, Br^-, I^-) and imidazolium alkyl chain length.

Switching on a different catalytic application, POSS nanocages, modified with imidazolium chloride moieties and grafted on mesostructured SBA-15, have been used as heterogeneous platform for Pd^{II} species. The resulting hybrid was successfully tested in Suzuki-Miyaura and Mizoroki-Heck couplings.

Then, POSS nanocages have been further employed as molecular bricks for the synthesis of imidazolium cross-linked networks to be tested in the fixation of carbon dioxide into epoxides. Two catalysts were synthesized for this purpose *via* a simple one-pot procedure based on the reaction between octakis(3-bromopropyl)-octasilsesquioxane or octakis(3-iodoopropyl)-octasilsesquioxane with 1,4-bis(imidazol-1-yl)-butane.

In this PhD dissertation, almost all the materials were easily recoverable and recyclable as well as highly active toward the formation of the desired products, showing high thermal stability and outstanding performances in terms of turnover number, productivity and selectivity. The adopted synthetic routes for the design of our hybrids pave the way to a huge spectrum of novel materials for additional catalytic applications. It is also noteworthy that the productivity and the efficiency of the catalysts for the CO_2 conversion could be improved by the insertion of co-

catalytic species, as Lewis acid sites. The further development of the catalytic systems can be deeply explored moving on their use in continuous-flow conditions.

List of abbreviations

AIBN	2,2′-Azobis(2-methylpropionitrile)
BE	Binding Energy
BET	Brunauer-Emmett-Teller
BJH	Barret, Joyner and Halanda
CNFs	Carbon Nanoforms
CNHs	Carbon Nanohorns
CNTs	Carbon Nanotubes
Conv.	Conversion
CP	Cross Polarization
CVD	Chemical Vapor Deposition
DE	Direct Excitation
DIPA	Diisopropylamine
DWCNTs	Double-walled carbon nanotubes
ICP-OES	Inductively Coupled Plasma – Optical Emission Spectrometry
ILs	Ionic Liquids
MAS	Magic Angle Spinning
MCM	Mobile Composite of Matter
MNPs	Metal Nanoparticles
MP-AES	Microwave Plasma - Atomic Emission Spectroscopy
MWCNTs	Multi-Walled Carbon Nanotubes
NMR	Nuclear Magnetic Resonance
NPs	Nanoparticles
OSs	Organic Salts
P	Productivity
P_i	Initial Pressure
POSS	Polyhedral Oligomeric Silsesquioxane
PSD	Pore Size Distribution

SAXS	Small-Angle X-ray Scattering
SAS	Synthetic Amorphous Silica
SBA	Santa Barbara Amorphous
SILs	Supported Ionic Liquids
SWCNTs	Single-Walled Carbon Nanotubes
TEM	Transmission Electron Microscopy
TEOS	Tetraethylorthosilicate
TGA	Thermogravimetric Analysis
TMB	1,3,5-trimethylbenzene
TON	Turnover Number
TOF	Turnover Frequency
TOSS	Total Suppression of Sidebands
TSILs	Task Specific Ionic Liquids
XPS	X-ray Photoelectron Spectroscopy
wt%	Weight%

Curriculum vitae

Carla Calabrese

Personal Information

Surname/First Name: Calabrese Carla

Address: 31, Via Monti Iblei, 90144, Palermo (Italy)

E-mail: carla.calabrese@unipa.it; carla.calabrese@unamur.be; carlacalabrese90@gmail.com

Nationality: Italian

Place and date of birth: Palermo (Italy), 28/05/1990

Professional Experience

• *10/12/2018 – on going*
Academic Tutor at the University of Palermo (Centro Orientamento e Tutorato): tutoring students of the University of Palermo about General Chemistry.

Education and Training

• *04/12/2018*
Qualifying examination to chemistry register obtained at University of Palermo.

• *01/11/2015 – on going*
PhD Student in Molecular and Biomolecular Sciences/ Doctorant en Science
Co-funded PhD fellowship between the University of Palermo (Italy) and the University of Namur (Belgium).
Project Title: "Design of Novel Imidazolium Based Nanostructures for Sustainable Catalytic Applications".
Tutors: Prof. Michelangelo Gruttadauria (University of Palermo) and Prof. Carmela Aprile (University of Namur).

• *15/06/2015 – 15/07/2015*
Internship (Research activity): Carbon Dioxide Conversion Catalyzed by Imidazolium Modified Polyhedral Silsesquioxanes in the Presence of Lewis Acid Species.
Laboratory of Applied Materials Chemistry, University of Namur, Rue de Bruxelles 61, 5000, Namur
Tutor: Prof. Carmela Aprile

• *26/01/2015 – 26/10/2015*
Internship (Research activity): Carbon Nanoforms in Catalytic Applications; Synthesis and Application of Imidazolium Based Hybrids.
Department of Biological, Chemical and Pharmaceutical Sciences and Technologies, University of Palermo, Viale delle Scienze, Ed. 17, 90128 Palermo (Italy)
Tutor: Prof. Michelangelo Gruttadauria, Prof. Francesco Giacalone

• *17/10/2011 – 17/01/2012*
Internship (Research activity): Synthesis and Charcterization of $LaFeO_3$ Powders from Biowaste-Sourced Soluble Substances.
ISMN-CNR UOS, Via Ugo La Malfa 153, 90146, Palermo
Tutor: Dr. Francesca Deganello

• *22/12/2014*
Master Degree in Chemistry – Curriculum Chemistry of Molecular Systems 110/110 with honors, University of Palermo (Italy)
Thesis Title: "Alcohol Oxidation Promoted by TEMPO/BAIB/TBAB Systems"
Tutor: Prof. Michelangelo Gruttadauria, Prof. Francesco Giacalone

• *08/07/2008*
High School Diploma (Classic Lyceum) with a final score of 100/100
Liceo-Ginnasio Statale "G. Meli", Palermo

Publications

• V. Campisciano, C. Calabrese, L. F. Liotta, V. La Parola, A. Spinella, C. Aprile, M. Gruttadauria, F. Giacalone, "Templating effect of Carbon Nanoforms on Highly Cross-Linked Imidazolium Network. Catalytic Activity of the Resulting Hybrids with Pd Nanoparticles", *Appl. Organometal. Chem.*, **2019**, doi: 10.1002/aoc.4848.

• C. Calabrese, L. F. Liotta, F. Giacalone, M. Gruttadauria, C. Aprile, "Supported Polyhedral Oligomeric Silsesquioxane-Based (POSS) Materials as Highly Active Organocatalysts for the Conversion of CO_2", *ChemCatChem* **2019**, *11*, 560-567.

• C. Calabrese, L. F. Liotta, E. Carbonell, F. Giacalone, M. Gruttadauria, C. Aprile, "Highly Performing Imidazolium Functionalized Carbon Nanohorns for the Conversion of Carbon Dioxide. Unprecedented Increase of Catalytic Activity after Recycling", *ChemSusChem*, **2017**, *10*, 1202-1209.

• F. Giacalone, V. Campisciano, C. Calabrese, V. La Parola, L. F. Liotta, C. Aprile, M. Gruttadauria, "Supported C60-IL-PdNP as extremely active nanocatalysts for C–C cross-coupling reactions", *J. Mater. Chem. A*, **2016**, *4*, 17193-17206.

• F. Giacalone, V. Campisciano, C. Calabrese, V. La Parola, Z. Syrgiannis, M. Prato, M. Gruttadauria, "Single-Walled Carbon Nanotube−Polyamidoamine Dendrimer Hybrids for Heterogeneous Catalysis", *ACS Nano*, **2016**, *10*, 4627-4636.

• F. Deganello, M. L. Tummino, C. Calabrese, M. L. Testa, P. Avetta, D. Fabbri, A. Bianco Prevot, E. Montoneri, G. Magnacca, "A new sustainable $LaFeO_3$ material prepared from biowaste sourced soluble substances", *New J. Chem.*, **2015**, *39*, 877-885.

Conference Communications

• Poster Communication to *International Winter School of Innovative Catalysis and Sustainability ICS2019, Bardonecchia (Turin, Italy)*, **January 07-11**, **2019**: C. Calabrese, L. F. Liotta, F. Giacalone, M. Gruttadauria, C. Aprile, "Imidazolium Based Cross-Linked Nanostructures from POSS molecular bricks for the Efficient Conversion of Carbon Dioxide".

• Oral Communication to *XXXVIII Convegno Nazionale della Divisione di Chimica Organica della Società Chimica Italiana CDCO, Milano (Italy)*, **September 09-13**, **2018**: C. Calabrese, L.F. Liotta, F. Giacalone, C. Aprile, M. Gruttadauria, "Supported Imidazolium Functionalized POSS Hybrids as Palladium Platform for C–C Cross-Couplings".

• Poster Communication to *12th International Symposium Scientific Bases for the Preparation of Heterogeneous Catalysts PREPA12, Louvain-La Neuve (Belgium)*, **July 8-12**, **2018**: C. Calabrese, F. Siragusa, L.F. Liotta, F. Giacalone, M. Gruttadauria, C. Aprile, "Design of POSS-Imidazolium Supported Hybrids for the Conversion of Carbon Dioxide into Cyclic Carbonates".

• Seminar at the University of Namur (Belgium) **June 29**, **2018**: C. Calabrese, "Design of Novel Imidazolium Based Nanostructures for Sustainable Catalytic Applications".

• Oral Communication to *Convegno congiunto delle sezioni Sicilia e Calabria della Società Chimica Italiana, Catania (Italy)*, **February 09-10**, **2018**: C. Calabrese, F. Siragusa, L.F. Liotta, F. Giacalone, M. Gruttadauria, C. Aprile, "Materiali Ibridi a base di POSS-Imidazolio per la Conversione della CO_2 in Carbonati Ciclici".

• Oral Communication to *Europacat 13th European Congress on Catalysis, Florence (Italy)*, **August 27-31**, **2017**: C. Calabrese, L. F. Liotta, E. Carbonell, F. Giacalone, M. Gruttadauria, C. Aprile, "Imidazolium-Functionalized Carbon Nanohorns for the Conversion of CO_2 Unprecedented Increase of Catalytic Activity after Recycling".

• Oral Communication to *Workshop delle sezioni Sicilia e Calabria della Società Chimica Italiana, Messina (Italy)*, **February 09-10**, **2017**: C. Calabrese, L.F.Liotta, E. Carbonell, F. Giacalone, M. Gruttadauria, C. Aprile, "Catalizzatori a base di Nanocorni di Carbonio-Liquidi Ionici per la conversione della CO_2".

• Oral Communication to *Convegno Congiunto delle Sezioni Sicilia e Calabria della Società Chimica Italiana, Catanzaro (Italy)*, **December 3-4**, **2015**: F. Giacalone, V. Campisciano, C. Calabrese, A. Scurria, V. La Parola, L. F. Liotta, M. Gruttadauria, "Ibridi C60-IL-Pd immobilizzati come catalizzatori estremamente attivi di nuova concezione".

• Poster Communication to *6th Czech-Italian-Spanish Conference on Molecular Sieves and Catalysis CIS-6 organized with GIC 2015 (XVIII National Congress of Catalysis) and AIZ 2015 (XII National Congress of Zeolites Science and Technology), Amantea (Italy)*, **June 14-17**, **2015**: V. Campisciano, C. Calabrese, V. La Parola, L. F. Liotta, C. Aprile, F. Giacalone, M. Gruttadauria: "Supported fullerene C60-ionic liquid hybrids as new catalytic materials".

Conference Attendance

• International Winter School of Innovative Catalysis and Sustainability ICS2019, Bardonecchia (Turin, Italy) **January 07-11**, **2019**.

• XXXVIII Convegno Nazionale della Divisione di Chimica Organica della Società Chimica Italiana CDCO, Milano (Italy) **September 09-13**, **2018**.

• 12th International Symposium Scientific Bases for the Preparation of Heterogeneous Catalysts PREPA12, Louvain-La Neuve (Belgium) **July 8-12**, **2018**.

• Convegno Congiunto delle Sezioni Sicilia e Calabria della Società Chimica Italiana, Catania (Italy) **February 09-10**, **2018**.

• Europacat 13th European Congress on Catalysis, Florence (Italy) **August 27-31**, **2017**.

• Workshop delle Sezioni Sicilia e Calabria della Società Chimica Italiana, Messina (Italy) **February 09-10**, **2017**.

• YBMRS 14th Young Belgium Magnetic Resonance Scientist Symposium, Blankenberge (Belgium) **November 30-December 01**, **2015**.

Supervisor of the experimental work of:

• Teresa Britz, erasmus bachelor student at University of Palermo (STEBICEF Department), **a.y. 2017-2018**.

• Fabiana Siragusa, master erasmus student at University of Palermo (STEBICEF Department) and at the University of Namur (Department of Chemistry), **a.y. 2016-2017**.

• Jennifer Braun, erasmus bachelor student at University of Palermo (STEBICEF Department), **a.y. 2016-2017**.

• Eleni Siefke, erasmus bachelor student, at University of Palermo (STEBICEF Department), **a.y. 2016-2017**.

• Gabriella Mastrantuoni, internship at University of Namur (Department of Chemistry), **05-07/2016**.

• Alexey Ryabov, master student at University of Namur (Department of Chemistry), **a.y. 2015-2016**.

• Carina Lemke, erasmus bachelor student, at University of Palermo (STEBICEF Department), **a.y. 2014-2015**.

Seminar and courses

• Seminar: "Factors determining activity of receptor tyrosine kinase inhibitors: FGFR as example", Prof. Walter Berger (Medical University of Vienna), **September 20**, **2018**, University of Palermo (Italy).

• Seminar: "Therapy resistance mechanisms in solid tumors: a multifaceted problem" Prof. Walter Berger (Medical University di Vienna), **September 18**, **2018**, University of Palermo (Italy).

• Workshop: "Pulmonary Drug Administration", **April 17**, **2018**, University of Palermo (Italy).

• Seminar: "Inside the review process", **April 4**, **2018**, University of Palermo (Italy).

• Seminar: "When I'm sixty-four…la sicurezza sociale dei giovani ricercatori: diritti e doveri degli studenti di dottorato di ricerca e situazione previdenziale", **March 12**, **2018**, University of Palermo (Italy).

• English Course: "Conversiazione in Lingua Inglese", Dr. Rachel Marion Garnett, 18 h **a.y. 2016-2017**, Centro Linguistico di Ateneo, University of Palermo (Italy).

• Seminar: "Spin-off accademico: fare impresa all'Università di Palermo", **March 29**, **2017**, Scuola Politecnica, University of Palermo (Italy).

• Training: "Presentazione della banca dati SciFinder", **December 13**, **2016**, Scuola Politecnica, University of Palermo (Italy).

• Seminar: "Occasioni di finanziamento della ricerca e della mobilità in ambito europeo". **November 15-17**, **2016**, University of Palermo (Italy).

• Seminar: "Le parcours administratif de la thèse", Prof. Jacques Ghiysen, (University of Namur), **May 19**, **2016**, Department of Chemistry, University of Namur (Belgium).

• Seminar: "Recent result of Molecular Gastronomy and its latest application: Note by Note cooking", Hervé This, (International Centre for Molecular Gastronomy AgroParisTech-INRA, Paris, France), **May 19**, **2016**, Department of Chemistry, University of Namur (Belgium).

• Seminar: "L'obésité: pas qu'une question d'alimentation" Thierry Arnould, (University of Namur), **May 19**, **2016**, Department of Chemistry, University of Namur (Belgium).

• Workshop: "Être un bon communiquant", Aude Fischer, Lexicom. **May 18 2016**, University of Namur (Belgium).

• Workshop: "How to make a great PowerPoint presentation", Laender, (University of Namur), **May 17**, **2016**, University of Namur (Belgium).

• Workshop: "Publishing in a Nature Research Journal", Bart Verberck, Nature Physics, London (UK), **May 17**, **2016**, University of Namur (Belgium).

• Seminar: "Culinary art and science" Christophe Lavelle, (CNRS/Museum National d'Histoire Naturelle/ISCC, Paris, France), **May 17**, **2016**, Department of Chemistry, University of Namur (Belgium).

• Seminar: "Food packaging: Challenges in biosourced polymers", Samira Benali, (University of Mons, Belgium), **May 17**, **2016**, Department of Chemistry, University of Namur (Belgium).

• Course: "Gestion du Risque chimique et Notions de Toxicologie", Prof. Steve Lanners (University of Namur), **February 17**, **2016**, Department of Chemistry, University of Namur (Belgium).

• Course: "Sécurité de laboratoire en Radioprotection", L. Blot (University of Namur), **February 15**, **2016**, Department of Chemistry, University of Namur, Namur (Belgium).

• Course of "Organometallic Synthesis and Catalysis", Prof. Steve Lanners (University of Namur), **a.y. 2015-2016**, Department of Chemistry, University of Namur, Namur (Belgium).